NASA Technical Memorandum 86671

A

# Improved Oxygen Sources for Breathing Apparatus

Peter C. Wood and Theodore Wydeven

May 1985



NASA
National Aeronautics and
Space Administration

U.S. DEPARTMENT OF THE INTERIOR
BUREAU OF MINES
SAFETY EFFICIENCY
MINERAL INDUSTRIES

NASA Technical Memorandum 86671

# Improved Oxygen Sources for Breathing Apparatus

Peter C. Wood, Department of Chemistry, San Jose State University, San Jose, California
and
Theodore Wydeven, Ames Research Center, Moffett Field, California

May 1985

National Aeronautics and
Space Administration

**Ames Research Center**
Moffett Field, California 94035

## FOREWORD

This report was prepared by the National Aeronautics and Space Administration Advanced Life Support Office, Ames Research Center, Moffett Field, CA 94035, under USBM Contract number HO242047. The contract was initiated under the Coal Mine Health and Safety Research Program. It was administered under the technical direction of Pittsburgh Mining and Safety Research Center with Mr. John Kovac acting as Technical Project Officer. Mr. Dennis D. Maez was the contract administrator for the Bureau of Mines. This report is a summary of the work recently completed as a part of this contract during the period April 14, 1974 to September 20, 1982. This report was submitted by the authors in August 1983.

The authors would like to acknowledge two coworkers, Dr. E. Vernon Ballou and Dr. LeRoy Spitze, for their significant contributions to the research described in this report.

TABLE OF CONTENTS

TABLE OF CONTENTS (cont.)

TABLE OF CONTENTS (cont.)

TABLE OF CONTENTS (cont.)

LIST OF TABLES

LIST OF TABLES (cont.)

LIST OF TABLES (cont.)

LIST OF TABLES (cont.)

LIST OF FIGURES

LIST OF FIGURES (cont.)

# 1. INTRODUCTION

## 1.1 Historical Background

Since the 1920s, the only respiratory protection which coal miners had available during exposure to toxic or irrespirable environments was a filter self-rescuer that catalytically converted carbon monoxide (CO) to carbon dioxide ($CO_2$). The deficiencies of this self-rescuer, which have been described elsewhere (37) led to the support by the Bureau of Mines of the development of a new generation of self-rescuers which utilized potassium superoxide ($KO_2$) as the air-revitalization chemical. Since $KO_2$ reacts with exhaled breath and releases oxygen ($O_2$) while it absorbs $CO_2$, the new self-rescuers were closed-circuit devices which isolated the miner from contact with toxic or irrespirable atmospheres. A device with a one-h duration developed by Lockheed under contract with the Bureau of Mines (18) utilized 1.5 lb of $KO_2$, weighed 4.54 lb and measured 6.5 by 3.6 by 7.7 in. Since the earlier, filter self-rescuer weighed about 2.5 lb and was worn continuously by the miner, the one-h, $KO_2$-based device represented a substantial addition to the equipment that the miner was accustomed to carrying and, therefore, was considered to be too large and too heavy.

## 1.2 Problems with $KO_2$

The size of the portable breathing apparatus is a function of the size of the $KO_2$ bed. When $KO_2$ is used as the air revitalization chemical in self-contained breathing apparatus, the amount of $KO_2$ in the bed is always larger than that needed to meet the metabolic $O_2$ requirements of the user. There are two reasons for this. First, upon exposure to the concentrations of water vapor and $CO_2$ existing in exhaled human breath, $KO_2$ tends to form a fused hydroxide coating on the exterior of the granules which can greatly limit the further utilization of the chemical. In addition to the coating of the granules, intergranule fusion can take place which can block off large sections of the superoxide bed from further contact with the exhalation gases, and thereby greatly increase the pressure drop through the bed. This formation of a fused hydrous coating results in chemical utilization efficiencies of only 50-80% (8) and requires that the $KO_2$ bed be made larger than if higher utilization efficiencies could be achieved.

Secondly, $KO_2$ overproduces $O_2$ relative to the amount of $CO_2$ it absorbs. The theoretical ratio of $CO_2$ absorbed to $O_2$ evolved for pure $KO_2$ is 0.67, if it is assumed that potassium carbonate ($K_2CO_3$) is the sole $CO_2/KO_2$ reaction product. This assumption is reasonable since under the high-temperature (>130°C) reaction conditions existing in the $KO_2$ bed of

a portable life support system, potassium bicarbonate ($KHCO_3$) is not thermally stable, and therefore is not a significant $CO_2$ reaction product (13,26). Since the respiratory quotient (RQ, volume $CO_2$ eliminated to volume of $O_2$ taken up) of a human engaging in moderate work ranges from 0.8 to 1.0 (15) it is apparent that to meet metabolic requirements, the $KO_2$ bed has to be oversized to match the $CO_2$ absorbing requirement or an auxiliary $CO_2$-absorbent bed must be provided.

## 1.3 Search for Improved Chemical-$O_2$ Sources

The deficiencies of $KO_2$ made it desirable to search for an alternative dual-function chemical to replace $KO_2$ which had a superior $O_2$ storage capacity and could be used in a new generation of lighter weight, smaller-sized, self-contained self-rescuers.

Table 1-1 lists the theoretical $O_2$ storage and $CO_2$ scrubbing capacities of the alkali and alkaline-earth metal peroxides, superoxides, and ozonides, all of which are potential, dual-function life-support chemicals. The capacities of the chemicals listed in table 1-1 are based on the following reactions:

M = Alkali Metal

$$M_2O_2 + CO_2 = M_2CO_3 + 1/2\ O_2 \quad \text{(peroxide)} \quad (1.1)$$

$$2MO_2 + CO_2 = M_2CO_3 + 3/2\ O_2 \quad \text{(superoxide)} \quad (1.2)$$

$$2MO_3 + CO_2 = M_2CO_3 + 5/2\ O_2 \quad \text{(ozonide)} \quad (1.3)$$

M = Alkaline Earth Metal

$$MO_2 + CO_2 = MCO_3 + 1/2\ O_2 \quad \text{(peroxide)} \quad (1.4)$$

$$M(O_2)_2 + CO_2 = MCO_3 + 3/2\ O_2 \quad \text{(superoxide)} \quad (1.5)$$

$$M(O_3)_2 + CO_2 = MCO_3 + 5/2\ O_2 \quad \text{(ozonide)} \quad (1.6)$$

For the alkali metals, the bicarbonate species ($MHCO_3$) was not included as a reaction product when the $CO_2$ scrubbing capacity was calculated since formation of $MHCO_3$ is not favored in the high-temperature environment of the bed in a portable breathing apparatus.

Most of the compounds listed in table 1-1 can be eliminated from consideration as replacements to $KO_2$ for one of the following reasons:

a. The compounds are known to be unstable at ambient temperature or only exist at cryogenic temperatures, [e.g.,

Table 1-1.- Available $O_2$ and $CO_2$ Scrubbing Capacities of Alkali and Alkaline Earth Metal Peroxides, Superoxides, and Ozonides.

| Compound | Theoretical Capacities | |
|---|---|---|
| | kg $O_2$ Evolved/kg Compound | kg $CO_2$ Absorbed/kg Compound |
| $Li_2O_2$ | 0.35 | 0.96 |
| $Na_2O_2$ | 0.21 | 0.56 |
| $K_2O_2$ | 0.15 | 0.40 |
| $Rb_2O_2$ | 0.08 | 0.22 |
| $Cs_2O_2$ | 0.05 | 0.15 |
| $MgO_2$ | 0.28 | 0.78 |
| $CaO_2$ | 0.22 | 0.61 |
| $SrO_2$ | 0.13 | 0.37 |
| $BaO_2$ | 0.09 | 0.26 |
| $LiO_2$ | 0.62 | 0.57 |
| $NaO_2$ | 0.44 | 0.40 |
| $KO_2$ | 0.34 | 0.31 |
| $RbO_2$ | 0.20 | 0.19 |
| $CsO_2$ | 0.15 | 0.13 |
| $Mg(O_2)_2$ | 0.50 | 0.54 |
| $Ca(O_2)_2$ | 0.46 | 0.42 |
| $Sr(O_2)_2$ | 0.32 | 0.29 |
| $Ba(O_2)_2$ | 0.24 | 0.22 |
| $LiO_3$ | 0.73 | 0.40 |
| $NaO_3$ | 0.56 | 0.31 |
| $KO_3$ | 0.46 | 0.25 |
| $RbO_3$ | 0.30 | 0.16 |
| $CsO_3$ | 0.22 | 0.12 |
| $Mg(O_3)_2$ | 0.66 | 0.37 |
| $Ca(O_3)_2$ | 0.59 | 0.33 |
| $Sr(O_3)_2$ | 0.44 | 0.24 |
| $Ba(O_3)_2$ | 0.34 | 0.19 |

$LiO_2$, $Mg(O_2)$, and all the ozonides, (46,38,30)]

b. The compounds possess no advantage over $KO_2$ in terms of $O_2$ capacity and $CO_2$ scrubbing capacity per unit weight [e.g., all peroxides except lithium peroxide ($Li_2O_2$), and Rb, Cs, Sr, and Ba superoxides, (table 1-1)]

The only compounds which remain for consideration are $Li_2O_2$, sodium superoxide ($NaO_2$), and calcium superoxide [$Ca(O_2)_2$].

### 1.3.1 Lithium Peroxide

Lithium peroxide has received considerable attention as an air-revitalization chemical because it is commercially available in high purity (30). However, its $O_2$-storage capacity is only slightly higher than $KO_2$ and its use would not significantly reduce the size and weight of self-rescuers if $O_2$-storage capacity is the criterion. Also, tests have shown that during the reaction of $Li_2O_2$ with humidified $CO_2$, $O_2$ evolution lags $CO_2$ absorption and thermal control of the exothermically reacting chemical bed is required to prevent thermal decomposition of the $Li_2O_2$ and the formation of lithium oxide ($Li_2O$) which does not absorb $CO_2$ (10).

### 1.3.2 Sodium Superoxide

Sodium superoxide has a $O_2$-storage capacity superior to $KO_2$ and is also commercially available in high purity. However, $NaO_2$ exhibits the same problems with fused hydroxide coatings that are seen with $KO_2$ and this prevents the full capacity of the chemical from being utilized.

### 1.3.3 Calcium Superoxide as a Potential Alternative to $KO_2$

One compound that is not excluded by the above criteria is $Ca(O_2)_2$. It has been studied in the United States and in the Soviet Union (46,28). The theoretical $O_2$-storage capacity of pure $Ca(O_2)_2$ is 35% greater than $KO_2$. In addition, the $Ca(O_2)_2$/water-vapor reaction product, calcium hydroxide [$Ca(OH)_2$], equivalent to potassium hydroxide (KOH) in the case of $KO_2$, does not form hydrates and decomposes at a high temperature (500°C) without melting. Thus $Ca(O_2)_2$ would not be expected to exhibit problems resulting from the formation of fused hydrous coatings. However, $Ca(O_2)_2$ is not commercially available and previous research on its synthesis yielded products containing only 30-55% $Ca(O_2)_2$.

Since personnel at the NASA Ames Research Center had previous experience in the synthesis of alkali and alkaline earth metal superoxides, the Bureau of Mines requested that a research program on $Ca(O_2)_2$ be carried out in order to produce higher purity material than had been previously

obtained.

## 1.4 Objectives of the Program

The overall objective of this research program was to prepare chemical $O_2$ sources which exhibited improved $O_2$ storage and reaction characteristics when compared to $KO_2$. Pursuit of this main objective was carried out by focusing on the following subobjectives:

(a) Synthesize $Ca(O_2)_2$ in the highest purity possible.

(b) Determine conditions for large-scale laboratory preparations of high-purity $Ca(O_2)_2$ to provide enough material for characterization and testing.

(c) Test the reactivity of $Ca(O_2)_2$ under conditions simulating those existing in the superoxide bed of a manned, self-contained self-rescuer and compare its reactivity with humidified $CO_2$ to that of $KO_2$.

(d) Synthesize and test mixtures of $KO_2$ with other materials to determine whether the reaction characteristics of $KO_2$ could be improved.

## 2. SYNTHESIS OF $Ca(O_2)_2$

### 2.1 Background

The most extensive research on the synthesis of $Ca(O_2)_2$ has been conducted in the Soviet Union by Vol'nov and his coworkers. In what appeared to be the culmination of 10 y of research, they found that up to 55.4% $Ca(O_2)_2$ could be obtained by disproportionating a thin layer (100 $cm^2/g$) of calcium peroxide diperoxyhydrate ($CaO_2 \cdot 2H_2O_2$) at 40°C for 60 min with a residual pressure above the layer of 6 mtorr (47). This purity level was close to the 58.4% value predicted by the $CaO_2 \cdot 2H_2O_2$ disproportionation reaction [i.e., eq. (2.1)] postulated by Vol'nov.

$$2CaO_2 \cdot 2H_2O_2 = Ca(O_2)_2 + Ca(OH)_2 + 3H_2O + 3/2O_2 \qquad (2.1)$$

Equation (2.1) was derived from a series of reaction mechanism equations that had been originally postulated by Kazarnovskii and Neiding (16) for the disproportionation of the related potassium compound, $K_2O_2 \cdot 2H_2O_2$. The reaction-mechanism equations for $CaO_2 \cdot 2H_2O_2$ according to Vol'nov (43) are as follows:

$$2CaO_2 \cdot 2H_2O_2 = Ca(O_2)_2 + Ca(OH)_2 + 2H_2O_2 + 2OH \qquad (2.2)$$

$$2H_2O_2 + 2OH = 2HO_2 + 2H_2O \qquad (2.3)$$

$$Ca(OH)_2 + 2HO_2 = Ca(O_2)_2 + 2H_2O \qquad (2.4)$$

Equations (2.2)-(2.4) yield the net reaction equation

$$2CaO_2 \cdot 2H_2O_2 = 2Ca(O_2)_2 + 4H_2O \qquad (2.5)$$

However, for the reaction in equation (2.5) to proceed, the reactions of equations (2.3) and (2.4) must be preferred over the decomposition of the OH free radicals

$$2OH + 2H_2O_2 = 3H_2O + 3/2O_2 \qquad (2.6)$$

According to Vol'nov, the production of $Ca(O_2)_2$ via reaction (2.4) is not significant because of the decomposition of the free radicals; therefore, equation (2.1) rather than equation (2.5) is the net disproportionation reaction. As a result, the purity of $Ca(O_2)_2$ varies from 0 to 58.4% depending on how efficiently the $H_2O$ generated in equation (2.1) is removed. Efficient removal of water vapor minimizes the following back reaction:

$$Ca(O_2)_2 + nH_2O = CaO_2 \cdot nH_2O + O_2 \qquad (2.7)$$

From a review of the work of Vol'nov and his coworkers, it did not appear that they had optimized the disproportion-

ation reaction conditions and that higher-purity products were still possible.

In the United States, $Ca(O_2)_2$ was produced by Petrocelli and Capostosto (29) through vacuum-drying a slurry of concentrated hydrogen peroxide ($H_2O_2$) and $Ca(OH)_2$. A review of this work indicated that the one-step sythesis process was too irreproducible with regard to the purity of $Ca(O_2)_2$ which was obtained; therefore, it was decided to try to improve upon the stepwise sythesis method used by Vol'nov.

## 2.2 Synthesis of $Ca(O_2)_2$ via the Disproportionation of $CaO_2 \cdot 2H_2O_2$

Calcium peroxide diperoxyhydrate can be produced in two forms: microcrystalline and macrocrystalline. Most of the work on the sythesis of $Ca(O_2)_2$ reported here was focused on the production of $Ca(O_2)_2$ from the disproportionation of the microcrystalline material (crystallite size 30-40 um) (22) since this was the material disproportionated by Vol'nov and his coworkers. However, a later search of the literature revealed the possibility that another crystalline form of $CaO_2 \cdot 2H_2O_2$ existed. A limited study was made of the sythesis of this material which was found to exist in the form of macrocrystals. A number of experiments were conducted in which the macrocrystalline $CaO_2 \cdot 2H_2O_2$ was disproportionated to yield $Ca(O_2)_2$.

Since $Ca(O_2)_2$ and the calcium peroxide ($CaO_2$) starting materials used in the sythesis of $Ca(O_2)_2$ are reactive with atmospheric $CO_2$, the calcium compounds involved in the synthesis process were handled whenever possible under dry nitrogen either inside a portable glove bag or in a glove box. All weighing of the materials was accomplished in tared, sealed containers. In this way, contamination of the $Ca(O_2)_2$ product material with $CaCO_3$ was minimized.

### 2.2.1 Synthesis of Microcrystalline $CaO_2 \cdot 2H_2O_2$

Microcrystalline $CaO_2 \cdot 2H_2O_2$ was produced in two steps. First, calcium peroxide octahydrate, $CaO_2 \cdot 8H_2O$, was sythesized and dried. Then the crystals of $CaO_2 \cdot 8H_2O$ were reacted with concentrated $H_2O_2$. The sythesis process is described in more detail in references (3) and (5). The summary of the process which follows describes the current techniques which have evolved from those described in references (3) and (5).

#### 2.2.1.1 Synthesis of $CaO_2 \cdot 8H_2O$

Calcium peroxide octahydrate was produced by mixing a 20.0% solution of calcium chloride ($CaCl_2$) with a solution which contained 2.0% ammonia ($NH_3$) and 2.5% $H_2O_2$ at $0^oC$. The

molar ratio of $CaCl_2$ to $H_2O_2$ was 1:4. The net reaction is shown in equation (2.8).

$$CaCl_2 + H_2O_2 + 2NH_3 + 8H_2O = CaO_2 \cdot 8H_2O + 2NH_4Cl \qquad (2.8)$$

The crystals of $CaO_2 \cdot 8H_2O$ which precipitated out were collected on a filter, washed with distilled $H_2O$, and dried. The current technique used for drying $CaO_2 \cdot 8H_2O$ utilizes a low-temperature distillation apparatus which allows large batches (up to 68 g) of $CaO_2 \cdot 8H_2O$ to be dried to the stoichiometric-8 waters of hydration without decomposition. The drying apparatus is shown in figure 2-1. The flask containing the $CaO_2 \cdot 8H_2O$ was maintained at 4°C while the trap was maintained at 0°C. Once the apparatus containing the crystals was evacuated down to ~4 torr, the 4°C temperature gradient between the crystal mass and the trap provided enough driving force to distill the excess water from the crystals. The pressure in the apparatus was controlled to a value equal to the vapor pressure of $H_2O$ at 0°C (4.6 torr) to prevent either the build-up of an air diffusion barrier (pressures higher than 4.6 torr) or dehydration of the crystals (pressures less than 4.6 torr). Calcium peroxide octahydrate is indefinitely stable when stored in sealed containers below 20°C.

2.2.1.2 Reaction of $CaO_2 \cdot 8H_2O$ and $H_2O_2$

Next, the microcrystalline $CaO_2 \cdot 2H_2O_2$ was prepared by reacting the dried $CaO_2 \cdot 8H_2O$ with 85-90% $H_2O_2$ at -15°C, decanting most of the liquid phase from the solid, and then removing the remaining $H_2O$ and $H_2O_2$ by freeze-drying. The $CaO_2 \cdot 2H_2O_2$ was freeze-dried on the apparatus shown in figure 2-2. The flask containing the $CaO_2 \cdot 2H_2O_2$ was placed in a cold bath at -10 to -15°C and the system was evacuated. When the pressure reached ~1 torr, the trap was immersed in a liquid-nitrogen bath, and the valve was opened to a diffusion pump. Water and $H_2O_2$ were collected in the trap, leaving the solid $CaO_2 \cdot 2H_2O_2$ in the flask. Using this technique, 17-g batches of dried $CaO_2 \cdot 2H_2O_2$ were obtained. The net-reaction equation is given below.

$$CaO_2 \cdot 8H_2O + 2H_2O_2 = CaO_2 \cdot 2H_2O_2 + 8H_2O \qquad (2.9)$$

The $CaO_2 \cdot 2H_2O_2$ which was produced by this method contained no moisture or excess $H_2O_2$. The material was a microcrystalline, fluffy, white powder and was stable indefinitely when stored in sealed containers below -60°C.

2.2.2 Disproportionation of Microcrystalline $CaO_2 \cdot 2H_2O_2$

The final step in the synthesis of $Ca(O_2)_2$ involves decomposing the $CaO_2 \cdot 2H_2O_2$ in a vacuum chamber. A series of parametric studies were undertaken to determine the reaction

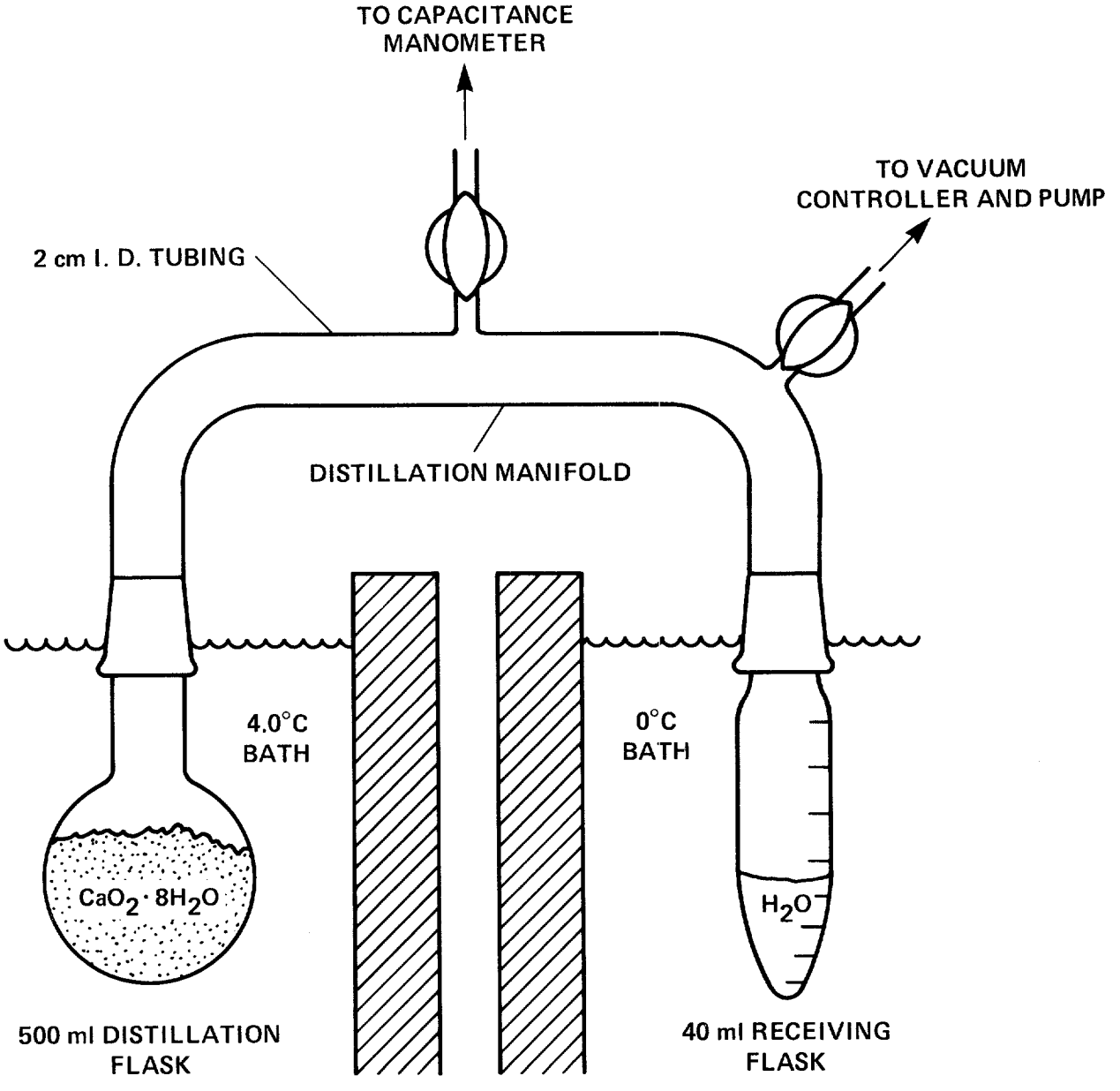


Figure 2-1.- Low-temperature distillation apparatus for removing excess $H_2O$ from $CaO_2 \cdot 8H_2O$.

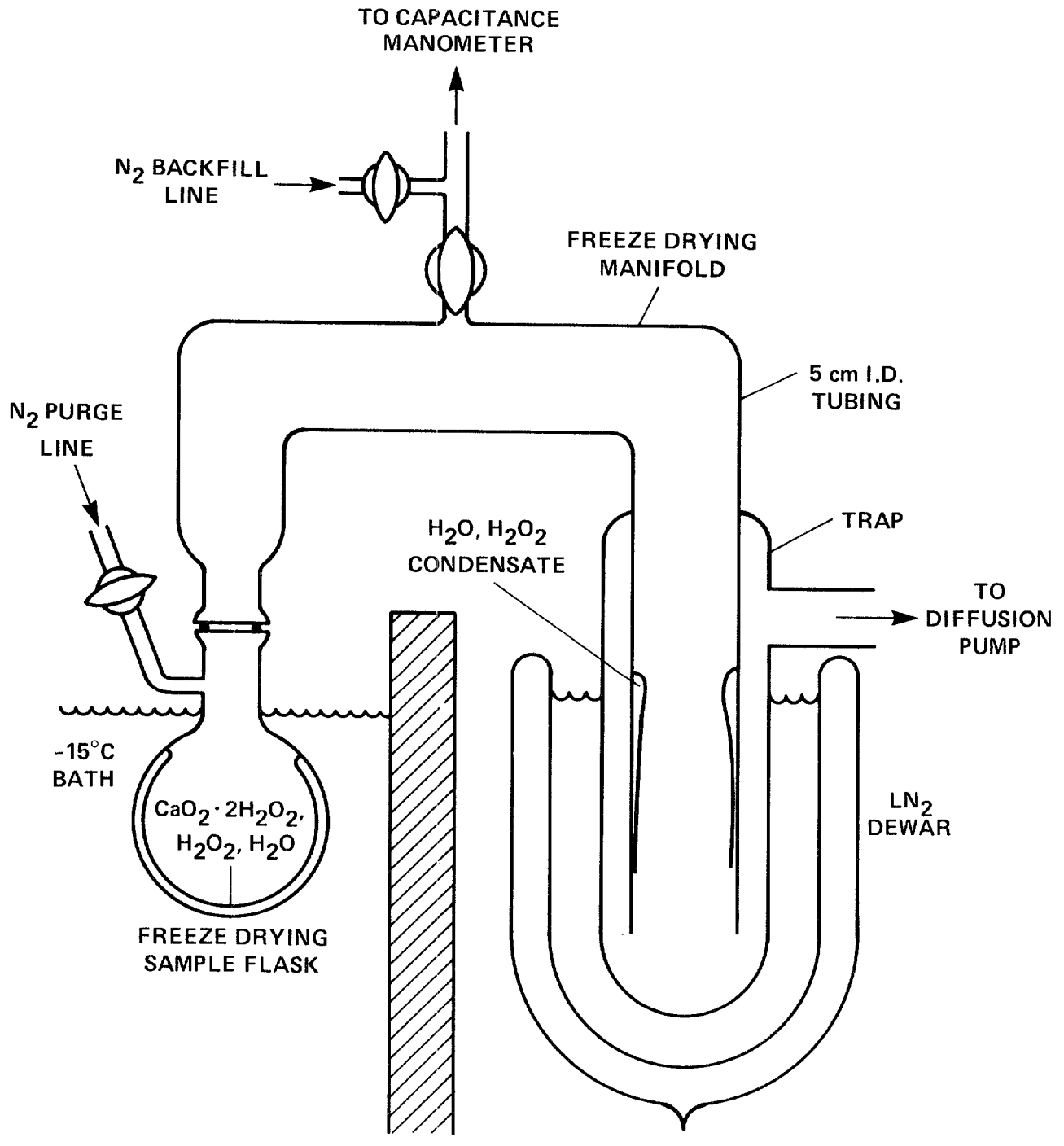


Figure 2-2.- Apparatus for freeze-drying $CaO_2 \cdot 2H_2O_2$.

conditions which yielded the highest purity of $Ca(O_2)_2$ from the disproportionation of microcrystalline $CaO_2 \cdot 2H_2O_2$.

2.2.2.1 Parametric Studies

First, the disproportionation reaction parameters of reaction temperature and reaction time were examined. A detailed description of these studies can be found in references (3) and (5). In this work, a cylindrical, glass-cross vacuum chamber was equipped with a heat lamp and a cooled sample platform to control the sample temperature and a liquid-nitrogen cold finger to trap evolved water vapor. The disproportionation reactor is shown in figure 2-3. The highest purity of $Ca(O_2)_2$ (i.e., up to 67%) was obtained by disproportionating thin layers of $CaO_2 \cdot 2H_2O_2$ (i.e., 150 $cm^2/g$ reactant) for 60-90 min at 30°C under a residual pressure of 6-90 mtorr. The purity of the $Ca(O_2)_2$ obtained under these conditions is significantly above the 58.4% purity level that Vol'nov had predicted would be the maximum possible from the disproportionation reaction [see eq. (2.1)]. This suggests that if Kazarnovskii's disproportionation mechanism holds, a significant quantity of $Ca(O_2)_2$ is being formed as a result of equation (2.4) by the reaction of $Ca(OH)_2$ with $HO_2$ radicals formed via equation (2.3). The 67% $Ca(O_2)_2$ obtained in the work described here is the highest-reported purity of $Ca(O_2)_2$ that has been sythesized.

At temperatures greater than 30°C, the disproportionation reaction was too vigorous and uncontrolled and the purity of $Ca(O_2)_2$ obtained was lower. The time required for completion of the disproportionation process increased with decreasing temperature. For example, at 0°C, products containing ~60% $Ca(O_2)_2$ were obtained by disproportionating $CaO_2 \cdot 2H_2O_2$ under a residual pressure of 1 mtorr. However, up to 24 h were required for the reaction to go to completion.

Next a parametric study was made of the effect of pressure on the purity of $Ca(O_2)_2$ obtained from the disproportionation of microcrystalline $CaO_2 \cdot 2H_2O_2$. The study has been described in reference (4). Two series of experiments were conducted in which thin layers of $CaO_2 \cdot 2H_2O_2$ (e.g., ~150 $cm^2/g$ reactant) were disproportionated for 90 min at 30°C under various residual pressures. In the first series of experiments, evolved water vapor was trapped by the liquid-nitrogen-filled cold finger located on the right-hand side of the reactor (figure 2-3); in the second series of experiments, molecular sieve pellets were mixed with the $CaO_2 \cdot 2H_2O_2$ powder and the cold finger was not used. In the first series of experiments, the highest purity of $Ca(O_2)_2$, approximately 63-64%, was obtained at pressures near to 90 mtorr. Increasing the pressure by a factor of 10 decreased the purity of $Ca(O_2)_2$ to 51% and increasing the pressure by a factor of 100 decreased the $Ca(O_2)_2$ purity level to 35%.

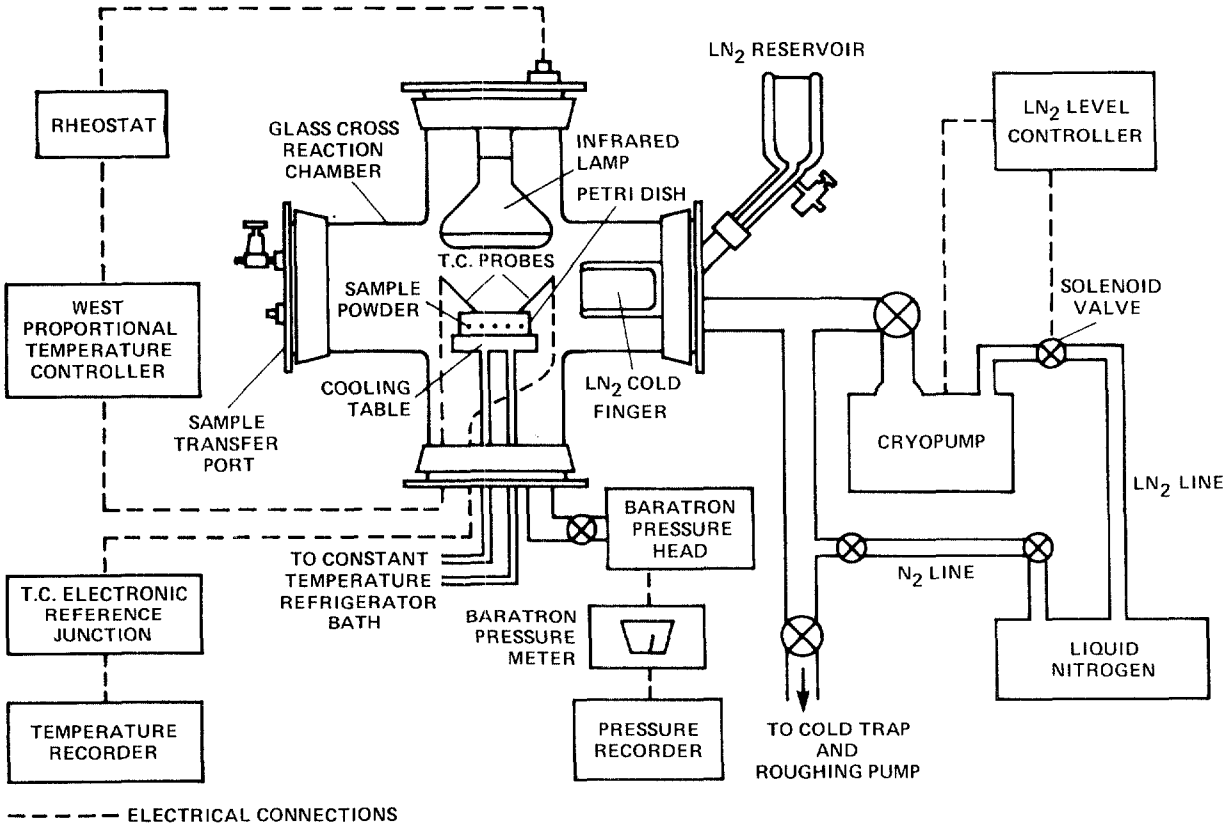


Figure 2-3.- Reaction chamber and auxiliary equipment for disproportionation of $CaO_2 \cdot 2H_2O_2$. (Copyright 1978 American Society of Mechanical Engineers. NTIS is authorized to reproduce and sell this copyrighted work. Permission for further reproduction must be obtained from the copyright owner.)

Lowering the pressure from 90 mtorr by a factor of 10 resulted in a slight (1-2%) decrease in the $Ca(O_2)_2$ content.

In the second series of experiments in which molecular sieve pellets were mixed with the $CaO_2 \cdot 2H_2O_2$, the effect of pressure followed the same general trend (i.e., increasing presssure resulted in decreasing $Ca(O_2)_2$ purity), but the effect was not as dramatic. In fact, 43% $Ca(O_2)_2$ was obtained at 300 torr using the molecular sieve, but only 35% $Ca(O_2)_2$ was present after disproportionation of $CaO_2 \cdot 2H_2O_2$ at 9 torr without molecular sieve. Thus higher purity $Ca(O_2)_2$ was obtained at 30 times the pressure using a molecular sieve as a water trap than when the desiccant was absent.

Finally, a parametric study was undertaken to determine the effect of a flow of inert gas through the disproportionating $CaO_2 \cdot 2H_2O_2$ layer on the purity of $Ca(O_2)_2$ in the product. A detailed description of this study can be found in reference (5). The experiments were carried out at 20°C in the reaction vessel pictured in figure 2-4. Thin layers (~160 $cm^2/g$) of $CaO_2 \cdot 2H_2O_2$ were spread over the surface of the 9-cm-diameter fritted glass disc and dry nitrogen was passed up through the reactant layer under a variety of mass flow rate and vessel pressure combinations. Over the pressure range of 25-150 mtorr, the purity of the $Ca(O_2)_2$ obtained from the disproportionation reaction was found to be a function of the linear velocity of the nitrogen gas flow through the $CaO_2 \cdot 2H_2O_2$ reactant layer. The highest purity of $Ca(O_2)_2$ (~65%) was obtained at the highest linear velocity of the nitrogen gas flow.

#### 2.2.2.2 Water-Vapor Removal Efficiency

The results obtained from the parametric studies can be explained in terms of the efficiency with which water vapor was removed from the layer of disproportionating $CaO_2 \cdot 2H_2O_2$. During the decomposition, the $CaO_2 \cdot 2H_2O_2$ disproportionates into $Ca(O_2)_2$ and $Ca(OH)_2$ and releases water vapor and $O_2$ [eq. (2.1)]. Unless the water vapor is removed from the $CaO_2 \cdot 2H_2O_2$ particle layer, it will back-react with the $Ca(O_2)_2$ that has been produced, forming $CaO_2$ and releasing $O_2$ [eq. (2.7)]. It was postulated that the maximum purity of $Ca(O_2)_2$ would be obtained under the conditions in which the efficiency of water vapor removal was maximized.

There are number of factors that must be optimized if the maximum possible water-vapor removal efficiency is to be achieved. First, the $H_2O$ generated within the particle must diffuse out of the pores of the reacting particles and into the void volume of the particle layer. Figure 2-5 is a photograph of a particle of disproportionated microcrystalline $CaO_2 \cdot 2H_2O_2$ taken using a scanning electron microscope

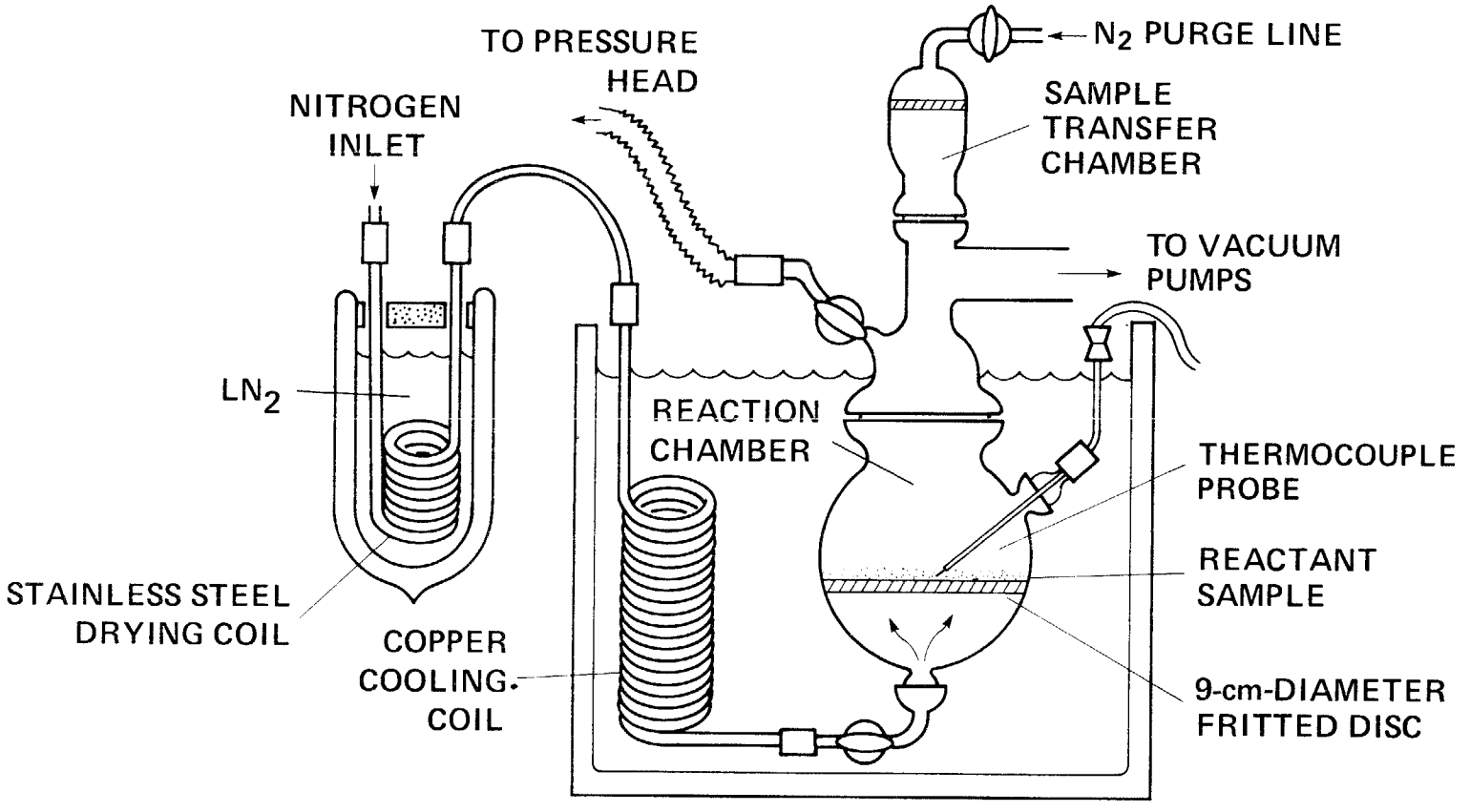


Figure 2-4.- Reaction vessel for the disproportionation of $CaO_2 \cdot 2H_2O_2$ with $N_2$ flow through the sample bed. (Copyright 1980 American Society of Mechanical Engineers. NTIS is authorized to reproduce and sell this copyrighted work. Permission for further reproduction must be obtained from the copyright owner.)

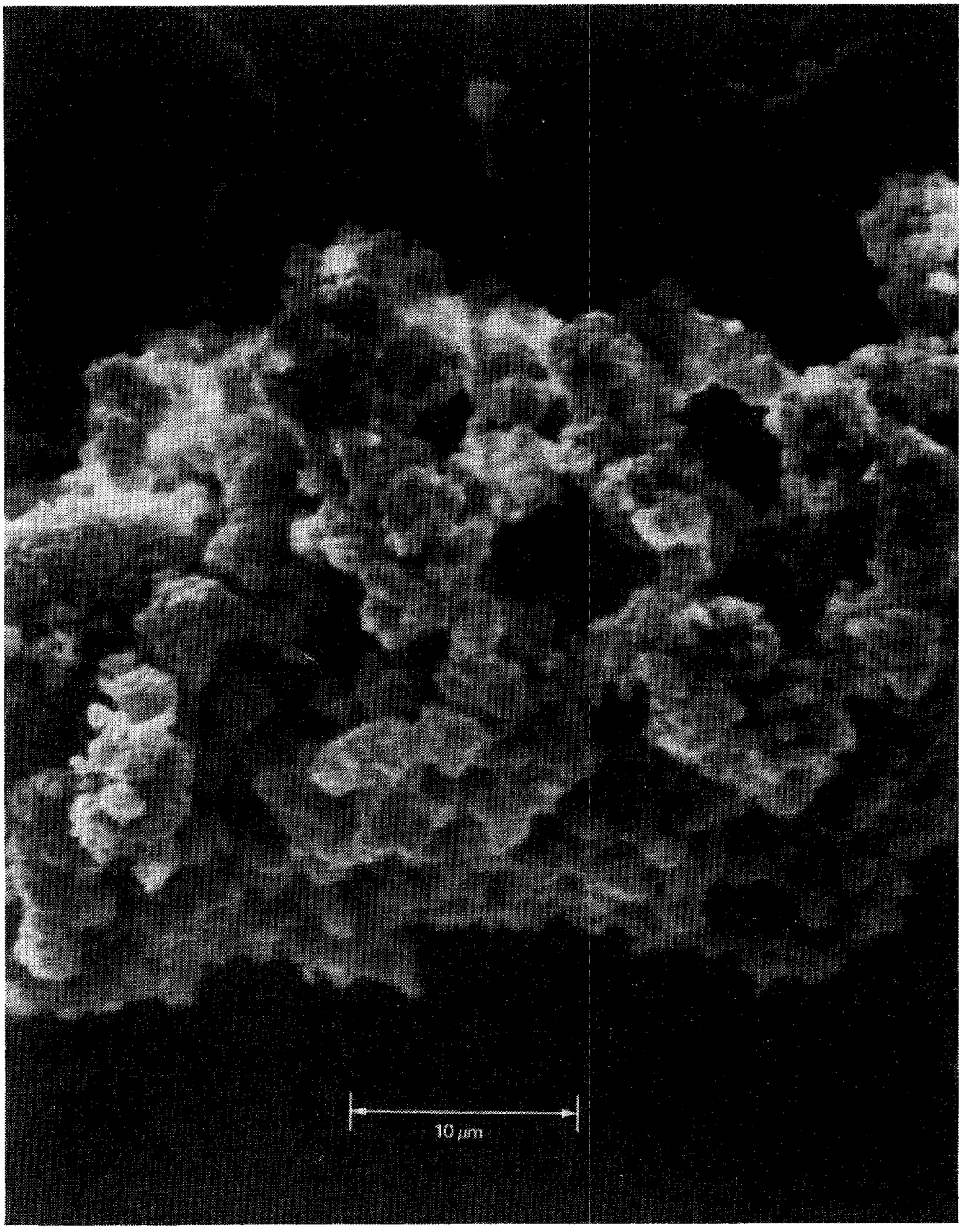


Figure 2-5.- Scanning-electron micrograph of a particle of disproportionated $CaO_2 \cdot 2H_2O_2$. (Copyright 1980 American Society of Mechanical Engineers. NTIS is authorized to reproduce and sell this copyrighted work. Permission for further reproduction must be obtained from the copyright owner.)

which shows the porous nature of the material. The diffusion time of $H_2O$ moving from within the particles to the void volume will be a function of the size distribution of pore diameters and lengths, the temperature of the particles, and the residual pressure of other gases in the pores and in the void space. Diffusion time would be minimized by high temperatures, small particles and low pressures.

However, the rate of release of $H_2O$ into the pores is a function of the rate of disproportionation which is directly dependent on the temperature of the particles. High particle temperatures result in a high partial pressure of water vapor in the pores and increase the likelihood that back reaction with product $Ca(O_2)_2$ will occur. Therefore, it is necessary to determine the temperature which balances the $H_2O$ diffusion and concentration effects. It was found that temperatures above ~30°C resulted in vigorous and uncontrolled reactions, rapid release of water vapor, and lower $Ca(O_2)_2$ purity. In the case of the experiments in which $CaO_2 \cdot 2H_2O_2$ was disproportionated at 0°C, it is postulated that the diffusion time of the $H_2O$ molecules out of the pores was long enough to permit significant back reaction of $H_2O$ to occur within the particles, despite the low $H_2O$ generation rates; therefore, the purity level was 7% less than that obtained at the optimum temperature of 30°C.

Secondly, the water vapor released from the pores into the interparticular void volume must be removed from the reactant layer. In a static vacuum system (with no gas flow through the particle layer) the efficiency of water vapor removal from the void volume is dependent on the depth of the particle layer and the residual pressure in the void space. Low pressures minimize the diffusion barrier, and therefore, minimize the diffusion time of $H_2O$ out of the particle layer. Thin layers of particles minimize the likelihood of $H_2O$ reacting with product as it exits from the layer.

However, the effect of pressure on the removal of $H_2O$ from the void space is complicated by the fact that the $CaO_2 \cdot 2H_2O_2$ disproportionation reaction is exothermic, and at low pressures heat generated within the particles and the particle layer is not conducted away from the layer fast enough to prevent a gradual temperature increase in the sample. The rising temperature in turn increases the rate of disproportionation and the release of $H_2O$ and additional heat. After a period of time, the length of which is dependent on the starting temperature of the particles, the temperature becomes high enough to produce a runaway, uncontrolled reaction in which $H_2O$ and heat are rapidly released from the particles and some of the particles are actually propelled out of the reactant bed. Therefore, it is necessary to determine the pressure at which thermal control

of the particle layer is possible while minimizing the diffusion barrier to escaping water vapor. In a static vacuum system in which thin layers of $CaO_2 \cdot 2H_2O_2$ are disproportionated (>100 $cm^2/g$ reactant), a pressure of ~100 mtorr was found to be optimum.

In a dynamic vacuum system in which a flow of inert gas (nitrogen or helium) passes through the reactant layer, the water vapor in the void volume is swept away by the gas stream. The importance of a diffusion barrier becomes less important. The efficiency of vapor removal was found to increase with the linear velocity of the gas sweep, and thermal control of the particles at low pressures (<100 mtorr) was improved.

Finally, the water vapor leaving the particle layer must be removed from the head space above the layer to prevent the back diffusion of $H_2O$ into the layer. This is accomplished in a static vacuum system by having an efficient water vapor trap adjacent to the reacting layer. To maximize the water vapor removal efficiency, it is necessary to have the water vapor trap as close as possible to the layer and thereby minimize the residual-gas diffusion barrier between the layer and the trap. However, since the thermal control of the particle layer is more difficult under very low pressures, the best approach is to move the water vapor trap close to the top of the layer and use a pressure of about 100 mtorr. The liquid-nitrogen-filled cold finger was very effective at this pressure although it was 5 cm away from the reactant layer. Also, it was found that mixing molecular sieve with the disproportionating $CaO_2 \cdot 2H_2O_2$ was effective in minimizing the back reaction of water vapor with $Ca(O_2)_2$ even at higher than optimum pressures, i.e., >100 mtorr. When a flow of dry nitrogen is passed through the disproportionating $CaO_2 \cdot 2H_2O_2$ layer, it is possible to eliminate the water vapor trap since the $H_2O$ does not back-diffuse and destroy the $Ca(O_2)_2$.

### 2.2.3 Synthesis of Macrocrystalline $CaO_2 \cdot 2H_2O_2$

Vannerberg, a Swedish chemist, had reported that $CaO_2 \cdot 2H_2O_2$ existed in two crystal modifications, alpha and beta, although he did not describe either the method of preparation he used or the unit cell dimensions of the beta form (40). His work on the alpha and beta crystal modifications of $SrO_2 \cdot 2H_2O_2$ and $BaO_2 \cdot 2H_2O_2$ indicated that the crystalline modifications had slightly different arrangements of $H_2O_2$ groups and thermal stabilities (39,41,42). His results suggested that the two crystalline forms of $CaO_2 \cdot 2H_2O_2$ might also have significantly different thermal stabilities. It was postulated that disproportionating a new crystalline form of $CaO_2 \cdot 2H_2O_2$, which had a different structure from the microcrystalline material studied earlier,

might yield $Ca(O_2)_2$ in a higher purity than had been obtained previously. Since no one had reported a method of growing the two crystal modifications of $CaO_2 \cdot 2H_2O_2$, a method for preparing macrocrystalline $CaO_2 \cdot 2H_2O_2$ was developed at the NASA Ames Research Center based on the techniques used by Vannerberg to prepare alpha and beta $SrO_2 \cdot 2H_2O_2$.

The crystal growing method involves making two solutions, one of $CaCl_2$ and $H_2O_2$ and the other of $NH_3$ and $H_2O_2$. Equal volumes of the two solutions were cooled to -10°C, carefully mixed, and allowed to stand 24 h at -10°C. The first crystals usually appeared within 1-10 h, depending on the concentration of the reactants. The crystals were collected on a fritted glass filter and washed with cold absolute ethanol and absolute ethyl ether. Then the last traces of solvent were removed by flowing dry nitrogen through the crystal mass. A number of combinations of various concentrations of $H_2O_2$, $NH_3$, and $CaCl_2$ were reacted, and the concentrations of the reactants in the mixed solutions are given in table 2-1. Two types of crystals, (I) clear and colorless particles with planar faces and (II) white spheroidal clusters, were obtained. The former, type I, came from solutions containing $H_2O_2$ in initial concentrations of 5.0 or 7.5 M. The latter, type II, were obtained from solutions containing $H_2O_2$ in initial concentrations of 10 M. Subsequent chemical analysis of the two types of crystals showed that type I were single crystals of $CaO_2 \cdot 8H_2O$ while type II had the same chemical composition of $CaO_2 \cdot 2H_2O_2$. The best conditions determined so far for obtaining macrocrystalline $CaO_2 \cdot 2H_2O_2$ are those listed in table 2-1 as combination No. 9.

Examination of the macrocrystals of $CaO_2 \cdot 2H_2O_2$ under a light microscope revealed that the clusters of spheroids had an apparent primary structure which consisted of tightly packed needles radiating out of the center of each spheroid. The crystals were not easily crushed, unlike the soft, fragile agglomerate particles of microcrystalline $CaO_2 \cdot 2H_2O_2$. It is not known for certain whether the type II crystals are either of the two crystal modifications reported by Vannerberg since no single crystal x-ray work was performed in this study. Further preparative work in conjunction with x-ray crystallography would be required to determine whether two crystal modifications do indeed exist.

### 2.2.4 Disproportionation of Macrocrystalline $CaO_2 \cdot 2H_2O_2$

A 16-g batch of the macrocrystalline $CaO_2 \cdot 2H_2O_2$ was prepared and had a chemical composition corresponding to 91% $CaO_2 \cdot 2H_2O_2$, 6.1% $CaO_2$, 2.1% calcium carbonate ($CaCO_3$), and 0.8% $H_2O$ (see Sec. 2.3.1.2 on pyrolytic analysis for further details on the analytical method). To obtain particles of a

Table 2-1.- Reactant Concentrations for Growing Macrocrystals of $CaO_2 \cdot 2H_2O_2$ at -10°C

| Combination No. | Reactant concentrations, M | | | Type of crystal obtained [1] |
|---|---|---|---|---|
| | $H_2O_2$ | $NH_3$ | $CaCl_2$ | |
| 1 | 5.0 | 1.5 | 0.10 | I |
| 2 | 5.0 | 1.5 | 0.25 | I |
| 3 | 7.5 | 1.5 | 0.10 | I |
| 4 | 7.5 | 1.5 | 0.25 | I |
| 5 | 10.0 | 0.25 | 0.25 | II |
| 6 | 10.0 | 0.50 | 0.25 | II |
| 7 | 10.0 | 1.0 | 0.25 | II |
| 8 | 10.0 | 1.5 | 0.25 | II |
| 9 | 10.0 | 1.5 | 0.50 | II |
| 10 | 10.0 | 2.0 | 0.25 | II |

[1] Type I crystals were clear and colorless with planar faces, Type II crystals were white clusters of spheroids.

smaller and more uniform size distribution, the crystals were ground in a dry-nitrogen-purged glass tube immersed in a -10°C cold bath. The particles were then sieved at 4°C in a cold room and the various sieve fractions were stored at -60°C until use.

Figure 2-6 is a schematic diagram of the vacuum system used to carry out the disproportionation of macrocrystalline $CaO_2 \cdot 2H_2O_2$. The glass-cross reaction chamber, which had been used previously to study the disproportionation of microcrystalline $CaO_2 \cdot 2H_2O_2$ (figure 2-3), had been modified to permit disproportionation of $CaO_2 \cdot 2H_2O_2$ with high-velocity inert gas flows through the reactant layer at low pressures (<10 mtorr). Figure 2-7 is a closeup of the reaction chamber and shows a cut away view of the sample dish. Once the sample was transferred to the chamber, the reactor was evacuated and a flow of helium was directed up through the $CaO_2 \cdot 2H_2O_2$ layer. Helium rather than nitrogen was used as the sweep gas because the diffusion pump had a higher pumping speed for helium and higher gas flows could be used while still keeping the pressure low (<10 mtorr).

Four samples of macrocrystalline $CaO_2 \cdot 2H_2O_2$ were disproportionated. A summary of the reaction conditions under which each of the experiments was carried out is given in table 2-2.

Table 2-3 lists the product analysis for the four samples of $CaO_2 \cdot 2H_2O_2$ which were disproportionated. The peroxide content in the disproportionation products could be viewed as coming from $CaO_2$, $CaO_2 \cdot 2H_2O_2$, or both, since in the case of three of the samples, the disproportionation reaction was not complete at the end of the allotted reaction time. Therefore, the analytical results for peroxide content are listed in three columns: % peroxide oxygen [% $O_2(p)$], % $CaO_2$, and % $CaO_2 \cdot 2H_2O_2$.

As had been the case with the disproportionation of microcrystalline $CaO_2 \cdot 2H_2O_2$, a gradual color change in the samples from white to yellow was observed during disproportionation. Since the evolved $O_2$ and $H_2O$ from the sample made a very small contribution to the total pressure, changes in pressure could not be used to determine the endpoint of the disproportionation reaction. For sample No. 4, the exhaust stream from the vacuum system was monitored for $O_2$ using an oxygen analyzer.

Sample No. 1 was yellow immediately after removal from the vacuum chamber. However, by the time it had been transferred into the glove box 10 min later, it was light tan. A small portion of the material was removed for analysis while the remainder was stored in a small bottle. Five minutes later, the cap was jettisoned from the bottle and condensate

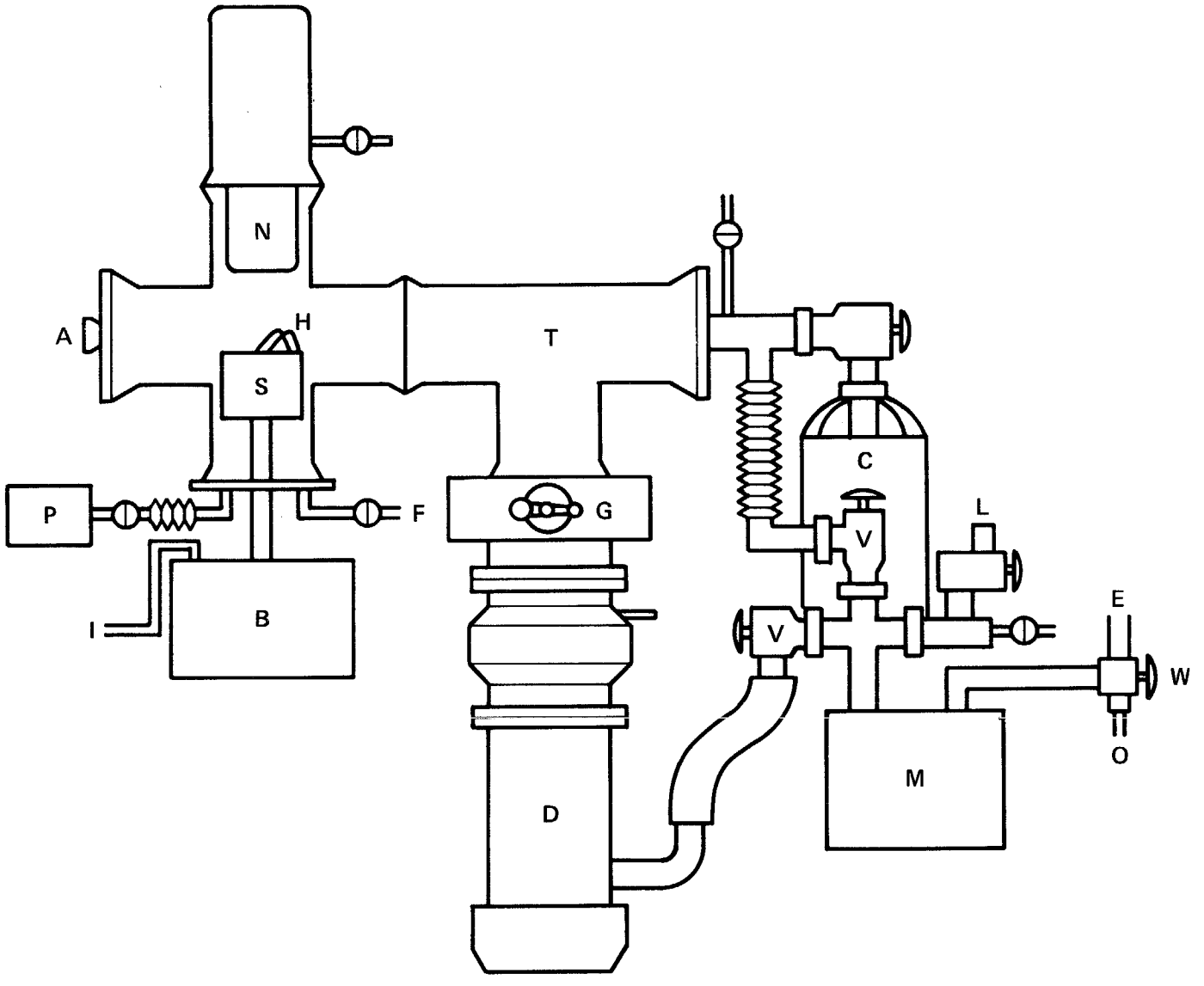


Figure 2-6.- Reaction chamber and auxiliary equipment for disproportionation of macrocrystalline $CaO_2 \cdot 2H_2O_2$. A - sample-loading port, B - constant-temperature bath, C - cryosorption pump, D - 6" diffusion pump, E - exhaust vent for rotary oil-sealed roughing pump, F - $N_2$ backfill port, G - diffusion-pump gate valve, H - copper-constantan thermocouples, I - helium inlet, L - leak test port, M - rotary oil-sealed roughing pump, N - $LN_2$ cold finger, O - pump exhaust vent to $O_2$ analyzer, P - capacitance manometer pressure gauge, S - sample platform, T - glass pipe "T", V - 1.75" high vacuum valves, W - 3-way valves.

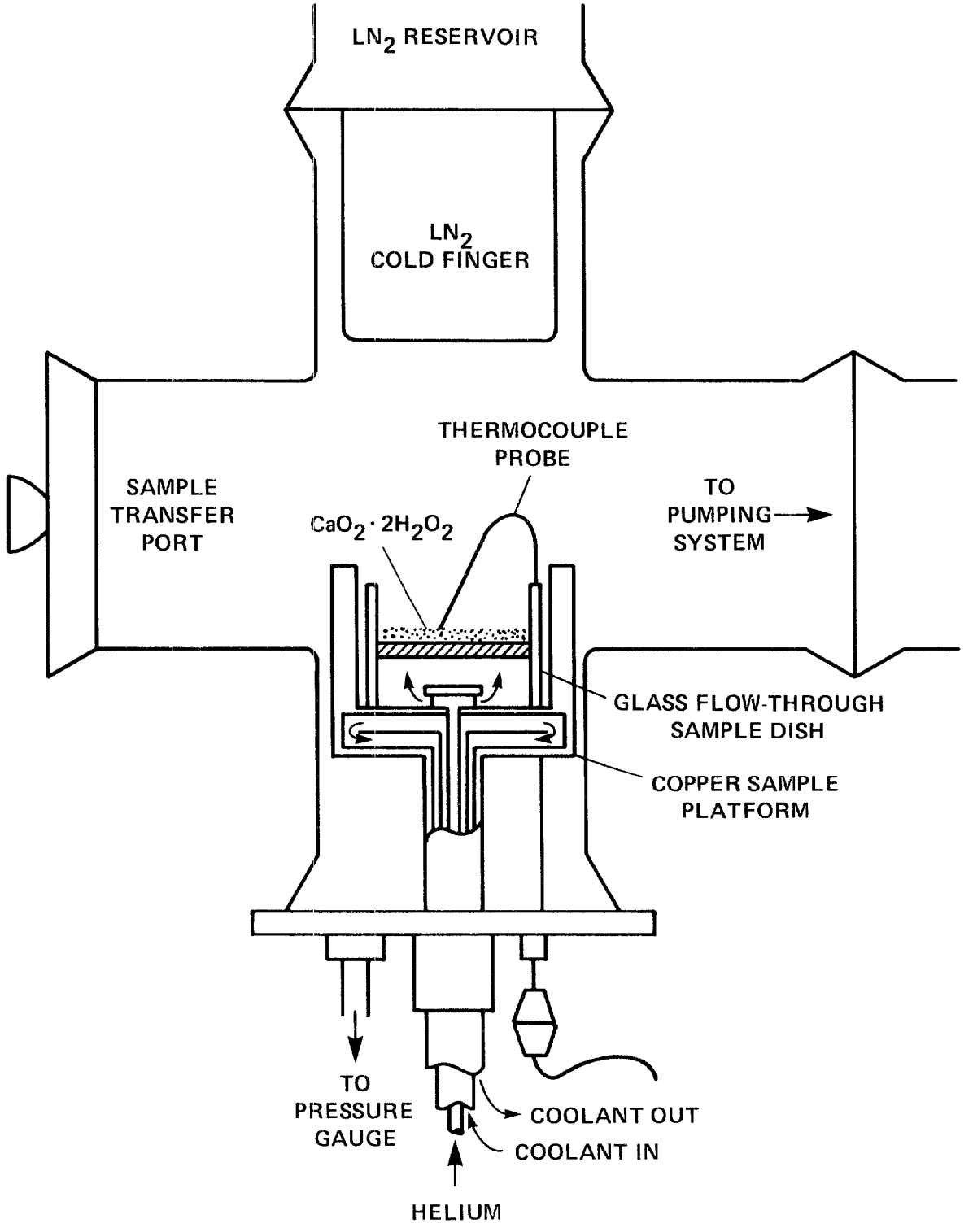


Figure 2-7.- Reaction chamber for disproportionation of macrocrystalline $CaO_2 \cdot 2H_2O_2$. Detail of sample dish and sample platform.

Table 2-2.- Disproportionation of Macrocrystalline $CaO_2 \cdot 2H_2O_2$ -- Sample and Disproportionation Reaction Parameters

| Sample No. | Sample wt., g | Particle size, mm | Sample spreading[1] area, $cm^2/g$ | Reaction temp., °C | He flow[2] rate, SCCM | Chamber pressure, mtorr | Reaction time, h |
|---|---|---|---|---|---|---|---|
| 1 | 1.16 | 0.45-0.86 | 38.1 | 13-22 | 90-95 | 9-10 | 7.0 |
| 2 | 1.16 | 0.45-0.86 | 38.1 | 17-30 | 90-95 | 9-10 | 7.5 |
| 3 | 1.30 | 0.28-0.45 | 34.0 | 15-26 | 90-95 | 9-10 | 10.5 |
| 4 | 1.05 | 0.14-0.23 | 42.1 | 16-20 | 90-95 | 9-10 | 25.3 |

[1] Based on a sample dish frit area of 44.2 $cm^2$.
[2] Linear velocity through sample layer = 2770-3250 cm/s at chamber pressures of 9-10 mtorr and 44.2 $cm^2$ sample area. SCCM = standard centimeters cubed per min at 20°C and 760 mm Hg.

Table 2-3.- Disproportionation of Macrocrystalline $CaO_2 \cdot 2H_2O_2$ -- Superoxide and Peroxide Analysis Results

| Sample No. | % $Ca(O_2)_2$ | Peroxide content[1] | | |
|---|---|---|---|---|
| | | as % $O_2(p)$ | as % $CaO_2$ | as % $CaO_2 \cdot 2H_2O_2$ |
| 1 | 0.99 | 28.6 | 129.0 | 83.5 |
| 2 | 21.8 | 13.4 | 60.4 | 39.1 |
| 3 | 30.8 | 9.3 | 42.0 | 27.2 |
| 4 | 34.3 | 8.1 | 36.4 | 23.6 |

[1] % $O_2(p)$ = peroxide oxygen content = available molecular $O_2$ which is released from the decomposition of $CaO_2$ and/or $H_2O_2$ constituents.

was observed on the inside of the bottle and on the sample. It was postulated that the disproportionation reaction was not complete after the 7-h reaction period at 20°C, and that the observed yellow color characteristic of superoxide was the result of the reaction of only the outside layers of the crystals.

For sample No. 2, the temperature of the sample was increased by increments up to 30°C during the reaction period until the sample began to exhibit apparent vigorous, uncontrolled reaction behavior, in which individual particles split apart. At this point the temperature of the sample platform was lowered until the sample dish surface was at 20°C and then this temperature was maintained for the remaining 4 h of the experiment. The yellow color of the material again faded to a light tan during transfer to the glove box.

Sample No. 3 was reacted at a slightly lower temperature of 26°C, but some sporadic vigorous reaction behavior was again observed. After 10.5 h of reaction only a slight fading of the yellow color of the product was observed during the 10-min period when the sample was transferred to the glove box.

Sample No. 4 was reacted for 25.3 h at 20°C. At the end of this period, the $O_2$ level in the pumped gas was 50 ppm (i.e., background level) and the rate of pressure rise was the same as for the empty chamber. Although the sample was yellow, the 34% $Ca(O_2)_2$ in the product was one-half the purity obtained when microcrystalline $CaO_2 \cdot 2H_2O_2$ was disproportionated under the same temperature conditions. It is postulated that the surface area of the macrocrystalline reactant is much less than that of the microcrystalline material. The less porous and more dense crystalline material may not permit evolution of product $H_2O$ from the crystalline particle interior without considerable back reaction with already-formed $Ca(O_2)_2$.

The results of the limited study of the disproportionation of macrocrystalline $CaO_2 \cdot 2H_2O_2$ indicate that this material was more thermally stable than microcrystalline $CaO_2 \cdot 2H_2O_2$ since complete disproportionation of the macrocrystalline $CaO_2 \cdot 2H_2O_2$ at 20°C required up to 25 h compared to the 3 h for the microcrystalline material. The lower-purity $Ca(O_2)_2$ obtained from the disproportionation of macrocrystalline $CaO_2 \cdot 2H_2O_2$ may be the result of the lower surface area, lower porosity, and higher density of this material compared to the microcrystalline $CaO_2 \cdot 2H_2O_2$. These factors inhibit the efficiency of product $H_2O$ removal from within the crystal. At the present time, it appears that disproportionation of the macrocrystalline $CaO_2 \cdot 2H_2O_2$ cannot be used to produce high-purity $Ca(O_2)_2$.

## 2.3 Characterization of $Ca(O_2)_2$ Synthesis Reactant and Product Materials

A variety of methods and techniques were used to characterize the $Ca(O_2)_2$ which was obtained from the synthetic processes described above. Classical wet-chemical methods of analysis were used to determine the chemical composition of $Ca(O_2)_2$ samples as well as the chemical compositions of the reactants used in the sythesis process. To provide a check on the wet chemical analysis, a pyrolytic analysis technique was later developed. The stability of $Ca(O_2)_2$ during storage was studied and differential scanning calorimetry (DSC) and thermogravimetric analysis (TGA) methods were used to determine the thermal stability of the material. Finally, x-ray powder crystallography was employed to determine what crystal structure, if any, the $Ca(O_2)_2$ exhibited.

### 2.3.1 Chemical Analysis Methods

#### 2.3.1.1 Classical, Wet-Chemical Analysis Methods

Perhaps the most widely used method for evaluating the purity of superoxide materials is that developed by Seyb and Kleinberg (35) in which the superoxide oxygen (i.e., the oxygen released as a result of the rupture of the $O_2$- bond thermally or through hydrolysis) of the material was measured volumetrically after release by reaction of a sample at 0°C with a mixture of acetic acid/diethyl phthalate. The peroxide content was determined by subtracting the volume of superoxide oxygen from the total $O_2$ content which was measured volumetrically after reaction of another sample with a hydrochloric acid/iron chloride catalyst solution. Figure 2-8 is a sketch of the apparatus. The method of Seyb and Kleinberg was employed initially during the work described here until it was determined that anomalously high $Ca(O_2)_2$ purities were being obtained using this method. These anomalies which are described in more detail in reference (3), resulted in an indicated superoxide content that was up to 4% too high because of the apparent decomposition of intermediate reaction products. Another weakness in the the method of Seyb and Kleinberg is that if a significant quantity of carbonate contamination is present in the sample to be analyzed, the $CO_2$ released by the carbonate upon reaction with acetic acid further increases the error in the superoxide and peroxide analyses. In the case of the samples described in reference (3), the $CO_2$ concentration in the $O_2$ released during decomposition with acetic acid was ~0.4%

Therefore, an alternate analytical method was developed in which the superoxide oxygen was released by reaction of the sample at 0°C with distilled $H_2O$ and then the peroxide content was determined by titrating the residue with potas-

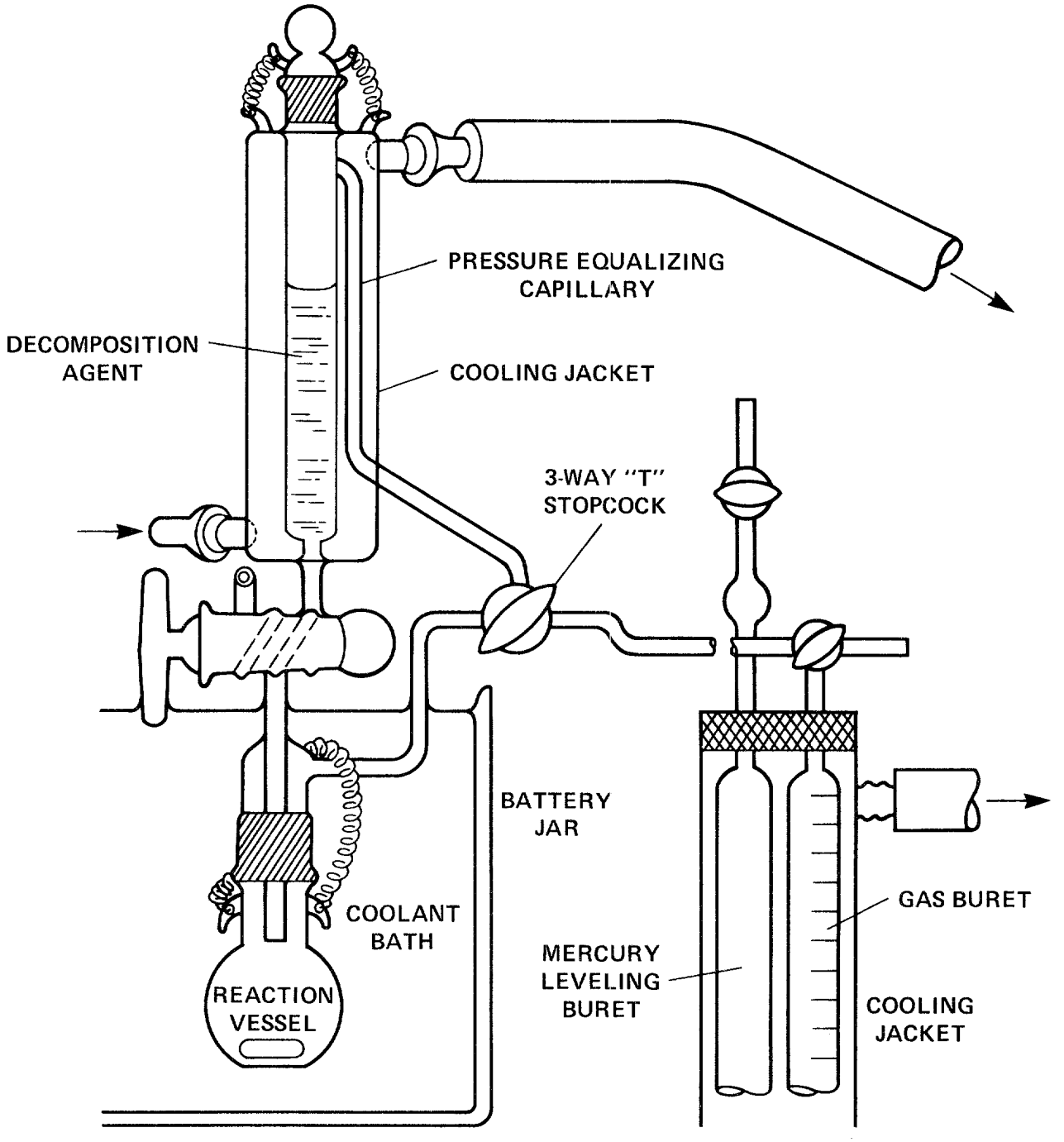


Figure 2-8.- Apparatus for the analysis of superoxides by measurement of $O_2$ released through wet chemical decomposition.

sium permanganate ($KMnO_4$) after it had been acidified with 3F phosphoric acid ($H_3PO_4$) (3). Since the residue remains alkaline during the release of the superoxide oxygen, the $H_2O$ decomposition/superoxide analysis method could potentially be applied to samples that contain a significant amount of $CaCO_3$ without any error resulting from the release of $CO_2$.

Analysis of the components used in the sythesis of $Ca(O_2)_2$, i.e., $CaO_2 \cdot 8H_2O$, $CaO_2 \cdot 2H_2O_2$ and $H_2O_2$, was accomplished recently at the NASA Ames Research Center using two steps: 1) titrating for peroxide content in one aliquot using potassium permanganate (34) and 2) determining the calcium content (in $CaO_2 \cdot 8H_2O$ and $CaO_2 \cdot 2H_2O_2$) in another aliquot by an EDTA titration (36) after destroying the peroxide though boiling the aliquot. the samples of $CaO_2 \cdot 8H_2O$ or $CaO_2 \cdot 2H_2O_2$ were dissolved in 1F nitric acid ($HNO_3$) or $H_3PO_4$, and samples of $H_2O_2$ were acidified with 1F sulfuric acid ($H2SO_4$).

2.3.1.2 Pyrolytic Analysis Method

BACKGROUND - There was a need to confirm the results of the wet chemical analysis of $Ca(O_2)_2$ and to determine the complete chemical composition of $Ca(O_2)_2$, $CaO_2 \cdot 2H_2O_2$, and $Ca(O_2)_2$/humidfied $CO_2$ products. Since it was not possible to determine directly the amount of $CaCO_3$ or $Ca(OH)_2$ by using only the wet chemical techniques described previously, the pyrolytic analysis technique originally described by Johnston, Osgood and Miller (14) was developed further for use in the complete analysis of each of the above compounds.

PROCEDURE - The pyrolytic analysis method involved the thermal decomposition of the samples in a dry nitrogen gas stream in a stepwise manner at two temperatures, 110 and 500°C. After the sample had been heated, the weight loss of the sample, and the weight of evolved moisture collected in an absorption tube were measured. The calcium content of the final residue was determined via an EDTA titration (36). The amount of $O_2$ evolved after heating the sample to a given temperature was determined by subtracting the weight of moisture on the absorption tube from the weight loss of the sample tube. As a check, the amount of $O_2$ (if any) evolved by the sample was also determined by measuring and integrating the $O_2$ present in the nitrogen gas purge stream using an oxygen analyzer and a computerized data acquisition system (see Sec 4.2.2). Figure 2-9 is a schematic diagram of the pyrolytic analysis apparatus.

To carry out a pyrolytic analysis, about 1 g of sample was placed on a quartz frit inside a tared quartz tube and the tube was reweighed. When superoxide samples were being loaded, the operations were carried out in a glove box. For

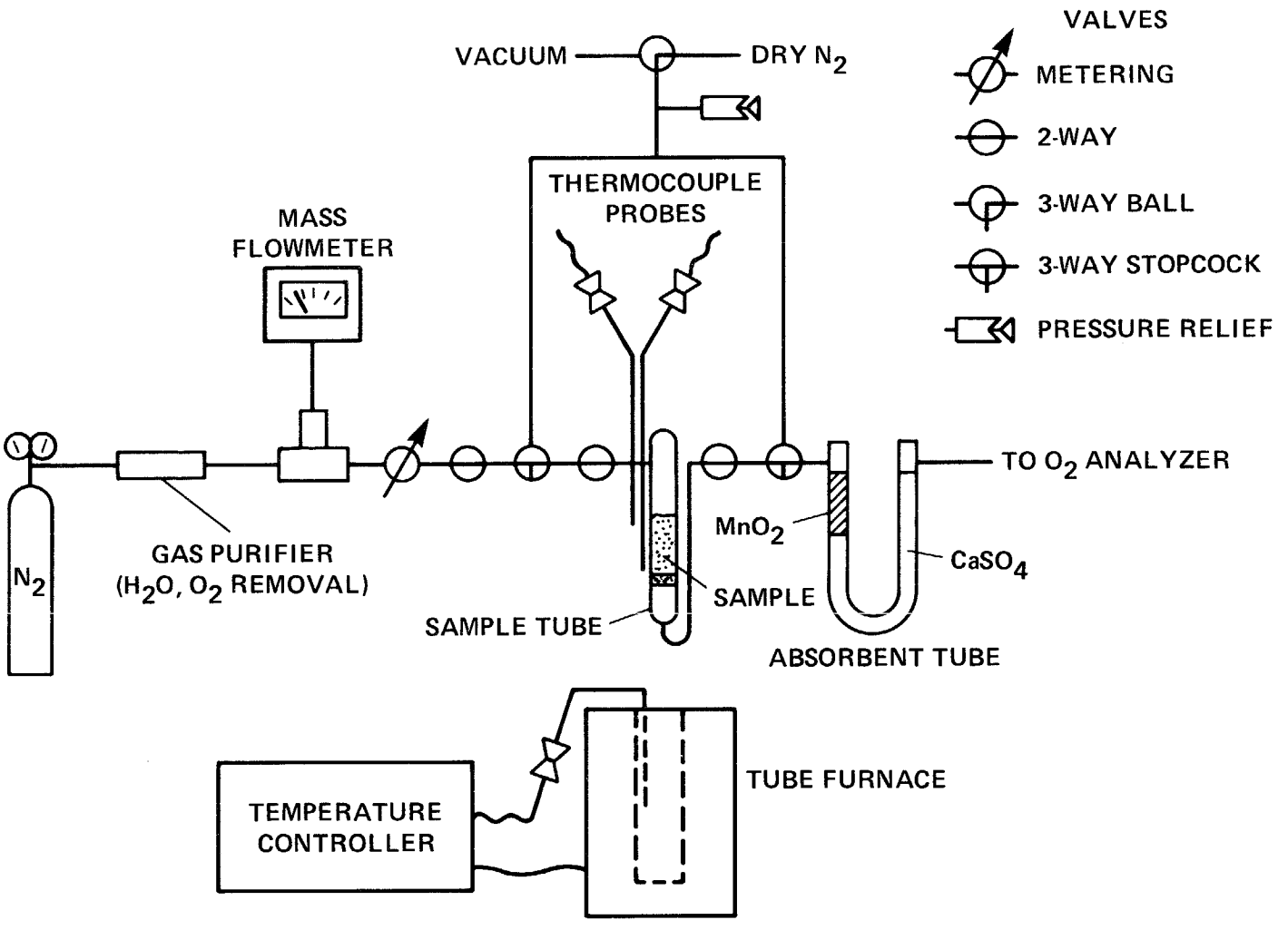


Figure 2-9.- Pyrolytic analysis apparatus.

samples of $CaO_2 \cdot 2H_2O_2$ or $Ca(O_2)_2$/humidified $CO_2$ reaction products, a nitrogen purged glove bag was used to prevent atmospheric contamination during loading of the sample. Room air between the sample and absorbent tubes was purged out by evacuation and backfilling with nitrogen. Then a 100-SCCM [standard (20°C, 1 atm) cubic centimeters per min] flow of dry nitrogen was passed through the tubes until a background level of $O_2$ was measured. Next, the furnace was placed around the sample until the weights of the sample and absorbent tubes had reached constant weight. The sample tube was heated at a given temperature until the $O_2$ level had returned to background levels and/or the condensation of moisture in the glass connecting lines had been swept into the absorption tube. It was determined experimentally that about 2 h at each temperature were required for the sample and drying tube weights to become constant.

CALCULATION OF COMPOSITION - Calcium superoxide obtained from the disproportionation of $CaO_2 \cdot 2H_2O_2$ contains $Ca(O_2)_2$, $CaO_2$, $Ca(OH)_2$, and traces of $CaCO_3$. When this superoxide-containing material is reacted with humidified $CO_2$ (as described in Sec. 4.3), the moist residue contains $CaCO_3$ as well as unreacted $Ca(O_2)_2$, $Ca(OH)_2$, and $CaO_2$. Any adsorbed $H_2O$ or water of hydration is removed from the sample by heating to 110°C. The carbonate component of the sample (if any) remains as part of the pyrolysis residue since the decomposition of $CaCO_3$ at 500°C is negligible. Therefore, excluding hydration products, there are only three components which undergo decomposition reaction upon heating samples of $Ca(O_2)_2$ or $Ca(O_2)_2$/humidified $CO_2$ reaction products to 500°C: $Ca(O_2)_2$, $CaO_2$, and $Ca(OH)_2$. The net thermal decomposition reactions are as follows:

$$Ca(O_2)_2 = CaO + 3/2O_2 \qquad (2.10)$$

$$CaO_2 = CaO + 1/2O_2 \qquad (2.11)$$

$$Ca(OH)_2 = CaO + H_2O \qquad (2.12)$$

$CaO_2 \cdot 2H_2O_2$ may also contain traces of $CaCO_3$. However, the net decomposition reaction upon heating this material to 500°C is

$$CaO_2 \cdot 2H_2O_2 = CaO + 3/2O_2 + 2H_2O \qquad (2.13)$$

Calculation of the composition of the sample was made in two steps based on the known decomposition reactions of the components. First, the composition of the sample after heating to 110°C was calculated. Then, the composition of the original sample (before heating it to 110°C) was calculated based on the composition of the sample after it had been heated to 110°C by using the original sample weight and the weight changes of the sample and absorbent tubes which

were observed when the sample was heated to 110°C.

The components remaining after heating to 110°C were assumed to consist of only one or more of the following: $Ca(O_2)_2$, $CaO_2$, $Ca(OH)_2$, and $CaCO_3$. The weight of $Ca(OH)_2$ in the sample after heating to 110°C was determined from the weight of $H_2O$ collected on the absorption tube while heating from 110 to 500°C; i.e.,

$$\text{wt. of } Ca(OH)_2 = (\text{wt. of } H_2O) \times \frac{(\text{F.W. } Ca(OH)_2)}{(\text{F.W. } H_2O)} \qquad (2.14)$$

Since the residue remaining after heating to 500°C contained only $CaCO_3$ and calcium oxide (CaO), the weight of the sample was calculated as

$$\text{wt. of sample[500°C]} = \text{wt. of } CaCO_3 + \text{wt. of CaO} \qquad (2.15)$$

and

$$\text{wt. of Ca} = (\%\text{Ca in } CaCO_3) \times (\text{wt of } CaCO_3) + (\%\text{Ca in CaO}) \times (\text{wt. of CaO}) \qquad (2.16)$$

The weight of $CaCO_3$ in the sample could be determined by combining equations (2.15) and (2.16),

$$\text{wt. of } CaCO_3 = \frac{(\%\text{Ca in } CaCO_3) \times (\text{wt. of sample[500°C]}) - \text{wt. of Ca}}{(\%\text{Ca in } CaCO_3 - \%\text{Ca in CaO})} \qquad (2.17)$$

Therefore, since

$$\text{wt. of sample[110°C]} = \text{wt. of } CaO_2 + \text{wt. of } Ca(O_2)_2 + \text{wt. of } Ca(OH)_2 + \text{wt. of } CaCO_3 \qquad (2.18)$$

and since there were only two $O_2$-releasing components, $Ca(O_2)_2$ and $CaO_2$,

$$\text{wt. of } O_2 = (\%O_2 \text{ in } Ca(O_2)_2) \times (\text{wt. of } Ca(O_2)_2) + (\%O_2 \text{ in } CaO_2) \times (\text{wt. of } CaO_2) \qquad (2.19)$$

the weight of $Ca(O_2)_2$ in the sample could be determined by combining equations (2.18) and (2.19)

$$\text{wt. of } Ca(O_2)_2 =$$

$$\frac{\text{wt. of } O_2 - (\%O_2 \text{ in } CaO_2) \times (\text{wt. of sample}[110^oC])}{(\%O_2 \text{ in } Ca(O_2)_2 - \%O_2 \text{ in } CaO_2)} - \frac{\text{wt. of } CaCO_3 - \text{wt. of } Ca(OH)_2}{(\%O_2 \text{ in } Ca(O_2)_2 - \%O_2 \text{ in } CaO_2)} \quad (2.20)$$

Finally, the weight of $CaO_2$ was determined by difference,

$$\text{wt. of } CaO_2 = \text{wt. of sample}[110^oC] - \text{wt. of } Ca(O_2)_2 - \text{wt. of } Ca(OH)_2 - \text{wt. of } CaCO_3 \quad (2.21)$$

RESULTS AND DISCUSSION - The method used for calculating the composition of the sample prior to heating to 110°C depended on the type of sample being analyzed. In the discussion below, each of the types of samples analyzed will be illustrated with example analyses and the calculation of the original composition of each sample type will be outlined based on the composition determined after heating to 110°C.

Analysis of $CaO_2 \cdot 2H_2O_2$ Disproportionation Products - Upon heating $CaO_2 \cdot 2H_2O_2$ disproportionation products to 110°C, there sometimes was a slight loss in the sample weight but no weight gain on the absorbent tube. Therefore, when a decrease in sample weight was observed this indicated that only $O_2$ was being lost from the sample. Therefore, in calculating the original composition of the samples before heating, it was assumed that the $O_2$ that had evolved during heating to 110°C was a result of the decomposition of $Ca(O_2)_2$ into $CaO_2$ and $O_2$;

$$Ca(O_2)_2 = CaO_2 + O_2 \quad (2.22)$$

The amount of $Ca(O_2)_2$ determined to be in the sample after heating to 110°C was therefore increased by an amount equivalent to the amount of $O_2$ lost upon heating to 110°C whereas the amount of $CaO_2$ was correspondingly decreased.

Table 2-4 gives the chemical composition of two different $CaO_2 \cdot 2H_2O_2$ disproportionation product materials before and after heating to 110°C and compares it with the composition of the sample as determined by the wet chemical analysis technique described above in Sec. 2.3.1.1. The values for the superoxide content as determined by the two analytical techniques agree to within 0.2-0.4%, but the peroxide content as determined by the pyrolytic analysis is consistently ~3% higher than for the wet chemical analysis.

Additional work on the pyrolytic analysis of $CaO_2 \cdot 2H_2O_2$

Table 2-4.- Pyrolytic Analysis of $CaO_2 \cdot 2H_2O_2$ Disproportionation Products

| Component | Composition, wt. % | | | |
|---|---|---|---|---|
| | $Ca(OH)_2$ | $CaCO_3$ | $Ca(O_2)_2$ | $CaO_2$ |
| Treatment of sample | | | | |
| Sample No. 1 | | | | |
| Wet chemical analysis[1] | ND | ND | 40.12 | 23.41 |
| Pyrolytic analysis | | | | |
| at 25°C | 30.41 | 2.93 | 39.70 | 26.96 |
| after heating to 110°C | 30.41 | 2.93 | 39.70 | 26.96 |
| Sample No. 2 | | | | |
| Wet chemical analysis[1] | ND | ND | 58.60 | 12.21 |
| Pyrolytic analysis | | | | |
| at 25°C | 26.06 | 0.48 | 58.42 | 15.03 |
| after heating to 110°C | 26.89 | 0.50 | 50.01 | 22.60 |

[1] Superoxide was determined by decomposition with liquid $H_2O$ at 0°C and peroxide was determined by $KMnO_4$ titration of residue (Sec. 2.3.1.1). ND = not determined.

disproportionation products will be necessary to determine the cause of the discrepancy between the two analytical methods with regard to the peroxide content of the samples.

Analysis of $Ca(O_2)_2$/Humidified $CO_2$ Reaction Products- The flow-system test residues obtained when $CaO_2 \cdot 2H_2O_2$ disproportionation products containing $Ca(O_2)_2$ were reacted with humidified $CO_2$ contained a significant amount of adsorbed $H_2O$ and water of hydration (Sec. 4.3.1). The pyrolytic analysis of the flow-system residues provided a method for determining the moisture content as well as the complete chemical composition of the solid material.

Upon heating the flow-system test residues to 110°C, $H_2O$ and a small amount of $O_2$ were released from the sample tube. The $O_2$ that was released was assumed to have come from the reaction of residual $Ca(O_2)_2$ with the warm water vapor that was evolved during the heating to 110°C. A study of the reaction of $Ca(O_2)_2$ with humidified $CO_2$ revealed that at reaction temperatures of 25-50°C, the major reaction product of the $Ca(O_2)_2/H_2O$ reaction was $Ca(OH)_2$ (Sec. 4.3.1). Therefore, it was assumed here that the $O_2$ that was released upon heating the flow test residue to 110°C resulted from the reaction

$$Ca(O_2)_2 + H_2O = Ca(OH)_2 + 3/2O_2 \qquad (2.23)$$

In the calculation of the composition of the sample prior to heating to 110°C, the amount of $O_2$ released upon heating to 110°C was converted [using the stoichiometry of equation (2.23)] to $Ca(O_2)_2$ and the amount of $Ca(OH)_2$ was correspondingly reduced. Table 2-5 gives the chemical composition of two different samples of $Ca(O_2)_2$/humidified $CO_2$ reaction products before and after heating to 110°C.

Analysis of $CaO_2 \cdot 2H_2O_2$- A pyrolytic analysis of $CaO_2 \cdot 2H_2O_2$ was desireable to determine the extent of carbonate contamination which was acquired during the sythesis process as well as the amount of free $H_2O$ that the material contained after drying. Two different samples of $CaO_2 \cdot 2H_2O_2$ were analyzed. The first sample was a macrocrystalline sample prepared according to the method given in Sec. 2.2.3. Since this was a new material it was important to determine the complete chemical composition of the crystals. The second sample consisted of a preparation of microcrystalline $CaO_2 \cdot 2H_2O_2$ which had been prepared by freeze-drying a slurry of $CaO_2 \cdot 8H_2O$ and $H_2O_2$ according the method given in Sec. 2.2.1.2, except that the liquid phase of the slurry was not decanted off before the freeze-drying process. Thus all the liquid phase was removed from the solid by evaporation. Since this was one of the early samples prepared by this method, it was necessary to determine whether the excess $H_2O$ and $H_2O_2$ had been completely removed in the freeze drying

Table 2-5.- Pyrolytic Analysis of $Ca(O_2)_2$/Humidified $CO_2$ Reaction Products

| Component | Composition, wt. % | | | | |
|---|---|---|---|---|---|
| | $Ca(OH)_2$ | $CaCO_3$ | $Ca(O_2)_2$ | $CaO_2$ | $H_2O$ |
| Treatment of sample | | | | | |
| Sample No. 1 | | | | | |
| at 25°C | 51.18 | 20.28 | 5.47 | 16.42 | 5.90 |
| after heating to 110°C | 55.28 | 21.48 | 4.29 | 18.95 | 0 |
| Sample No. 2 | | | | | |
| at 25°C | 36.84 | 24.47 | 6.87 | 22.03 | 9.80 |
| after heating to 110°C | 41.10 | 27.15 | 7.31 | 24.44 | 0 |

process.

Both types of $CaO_2 \cdot 2H_2O_2$ samples exhibited similar behavior when they were heated to 110°C. A large amount of $O_2$ and moisture were evolved from the samples when the temperature of the sample tube reached about 50°C. Table 2-6 gives the chemical compositions of the two samples after heating to constant sample weight at 110°C. Both materials yield a compound that has a chemical composition corresponding to that of high purity (90+%) $CaO_2$.

The approach used to determine the chemical composition of the $CaO_2 \cdot 2H_2O_2$ samples was different than that used to determine the composition of the other materials discussed above. Since extensive amounts of $O_2$ and $H_2O$ were evolved from the sample, the chemical composition after heating the sample to 110°C had little relation to that existing before heating. The presence of $Ca(O_2)_2$ in the sample after heating indicated that during the thermal decomposition process at least some disproportionation of the $CaO_2 \cdot 2H_2O_2$ had taken place. Therefore, rather than calculating back from the chemical composition values obtained after heating the sample to 110°C, the chemical composition was determined using the total amounts of $O_2$ and $H_2O$ evolved by the sample and the total calcium content.

The chemical composition of the samples prior to heating to 110°C can be expressed in several ways. Without making any assumptions about the association of the fundamental components of the material (those species which appear in the net pyrolysis reaction [i.e., CaO, $O_2$, and $H_2O$, eq. (2.13),], the chemical composition can be expressed as in table 2-7 and an assessment of the composition can be made by comparing it to the theoretical composition.

The values for the $O_2$ content of the two samples given in table 2-7 were checked by titrating another portion of each sample for peroxide with $KMnO_4$. The $O_2$ values obtained from the titrated samples were 32.91% and 37.74%, respectively, for the macrocrystalline and microcrystalline $CaO_2 \cdot 2H_2O_2$ samples. Thus, the two different analytical methods yield results which agree to within 0.2-0.5% for the peroxide-oxygen content of the sample. It is apparent from table 2-7 that the composition of the macrocrystalline material was closer to the theoretical values than the microcrystalline material.

By making some assumptions about the association of the components (i.e., CaO, $O_2$ and $H_2O$), it was possible to get a more informative picture of the chemical composition of the materials. The following assumptions were made:

(a) All of the calcium not tied up as $CaCO_3$ was present in $CaO_2$

Table 2-6.- Pyrolytic Analysis of $CaO_2 \cdot 2H_2O_2$ Thermal Decomposition Products

| Component | Composition, wt. % | | | |
|---|---|---|---|---|
| | $Ca(OH)_2$ | $CaCO_3$ | $Ca(O_2)_2$ | $CaO_2$ |
| Sample Type Thermally Decomposed at 110°C: | | | | |
| Macrocrystalline $CaO_2 \cdot 2H_2O_2$ | 0.96 | 3.69 | 5.57 | 89.78 |
| Microcrystalline $CaO_2 \cdot 2H_2O_2$ | 0.10 | 0.94 | 2.04 | 96.92 |

Table 2-7.- Pyrolytic Analysis of $CaO_2 \cdot 2H_2O_2$ -- Comparison of Theoretical and Experimental Compositions

| Sample Type | Chemical Composition, wt. % | | |
|---|---|---|---|
| | Experimental | | |
| | Macrocrystalline $CaO_2 \cdot 2H_2O_2$ | Microcrystalline $CaO_2 \cdot 2H_2O_2$ | Theoretical |
| Component | | | |
| CaO | 41.21 | 24.07 | 40.03 |
| $O_2$ | 32.54 | 37.97 | 34.26 |
| $H_2O$ | 24.18 | 37.89 | 25.72 |
| $CaCO_3$ | 2.06 | 0.30 | 0.0 |
| Mole ratio ($CaO:O_2:H_2O$) | 1 : 1.35 : 1.78 | 1 : 2.74 : 4.85 | 1 : 1.50 : 2.00 |

(b) The $O_2$ that was released came only from $CaO_2$ and $H_2O_2$. That is, the amount of $O_2$ tied up in the $CaO_2$ could be subtracted from the total amount released during the pyrolysis to determine the amount of $O_2$ present in $H_2O_2$.

(c) The $H_2O$ released from the sample came from either decomposition of $H_2O_2$ or from superficial moisture in the sample. Thus, the amount of $H_2O$ that was released from the $H_2O_2$ upon decomposition could be subtracted from the total amount of $H_2O$ released to determine the amount of moisture in the original sample.

(d) Each mole of $CaO_2$ was associated with 2 moles of $H_2O_2$. Any excess $CaO_2$ or $H_2O_2$ "left over" after determining the % of $CaO_2 \cdot 2H_2O_2$ was postulated to be an additional component in the $CaO_2 \cdot 2H_2O_2$.

Table 2-8 gives the chemical composition of the material calculated on the basis of the above assumptions. Two ways of listing the composition of the $CaO_2 \cdot 2H_2O_2$ samples are used in table 2-8. Component set No. 1 lists the composition of the samples based on assumptions (a)-(c) given above, and component set No. 2 lists the composition of the samples based on assumptions (a)-(d). In the case of the macrocrystalline material, it appeared that some decomposition of the material had occurred during the handling process (grinding and sieving), since $CaO_2$ was present as a separate component in the sample (component set No. 2, table 2-8). The $H_2O$ content in the macrocrystalline material was negligible but the carbonate contamination was significant and indicated that there may have been some dissolved $CO_2$ in the starting reagents used in the sythesis process, or some reaction with ambient $CO_2$ during the sieving process.

From the composition given in table 2-8, the microcrystalline material apparently contained a large excess of "free" (uncomplexed) $H_2O_2$ and a significant proportion of superficially bound moisture (component set No. 2). As a result of the information gained through the pyrolytic analysis, the method for drying $CaO_2 \cdot 2H_2O_2$ was changed as follows. The bulk of the $H_2O_2/H_2O$ liquid phase was decanted away from the solid phase before freeze-drying, and the freeze-drying time was lengthened.

### 2.3.2 Storage Stabilty Studies

During a parametric study in which the purity of $Ca(O_2)_2$ obtained from the disproportionation of $CaO_2 \cdot 2H_2O_2$ at 30°C was followed as a function of disproportionation time, it was observed that the purity of $Ca(O_2)_2$ reached a maximum (~67%) after 60 min. Then the purity decreased after this point such that 58-60% $Ca(O_2)_2$ was obtained after 240 min [see ref. (18)]. It was postulated that either a) $Ca(O_2)_2$ was unstable under a high-vacuum environment or b) residual $CaO_2 \cdot 2H_2O_2$ in the interior of the disproportion-

Table 2-8.- Pyrolytic Analysis of $CaO_2 \cdot 2H_2O_2$ -- Determination of the "Free" $H_2O_2$ and $H_2O$ Content

| Sample type | Chemical composition, wt. %: Macrocrystalline $CaO_2 \cdot 2H_2O_2$ | Chemical composition, wt. %: Microcrystalline $CaO_2 \cdot 2H_2O_2$ |
|---|---|---|
| [1] Component set No. 1 | | |
| $CaO_2$ | 52.97 | 30.93 |
| $H_2O_2$ | 44.19 | 65.89 |
| $H_2O$ | 0.77 | 2.88 |
| $CaCO_3$ | 2.06 | 0.30 |
| [1] Component set No. 2 | | |
| $CaO_2 \cdot 2H_2O_2$ | 91.01 | 60.13 |
| $CaO_2$ | 6.15 | 0.0 |
| $H_2O_2$ | 0.0 | 36.70 |
| $H_2O$ | 0.77 | 2.88 |
| $CaCO_3$ | 2.06 | 0.30 |

[1] See text for explanation of component sets.

ation product particles continued to react, releasing $H_2O$ which reacted with $Ca(O_2)_2$. The instability of $Ca(O_2)_2$ under vacuum was later ruled out since the purity of $Ca(O_2)_2$ in disproportionation products stored at atmospheric pressure also decreased. Table 2-9 illustrates the decrease in $Ca(O_2)_2$ content upon storage for three different samples. Each of the samples was analyzed immediately after sythesis and then additional portions of the sample were analyzed after various periods of storage inside a dry nitrogen-purged glove box.

Continued disproportionation of residual $CaO_2 \cdot 2H_2O_2$ within the interior of the product particles at room temperature could be used to explain the drop in $Ca(O_2)_2$ content over a period of a few hours. However, since the $Ca(O_2)_2$ content of the samples which were stored at room temperature (20-25°C) continued to decrease over a period of days, another explanation of the degradation in the superoxide purity was needed. Two possible explanations have been envisioned. For the first explanation, it was postulated that residual water of hydration present in the disproportionation product from the back reaction of $Ca(O_2)_2$ with evolved $H_2O$, i.e.,

$$Ca(O_2)_2 + nH_2O = CaO_2 \cdot nH_2O + O_2 \qquad (2.7)$$

continues to react with additional $Ca(O_2)_2$ by migrating from $CaO_2$ sites;

$$CaO_2 \cdot nH_2O = CaO_2.(n-1)H_2O + H_2O \qquad (2.24)$$

This "recycling" of $H_2O$ would continue indefinitely until a hydrate with a low vapor pressure was formed, or $H_2O$ reacted with $Ca(O_2)_2$ to form $Ca(OH)_2$

$$Ca(O_2)_2 + H_2O = Ca(OH)_2 + 3/2O_2 \qquad (2.23)$$

The second possible explanation for the degradation of $Ca(O_2)_2$ purity upon storage is tied to the fact that the $CaO_2 \cdot 2H_2O_2$ disproportionation products containing a significant percentage of $Ca(O_2)_2$ (>40%) apparently possess an amorphous solid-state structure (Sec. 2.3.4). Therefore, products containing >55% $Ca(O_2)_2$ may not be able to stablize the superoxide anions in high concentration at room temperature. Therefore, the reaction

$$Ca(O_2)_2 = CaO_2 + O_2 \qquad (2.25)$$

would continue until the remainder of the $Ca(O_2)_2$ could be stablized in an amorphous "lattice" structure. If this is the case, then it would appear that ~55% $Ca(O_2)_2$ is the highest purity material which is indefinitely stable at room temperature. Further work on the stability of $Ca(O_2)_2$

Table 2-9.- Storage Stablility of $CaO_2 \cdot 2H_2O_2$ Disproportionation Products

| Sample No. | Storage time,[1] days | Composition,[2] wt. % $Ca(O_2)_2$ | $CaO_2$ |
|---|---|---|---|
| 1 | 0 | 67.18 | 7.39 |
| | 14 | 58.29 | 14.49 |
| 2 | 0 | 62.82 | 9.81 |
| | 2 | 59.69 | 11.48 |
| | 30 | 55.35 | 14.36 |
| 3 | 0 | 58.60 | 12.21 |
| | 2 | 57.01 | 12.23 |
| | 5 | 56.01 | 13.52 |
| | 6 | 55.65 | 14.14 |

[1] Products were stored in sealed glass bottles inside a dry-nitrogen-atmosphere glove box at 20-25°C.

[2] The compositions of the products were determined using the method outlined in Sec. 2.3.1.1.

containing materials will be needed before a choice between the two explanations can be made.

### 2.3.3 Thermal Stability Studies

The thermal stability of $Ca(O_2)_2$ produced here was examined using two techniques; DSC and TGA. The goal of the DSC study was to detect thermal effects occurring at different temperatures when $Ca(O_2)_2$ is heated to ~500°C and to measure the amount of heat associated with these effects. Thermogravimetric analysis was used to determine the decomposition temperatures of the components of the calcium superoxide products, namely $Ca(O_2)_2$, $CaO_2$, and $Ca(OH)_2$, and to help interpret through weight loss changes the heat effects which were observed using the DSC.

#### 2.3.3.1 Differential Scanning Calorimetry

APPARATUS - Thermal analysis of samples containing $Ca(O_2)_2$ was made using a Perkin-Elmer Model DSC-2 [1] DSC equipped with a dry nitrogen purged glove box.

PROCEDURE - A 3.0 to 4.5-mg sample was loaded into a tared-aluminum or gold sample pan, and hermetically sealed while inside a glove box. The sealed pan was weighed to the nearest 0.001 mg and transferred into the DSC glove box where a pinhole was made in the top of the sample pan to permit decomposition gases to escape. Then the sample was loaded into the calorimeter, and after a short equilibration period, the sample temperature was increased at a constant rate and the differences in heating rates between the sample and a reference material were recorded as a function of time and temperature. After the upper limit of the temperature program had been reached, the sample was cooled to the initial temperature and the decomposed sample was rescanned over the same temperature range to obtain the baseline. Table 2-10 lists the DSC parameters for each of the samples analyzed.

RESULTS - Figure 2-10 is the DSC recorder trace for sample No. 4 and shows the three thermal-transition peaks which were observed for all the $Ca(O_2)_2$ samples analyzed. Peaks below the baseline are a result of exothermic processes whereas peaks above the baseline are a result of endothermic processes. There was an apparent change in the heat capacity of the samples following decomposition; therefore, when the baseline scan was made following the decomposition

---

[1] Reference to specific brands, equipment, or trade names in this report is made to facilitate understanding and does not imply endorsement by the Bureau of Mines.

Table 2-10.- DSC Analysis of $CaO_2 \cdot 2H_2O_2$ Disproportionation Products -- Sample and Differential Scanning Calorimeter Parameters

| Sample No. | Sample Composition | | Sample weight, mg | [1] Pan material | refence material | Temp. scan range, °C | Temp. scan rate, °C/min | Sensitivity, mcal/sec |
|---|---|---|---|---|---|---|---|---|
| | % $Ca(O_2)_2$ | % $CaO_2$ | | | | | | |
| 1 | 50.9 | 18.2 | 3.296 | Al | CaO | 45-500 | 10 | 2 |
| 2 | 50.9 | 18.2 | 3.204 | Al | CaO | 49-500 | 5 | 2 |
| 3 | 50.9 | 18.2 | 3.660 | Au | empty pan | 50-600 | 2.5 | 2 |
| 4 | 41.4 | 22.7 | 4.488 | Al | empty pan | 50-500 | 2.5 | 1 |

[1] Sample and reference pan material were the same. Al = aluminum, Au = gold.

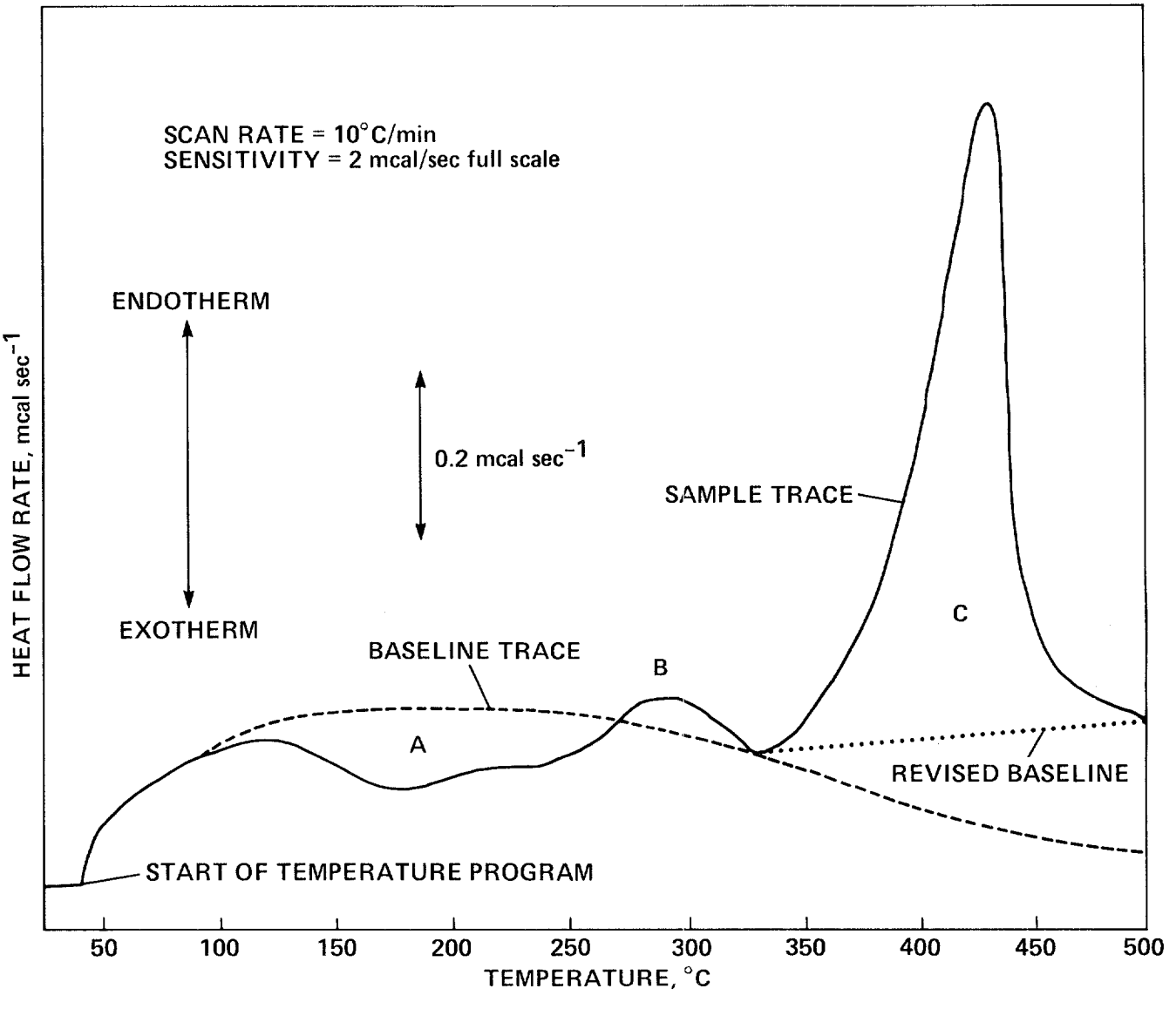


Figure 2-10.- Differential scanning-calorimeter recorder traces of the thermal decomposition of $CaO_2 \cdot 2H_2O_2$ disproportionation products.

scan, the two traces did not match up. To estimate the heat of decomposition value associated with the peak "C", it was necessary to draw in a revised baseline below the peak.

DISCUSSION - Prior to the TGA study, peak "A" was assigned to the thermal decomposition of the $Ca(O_2)_2$ component of the $CaO_2 \cdot 2H_2O_2$ disproportionation product sample. In this reaction, which is known to be exothermic (43), $Ca(O_2)_2$ decomposes, forming $CaO_2$ and releasing $O_2$:

$$Ca(O_2)_2 = CaO_2 + O_2 \qquad (2.25)$$

Initially it was thought that this decomposition reaction began near a temperature of 80°C and continued until a temperature of ~270°C.

The process responsible for peak "B" could not be determined based on the DSC work alone. However, it was postulated to be the result of some endothermic crystal transition.

Peak "C" was postulated to result from the two endothermic decomposition reactions

$$CaO_2 = CaO + 1/2O_2 \qquad (2.11)$$

and

$$Ca(OH)_2 = CaO + H_2O \qquad (2.12)$$

which are known to occur in the range of 300-500°C (14,43, 46). The $CaO_2$ contributing to peak "C" was thought to originate from $CaO_2$ originally in the sample and from $CaO_2$ formed from $Ca(O_2)_2$ via equation (2.25).

Since there was some uncertainty over the assignment of the thermal effects seen on the DSC trace it was felt that additional information was needed before the heats of the proposed decomposition reactions could be estimated. Therefore a thermogravimetric analysis of $CaO_2 \cdot 2H_2O_2$ disproportionation products was carried out to aid in the interpretation of the DSC thermal effects. Further discussion of the significance of the DSC results will be deferred to the next section on the TGA study.

### 2.3.3.2 Thermogravimetric Analysis

APPARATUS - Thermograms of $CaO_2 \cdot 2H_2O_2$ disproportionation products samples were recorded on a Texas Instruments Servo-riter II chart recorder using a Perkin-Elmer model TGS-1 thermobalance which was programmed by a Perkin-Elmer UU-1 temperature program controller. The TGS-1 thermobalance furnace was calibrated over the temperature range of

25-650°C using magnetic standards[2].

PROCEDURE - A 2.3 to 5.3 mg sample was loaded into a tared-aluminum or gold volatile-sample pan and hermetically sealed while inside a dry glove box. The sealed pan was weighed to the nearest 0.001 mg and the outside rim of the pan was removed so that the pan would hang in the thermobalance stirrup. Once the sample was loaded in the balance, the balance case was purged with dry nitrogen before a small pinhole was made in the top of the sample pan to permit decomposition gases to escape. After an additional dry-nitrogen purge, the flow rate of nitrogen was adjusted to 40 SCCM. Then the temperature of the furnace was increased at a constant rate and the weight of the sample was recorded as a function of the temperature. After the maximum temperature had been reached, the temperature was maintained at this value until the weight remained constant. The time required to reach constant sample weight was usually 10-15 min. Table 2-11 lists the sample and TGS-1 instrument parameters for each of the samples analyzed.

RESULTS - Using values taken off the chart trace, the rate of weight change, dM/dt (mg/sec), was calculated as a function of sample temperature. Using the total weight loss value, the percentage of the total weight loss as a function of temperature was calculated. Figure 2-11 contains a plot of the weight loss curve and a plot of the differential weight-loss curve for sample No. 2. Figure 2-12 is a plot of the percentage of the total-sample weight loss as a function of temperature for sample No. 2. The general features of the three plots are representative of the data obtained for the other three samples.

Figures 2-11 and 2-12 have been divided into three temperature regions. Region I (25-155°C) is the temperature region over which the sample is relatively thermally stable with respect to weight loss or decomposition. In regions II and III, (155-341°C and 341-498°C, respectively), the samples underwent decomposition reactions which were accompanied by significant weight losses. The weight loss curve for sample No. 4 (not shown) had a fourth region (IV), (498-644°C) in which the percentage of decomposition was insignificant.

The differential weight-loss curve for sample No. 2 (fig. 2-11), shows that the rate of weight loss maximized in region II near 300°C and in region III near 450°C. At 340°C,

---

[2] Reference to specific brands, equipment, or trade names in this report is made to facilitate understanding and does not imply endorsement by the Bureau of Mines.

Table 2-11.- Thermogravimetric Analysis of $CaO_2 \cdot 2H_2O_2$ Disproportionation Products -- Sample and TGS-1 Thermobalance Parameters

| | | TGS-1 thermobalance parameters | | | | |
|---|---|---|---|---|---|---|
| Sample No. | Initial sample weight, mg [1] | sample pan material [2] | Temp. scan range, °C | Temp. scan rate, °C/min | Mass range, mg | Recorder range, mg |
| 1 | 4.940 | Al | 25-498 | 10 | 10 | 0.2 |
| 2 | 5.324 | Al | 26-498 | 10 | 10 | 0.4 |
| 3 | 4.084 | Al | 27-498 | 10 | 10 | 1.0 |
| 4 | 3.340 | Au | 25-644 | 10 | 10 | 1.0 |

1 All samples had a chemical composition of 41.4% $Ca(O_2)_2$, 22.7% $CaO_2$, and 35.9% $Ca(OH)_2$. % $Ca(OH)_2$ obtained by difference, i.e., % $Ca(OH)_2$ = 100 - % $Ca(O_2)_2$ - % $CaO_2$.

2 Al = aluminum, Au = gold.

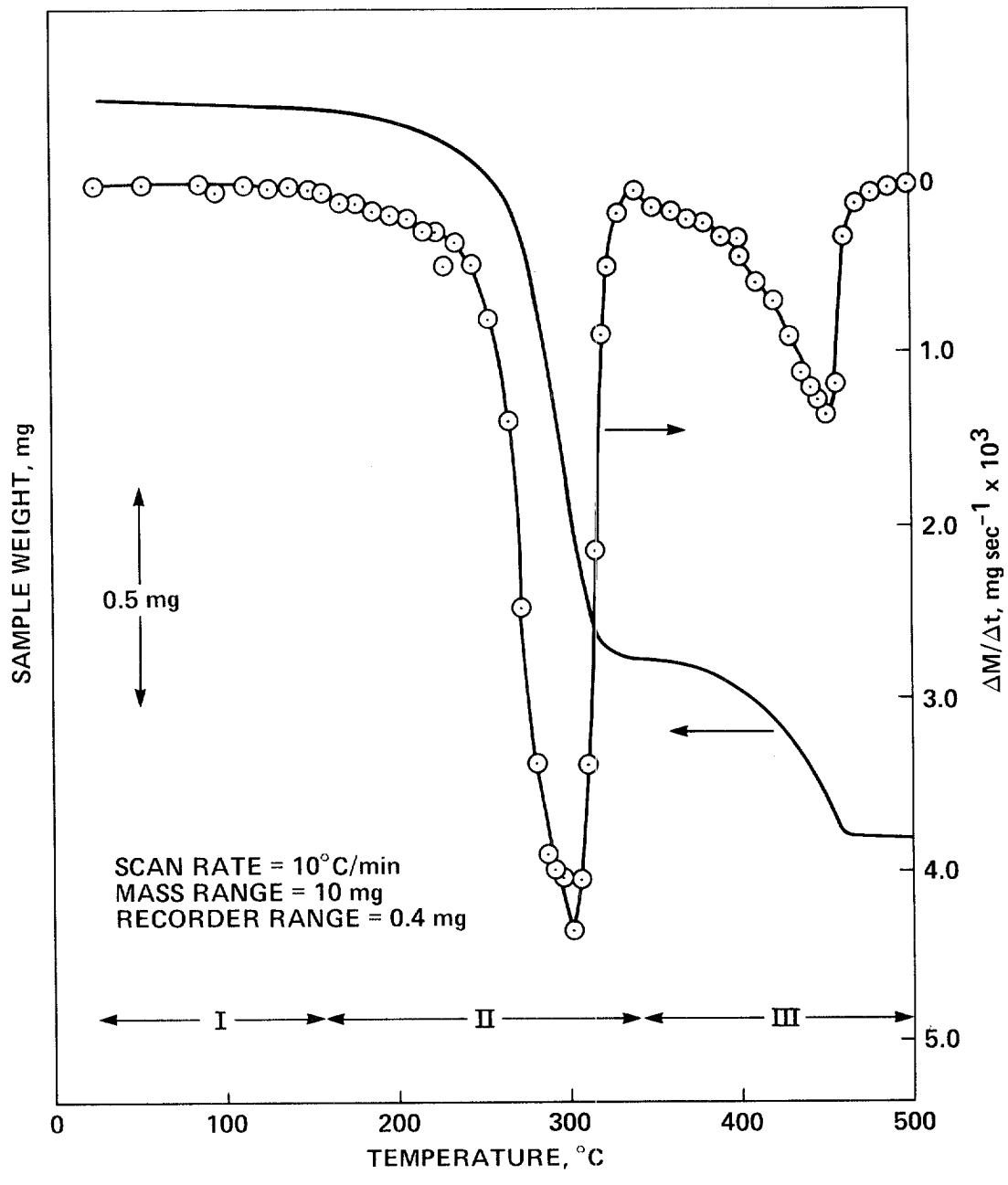


Figure 2-11.- Thermogravimetric analysis of $CaO_2 \cdot 2H_2O_2$ disproportionation products. Weight loss and differential weight loss curves.

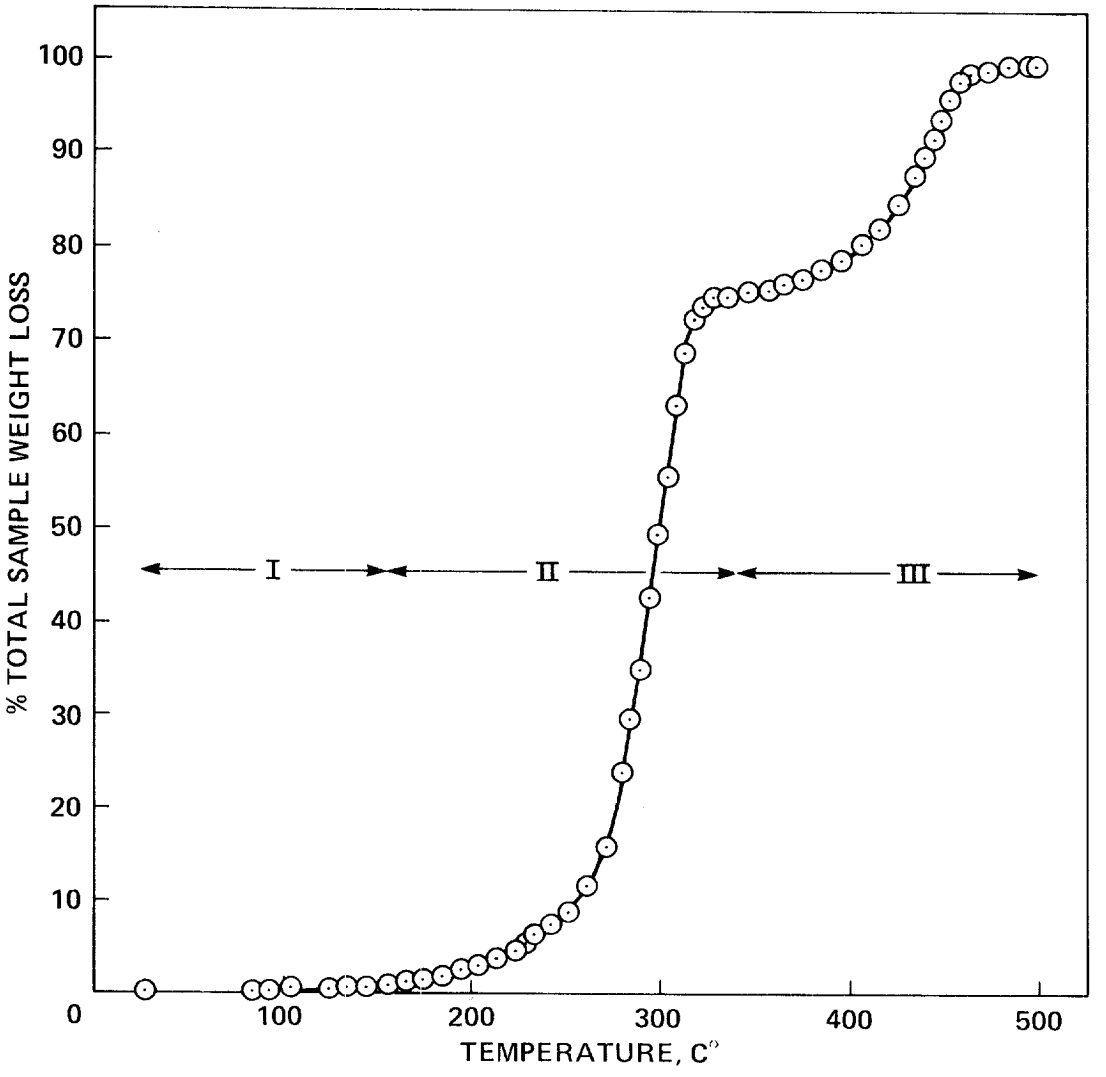


Figure 2-12.- Thermogravimetric analysis of $CaO_2 \cdot 2H_2O_2$ disproportionation products. Percentage of the total sample weight loss as a function of temperature.

the rate of sample weight loss was low, indicating that the first decomposition process was complete before the second decomposition process had begun. In table 2-12, the temperature at which the maximum and minimum rates of weight loss occurred in regions II and III for the four samples are compared. The temperatures at which the maximum and minimum rates of weight loss occurred for each sample are slightly different from sample to sample probably because of slight differences in sample size, packing in the sample pan and position in the furnace. Sample size, packing and position could determine the degree to which the sample temperature lagged behind the furnace temperature. A sample temperature lag would shift the maximum and minimum rates of weight loss to higher temperatures values.

Table 2-13 lists the percentage of the total sample weight loss observed for each of the four samples at the upper limits of the three temperature regions. Up to 155°C, none of the samples had lost more than 2% of the total weight loss. When the temperature reached 341°C (the upper limit of region II), the majority of the samples had lost ~75% of the total sample weight loss. Subsequent to the TGA of sample No. 1, it was found that the chart recorder was not in calibration with the TGS-1 thermobalance output and this may account for the significant difference in both the total-percentage weight-loss value and the percentage of the total weight loss at 341°C when sample No. 1 is compared to sample Nos. 2-4.

Sample No. 4 was heated from 500°C to 644°C to determine if the $CaO_2 \cdot 2H_2O_2$ disproportionation product had completely decomposed after heating to 500°C. The weight loss for sample No. 4 above a temperature of 500°C was slightly more than 1% of the total sample weight loss and this indicates that the decomposition of the $Ca(O_2)_2$, $CaO_2$, and $Ca(OH)_2$ components of the mixture is essentially complete by 500°C.

DISCUSSION - Indentification of the decomposition reactions responsible for the two bands on the differential weight-loss curve (fig. 2-11) was done by using the initial chemical composition of the batch of $CaO_2 \cdot 2H_2O_2$ disproportionation product and the weight loss data from the four TGA runs:

(a) Thermal Decomposition Reactions - Table 2-14 lists the decomposition reactions of the three known components of the $CaO_2 \cdot 2H_2O_2$ disproportionation product. Also given in table 2-14 are the weights of $H_2O$ or $O_2$ which would be released during the decomposition of each component for a 1-g disproportionation product sample containing 41.4% $Ca(O_2)_2$, 22.7% $CaO_2$, and 35.9% $Ca(OH)_2$. The amounts of $H_2O$ and $O_2$ are also presented in terms of the percentage of the

Table 2-12.- Thermogravimetric Analysis of $CaO_2 \cdot 2H_2O_2$ Disproportionation Products -- Temperatures at Which Maximum and Minimum Rates of Weight Loss (dM/dt) Were Observed

| Sample No. | Temperature of maximum dM/dt, °C | | Temperature of minimum dM/dt, °C [1] |
|---|---|---|---|
| | Region II | Region III | |
| 1 | 292 | 450 | 342 |
| 2 | 302 | 452 | 342 |
| 3 | 297 | 447 | 346 |
| 4 | 297 | 445 | 332 |
| Average | 297 | 448 | 341 |

[1] This temperature fixed the boundary between temperature regions II and III

Table 2-13.- Thermogravimetric Analysis of $CaO_2 \cdot 2H_2O_2$ Disproportionation Products -- Total Weight Loss and Cumulative Weight Loss at Selected Temperatures

| Sample No. | Total sample weight loss, mg | Total sample weight loss, % of initial sample weight | Cumulative weight loss at selected temperatures, as % of total weight loss: [1] 155°C | [2] 341°C | [3] 498°C |
|---|---|---|---|---|---|
| 1 | 1.738 | 35.2 [4] | 1.7 | 69.3 | 99.5 |
| 2 | 1.736 | 32.6 | 1.1 | 75.0 | 99.2 |
| 3 | 1.322 | 32.4 | 0.2 | 75.1 | 99.4 |
| 4 | 1.083 | 32.4 | 1.1 | 74.7 | 98.6 |

1 Upper limit of temperature region I.
2 Upper limit of temperature region II.
3 Upper limit of temperature region III.
4 Chart recorder out of calibration with TGS-1 thermobalance.

Table 2-14.- Thermogravimetric Analysis of $CaO_2 \cdot 2H_2O_2$ Disproportionation Products -- Decomposition Reactions and Calculated Weight Losses for Superoxide, Peroxide, and Hydroxide Components

| Component decomposing | Decomposition reaction(s)[2] | Calculated weight loss of components[1]: $O_2$ released, g | $O_2$ released, % of total weight loss[3] | $H_2O$ released, g | $H_2O$ released, % of total weight loss[3] |
|---|---|---|---|---|---|
| Superoxide | $Ca(O_2)_2 = s\text{-}CaO_2 + O_2$ | 0.127 | 38.7 | 0 | 0 |
| | $s\text{-}CaO_2 = CaO + 1/2O_2$ | 0.064 | 19.4 | 0 | 0 |
| Peroxide | $o\text{-}CaO_2 = CaO + 1/2O_2$ | 0.050 | 15.3 | 0 | 0 |
| Hydroxide | $Ca(OH)_2 = CaO + H_2O$ | 0 | 0 | 0.087 | 26.6 |

1 Values based on a 1 g sample of $CaO_2 \cdot 2H_2O_2$ disproportionation product containing 41.4% $Ca(O_2)_2$, 22.7% $CaO_2$, and 35.9% $Ca(OH)_2$.

2 $s\text{-}CaO_2$ = peroxide arising from the thermal decomposition of $Ca(O_2)_2$, $o\text{-}CaO_2$ = peroxide in original sample.

3 Total calculated weight loss = 0.329 g / g sample.

total sample weight loss which would be expected after decomposition of a given component.

(b) Proposed Thermal Decomposition Schemes - On the basis of the theoretical weight loss values presented in table 2-14, four possible schemes have been proposed which outline the temperature regions in which the various components of the disproportionation product decompose. Table 2-15 lists the decomposition schemes and the corresponding expected percentage of the total weight loss which would be observed in temperature regions I, II, and III. For comparison, the actual percentages of total weight loss observed for each sample in each temperature region are also given in table 2-15. Scheme Nos. 3 and 4 appear less probable for the following reasons. Scheme No. 3 is unlikely to occur due to the low decomposition temperature range required of $Ca(OH)_2$ and scheme No.4 is unlikely to occur in that the two "types" of $CaO_2$ have to decompose at different temperatures. Scheme No. 1 is essentially the same as that initially proposed following the DSC study described previously (Sec. 2.3.3.1). Of the four schemes, scheme No. 2 gives the best correlation to the observed weight loss values for the four samples.

(c) Examination of Earlier DSC Results - As can be seen from table 2-15, scheme No. 2 is significantly different from the scheme proposed after the DSC study (i.e., scheme No. 1). Examination of the DSC results in the light of the data obtained from the TGA study led to a new interpretation of the processes responsible for the peaks on the DSC trace.

First, since less than 3% of the total weight loss occurred below 200°C, it seems unlikely that the decomposition reaction of the $Ca(O_2)_2$ component was occurring to any significant extent below this temperature. Peak "A" on the DSC trace appears as a shallow doublet. It is postulated that the exothermic heat effect seen below 200°C is the result of the $CaO_2 \cdot 2H_2O_2$ disproportionation product undergoing a solid state transition. During this transition a metastable amorphous structure, left after the release of $H_2O$ and $O_2$ during the disproportionation process, collapses to a more stable structure. This solid state transition is likely in the light of the gentle conditions used for $CaO_2 \cdot 2H_2O_2$ disproportionation. All of the products analyzed by TGA or DSC were obtained from disproportionations carried out below 0°C and were stored at ambient temperature (~25°C) following disproportionation. Therefore, heating during the DSC analysis would "anneal" the sample for the first time and release heat.

Secondly, the presence of peak "B", previously not assigned to any decomposition process, can now be attributed to the last part of the endotherm resulting from the decomposition of $CaO_2$. According to the TGA results, the superox-

Table 2-15.- Thermogravimetric Analysis of $CaO_2 \cdot 2H_2O_2$ Disproportionation Products -- Comparison of Actual Weight Loss Values with Theoretical Weight Loss Values for Proposed Decomposition Schemes

| Decomposition scheme No. | Components decomposing,[1] Temp. regions I + II | Components decomposing,[1] Temp. region III | Theoretical weight loss, as % of total sample weight loss,[2] Temp. regions I + II | Theoretical weight loss, as % of total sample weight loss,[2] Temp. region III |
|---|---|---|---|---|
| 1 | $Ca(O_2)_2$ | s-$CaO_2$, o-$CaO_2$ $Ca(OH)_2$ | 38.7 | 61.3 |
| 2 | $Ca(O_2)_2$, s-$CaO_2$, o-$CaO_2$ | $Ca(OH)_2$ | 73.5 | 26.6 |
| 3 | $Ca(O_2)_2$, $Ca(OH)_2$ | s-$CaO_2$, o-$CaO_2$ | 65.3 | 34.7 |
| 4 | $Ca(O_2)_2$, s-$CaO_2$ | o-$CaO_2$, $Ca(OH)_2$ | 58.1 | 41.9 |

| Sample No. | Weight loss, as % of total sample weight loss, Temp. regions I + II | Weight loss, as % of total sample weight loss, Temp. region III |
|---|---|---|
| 1 | 69.3 | 30.7 |
| 2 | 75.0 | 25.0 |
| 3 | 75.1 | 24.9 |
| 4 | 74.7 | 26.3 |

1 See Table 2-14 for reaction equations.
2 Based on values listed in table 2-14.

ide and peroxide components decompose in the same temperature region and the decomposition of the two components cannot be distinguished on the weight loss curve, but appear instead as a single decomposition. Therefore, on the DSC trace, one would expect the exotherm caused by the decomposition of the superoxide to be superimposed on the endotherm caused by the decomposition of the peroxide. However, unless the exotherm and endotherm were identical in magnitude and maximized at the same temperature value, portions of both heat effects would be visible on the trace. In the actual DSC trace (fig. 2-10), it appears that the exotherm caused by $Ca(O_2)_2$ decomposition preceeds the endotherm caused by $CaO_2$ decomposition, since the last part of the endotherm is visible as peak "B". This could mean that the superoxide decomposition is finished slightly before the decomposition of the $CaO_2$ is complete. The use of a slower scan rate than 1100°C/min on the TGS-1 instrument may make it possible to partially separate the two decomposition processes, but since the superoxide and peroxide decomposition are superimposed, it seems unlikely that one can obtain delta-H values for either species using the DSC technique.

Thirdly, if one examines the DSC trace in figure 2-10, the "valley" between peak "B" and peak "C" corresponds to the minimum present on the differential weight-loss curve (fig. 2-11) observed at 340-350°C. This valley suggests that the superoxide and peroxide have completely decomposed before the $Ca(OH)_2$ decomposition begins.

Finally, the TGA results indicate that peak "C" of the DSC trace is the consequence of the thermal decomposition of $Ca(OH)_2$ alone, rather than the combined decomposition of $CaO_2$ and $Ca(OH)_2$ (scheme No. 1). Assuming that this is true, it is possible to calculate the weight of $Ca(OH)_2$ in the samples using the delta-H values obtained from peak "C" and a value of delta-H(670)[3] for the decomposition of $Ca(OH)_2$ to CaO and $H_2O$ [i.e., 23.3 $\pm$ 2.0 kcal/mole, calculated based on the data and method given in reference (31)]. Alternatively, one could calculate an experimental delta-H(670) for the decomposition of $Ca(OH)_2$ using the heat values from peak "C" and the known weight of $Ca(OH)_2$ in the samples. The results of both types of calculations are given in table 2-16. It can be seen that (except for sample No. 3), all of the DSC runs give high values for the percentage of $Ca(OH)_2$ in the samples, and for the experimental delta-H(670) value for $Ca(OH)_2$ decomposition. The reason for these higher than expected values is not known at this time although it could be due to the error in drawing the baseline beneath peak "C".

---

[3] delta-H(670) is the heat of decomposition at 670 K

Table 2-16.- Thermal Analysis of $CaO_2 \cdot 2H_2O_2$ Disproportionation Products by DSC -- Experimental Values for % $Ca(OH)_2$ in Product Samples and delta-H(670) for the Decomposition of $Ca(OH)_2$

| Sample No. | Actual amount of $Ca(OH)_2$ in sample, | | delta-H, peak "C",[2] mcal/sample | Calculated amount[1] of $Ca(OH)_2$ in sample, | | Experimental delta-H(670), kcal/mole |
|---|---|---|---|---|---|---|
| | mg | % sample wt. | | mg | % sample wt. | |
| 1 | 1.018 | 30.9 | 443 | 1.41 ± 0.11 | 42.7 ± 3.3 | 32.3 |
| 2 | 0.990 | 30.9 | 399 | 1.27 ± 0.10 | 39.6 ± 3.1 | 29.9 |
| 3 | 1.131 | 30.9 | 332 | 1.06 ± 0.09 | 28.8 ± 2.5 | 21.8 |
| 4 | 1.611 | 35.9 | 657 | 2.09 ± 0.17 | 46.6 ± 3.8 | 30.2 |

1 Calculation was based on a thermodynamically estimated value of delta-H(670) for $Ca(OH)_2 = CaO + H_2O$ of 23.3 ± 2.0 kcal/mole [estimation of delta-H(670) was made using method given in ref. (17)].

2 See figure 2-10 for peak assignment. Values obtained by integrating areas under the peak using revised baseline.

SUMMARY AND CONCLUSIONS - The results from the DSC and TGA indicate that $CaO_2 \cdot 2H_2O_2$ disproportionation products are thermally stable with respect to decomposition up to a temperature of 155°C. Significant decomposition of the material does not begin until above 200°C. However, in the temperature range of 80-200°C, it is postulated that the metastable solid-state structure of the product mixture undergoes a change giving rise to the observed exotherm on the DSC trace.

The $Ca(O_2)_2$ and $CaO_2$ components of the disproportionation mixture decompose over the same temperature range of 200-340°C but the superoxide decomposition appears to be complete slightly before the peroxide decomposition is finished. Neither the heat effects nor the weight loss values for the superoxide component could be distinguished from those for the peroxide component. However, the combination of the TGA and DSC data allowed a portion of the peroxide decomposition endotherm to be identified on the DSC trace. Both the superoxide and peroxide components had completely decomposed before $Ca(OH)_2$ decomposition began near 350°C. The $Ca(OH)_2$ decomposition was complete near 470°C. No further significant decomposition of the $CaO_2 \cdot 2H_2O_2$ disproportionation product occurred from 500-644°C.

### 2.3.4 X-ray Crystallography Study of Calcium Superoxide

INTRODUCTION - It was of interest to determine if the $Ca(O_2)_2$ which was obtained from the disproportionation of $CaO_2 \cdot 2H_2O_2$ possessed a solid state structure which could be indexed by its x-ray powder-diffraction pattern. It was postulated that the information obtained from an x-ray analysis of the superoxide material might lead to a better understanding of why higher purity $Ca(O_2)_2$ was not produced by the $CaO_2 \cdot 2H_2O_2$ disproportionation reaction.

X-RAY SAMPLE CELL - Figure 2-13 shows the cell that was used to contain samples during the x-ray analysis. The cell was designed to fit into the flat sample holder bracket of the General Electric[4] Model SPG-2 x-ray spectrogoniometer which was used to detect and record the powder diffraction pattern. A thin film of Mylar[5] or Kapton[5] was glued onto the aluminum window frame using DuPont 49001 polyester resin and RC-803 curing agent. A special stretcher was made to permit the bonding of the tensioned plastic film to the

---

[4] Reference to specific brands, equipment, or trade names in this report is made to facilitate understanding and does not imply endorsement by the Bureau of Mines.
[5] Registered trademark DuPont

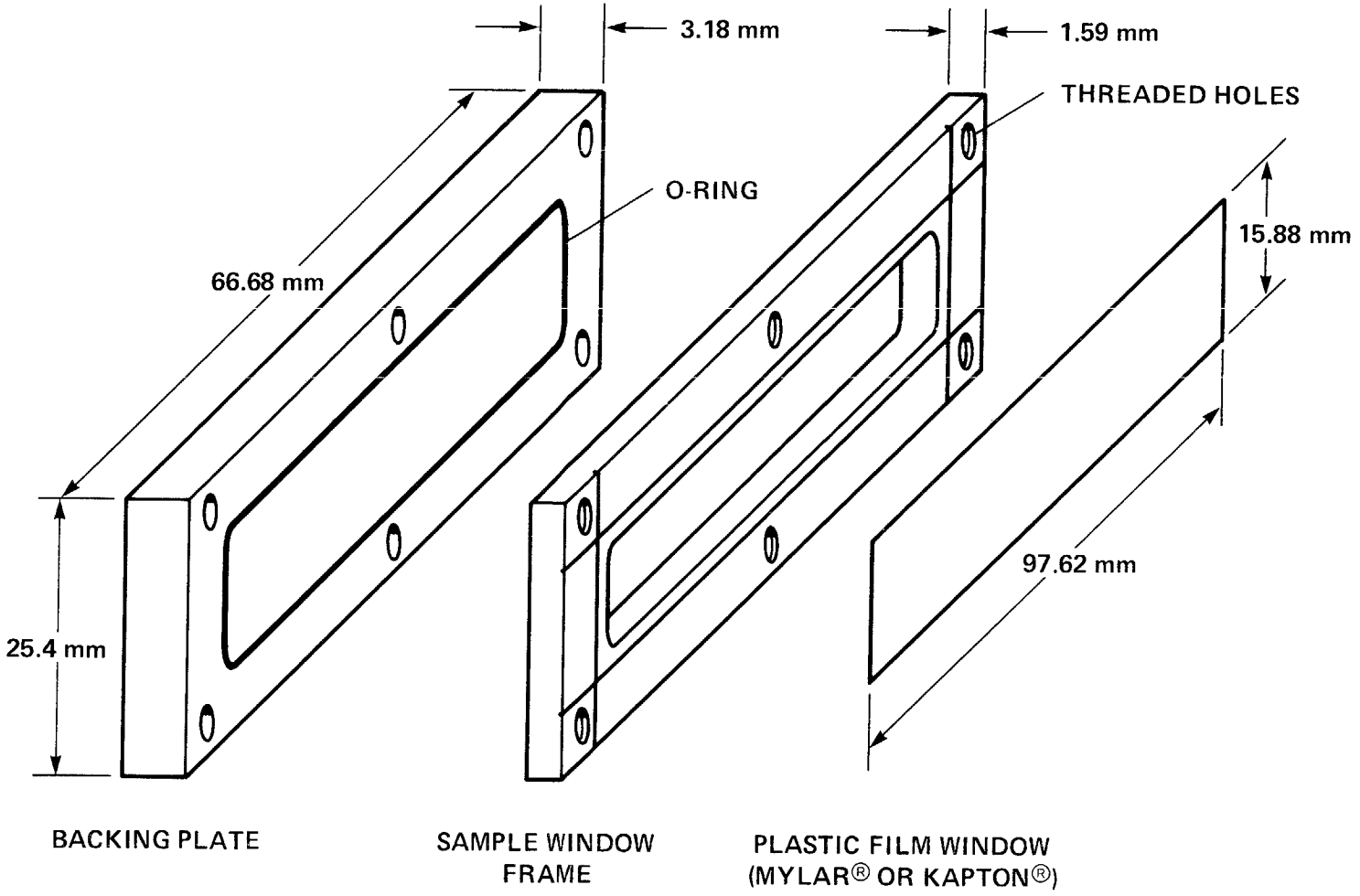


Figure 2-13.- X-ray sample cell.

aluminum frame.

PROCEDURE - After loading the sample into the aluminum frame behind the plastic window, a backing plate with an O-ring seal was attached to the frame using screws. The cell was then stored and transported in a small desiccator filled with anhydrous calcium sulfate to prevent reaction of the sample with atmospheric moisture which slowly diffused through the thin plastic window.

A sample containing 41% $Ca(O_2)_2$, 36% $Ca(OH)_2$, and 23% $CaO_2$ was loaded into the x-ray sample cell behind a 0.5 mil (0.012 mm) Mylar[6] window. Using Copper K-alpha incident radiation and a nickel filter, a scan through a 2-theta range of 15-90o was made at a rate of 2o/min and 1000-counts/sec (full scale) sensitivity. Two bands were recorded on the chart trace output and both were the result of low angle and amorphous scattering from the Mylar window.

RESULTS AND DISCUSSION - The superoxide sample had been prepared and stored under relatively mild conditions (i.e., disproportionation of $CaO_2 \cdot 2H_2O_2$ at -10°C and storage at room temperature). It was postulated that the sample might be in an amorphous state and that annealing it at a higher temperature might convert the material to a crystalline structure. This postulate was based upon the prior results obtained using TGA and DSC (Sec. 2.3.3) which had revealed that the same 41% $Ca(O_2)_2$ sample was stable up to about 155°C, but a broad exothermic peak had been observed on the DSC trace over the temperature range of 80-200°C. The exothermic peak had been attributed to a solid state structural transition. However, when another $Ca(O_2)_2$ sample was annealed at 150°C for 4 h in an inert (dry nitrogen) atmosphere, no x-ray diffraction pattern attributable to anything but low-angle scattering by the Mylar window was observed. Therefore, the x-ray analysis did not confirm a transition from an amorphous to a crystalline state.

To insure that no weak diffraction bands caused by $Ca(O_2)_2$, $CaO_2$, or $Ca(OH)_2$ were being obscured by the Mylar scattering bands, another sample was loaded into the sample cell behind a 0.3 mil Kapton[6] window. The Kapton material did not exhibit the strong amorphous scattering bands that had characterized the Mylar. The sample was scanned over a 2-theta angle range of 15-90o at 2o/min and at 4 times the sensitivity (i.e., 250 counts/sec) that had been used for the previous samples. No diffraction bands above background were observed.

---

[6] Registered trademark DuPont

Brosset and Vannerberg obtained an x-ray powder pattern for $CaO_2$ preparations which contained up to 23% $Ca(O_2)_2$ (7). The material was prepared by dehydrating $CaO_2 \cdot 8H_2O$ at room temperature, and then heating the dehydration product to a temperature of 100-250°C. The powder pattern showed only one phase, and was consistent with a $CaO_2$ lattice in which some of the peroxide anions were statistically replaced with superoxide, oxide and hydroxide anions. However, Vol'nov and Chamova (45) have demonstrated that no $Ca(O_2)_2$ was obtained from the dehydration of pure $CaO_2 \cdot 8H_2O$ and that the presence of $H_2O_2$ on the crystal faces or excessive $H_2O_2$ in the liquid phase during the preparation of $CaO_2 \cdot 8H_2O$ was required to produce any $Ca(O_2)_2$ when the octahydrate was dehydrated. They postulated that the $Ca(O_2)_2$ arose from the formation of significant quantities of $CaO_2 \cdot 2H_2O_2$ which disproportionated to form $Ca(O_2)_2$. If this is true, then Brosset and Vannerberg's preparations are similar to those examined in this work, except for the purity of $Ca(O_2)_2$. Apparently at lower superoxide concentrations [~25% $Ca(O_2)_2$], an x-ray powder pattern equivalent to $CaO_2$ is observed.

Bakulina, Zimina, and Tsentsiper (2) observed an x-ray powder pattern for a mixture of 35% $Ca(O_2)_2$, 25% $CaO_2$, 35% $Ca(OH)_2$, and 5% $CaCO_3$. They obtained their material from the disproportionation of $CaO_2 \cdot 2H_2O_2$ at 50°C. The powder pattern was similar to that for $Ca(OH)_2$ except that the lines were weaker and more diffuse and a strong halo was present. Since the only crystalline phase present was $Ca(OH)_2$, they concluded that the $Ca(O_2)_2$ and $CaO_2$ were present in an amorphous state; therefore, the product was nonhomogeneous. In the work described in this section a sample containing 41% $Ca(O_2)_2$ showed no x-ray diffraction pattern for $Ca(OH)_2$ or any other component. It is possible that a diffraction pattern for $CaO_2$ and $Ca(OH)_2$ would appear if the sample were annealed at 150°C for a longer period of time.

CONCLUSIONS - The x-ray diffraction studies one samples containing 41% $Ca(O_2)_2$ led to the following tentative conclusions. First, it is possible that the $Ca(O_2)_2$ prepared here from the disproportionation of $CaO_2 \cdot 2H_2O_2$ was stable only in an impure and amorphous structure which possessed no characteristic x-ray diffraction pattern. Second, the $Ca(O_2)_2$ in the sample may be crystalline, but the crystallite size is too small (<100 micrometers) to produce a diffraction pattern. Third, it is possible that longer annealing times at 150°C or higher annealing temperatures are necessary to convert the amorphous structure into a crystalline state.

## 3. SCALED-UP SYNTHESIS OF $Ca(O_2)_2$

A series of parametric studies on the disproportionation of microcrystalline $CaO_2 \cdot 2H_2O_2$ showed that up to 67% $Ca(O_2)_2$ could be obtained by disproportionating thin layers of the material (Sec. 2.2.2). However, using the disproportionation apparatus previously described (fig. 2-3) only ~0.5 g of 67% $Ca(O_2)_2$ could be obtained at one time. It became necessary to produce larger amounts of $Ca(O_2)_2$ for use in the characterization and reaction studies. Therefore, work was undertaken to increase the amount of $Ca(O_2)_2$ that could be prepared from a single batch of $CaO_2 \cdot 2H_2O_2$.

The first approach taken to scaleup was to increase the thickness of the layer of $CaO_2 \cdot 2H_2O_2$ that was disproportionated. When this approach was attempted at ambient temperature under the conditions which had given 67% $Ca(O_2)_2$ from the disproportionation of thin layers of $CaO_2 \cdot 2H_2O_2$, the temperature of the reactant layer could not be controlled. The heat given off from the exothermic disproportionation reaction resulted in a rapid increase in the temperature of the reactant layer and caused a runaway, vigorous reaction which resulted in low-purity $Ca(O_2)_2$. These results led to a study of the scaleup of the disproportionation reaction at subambient temperatures.

### 3.1 Subambient Temperature Scaleup

Since the rate of disproportionation had been found to be dependent on temperature, it was postulated that better thermal control of the $CaO_2 \cdot 2H_2O_2$ reactant layer could be obtained by reducing the temperature during disproportionation. Also, since the rate of $H_2O$ release from the reactant would be lower at subambient temperatures, it appeared possible that more efficient water vapor removal could be achieved.

#### 3.1.1 Experiments Near 0°C

A parametric study was undertaken in which the thickness of the $CaO_2 \cdot 2H_2O_2$ layer was increased while the other reaction conditions of chamber pressure and sample platform temperature were held constant at 1 mtorr and $0 \pm 4$°C, respectively. Reaction times of up to 24 h were required when the disproportionation reaction chamber shown in figure 2-4 was used. A more detailed description of this study can be found in reference (4). The purity of the $Ca(O_2)_2$ product remained approximately constant at 59-61% over the reactant spreading area range of 36-312 $cm^2/g$. No vigorous reactions were observed during any of the experiments.

However, when a $CaO_2 \cdot 2H_2O_2$ reactant spreading area of 18 $cm^2/g$ was tested, the sample underwent extensive vigorous

reaction after an induction period. It was postulated that at the low-pressure conditions of 1 mtorr, the removal of the exothermic heat of reaction by conduction and radiation processes was insufficient to prevent an increase in temperature. The increase in temperature led to an uncontrolled reaction. Visual examination of the white $CaO_2 \cdot 2H_2O_2$ during disproportionation revealed that the upper portion of the layer turned yellow (the color characteristic of superoxides) before the lower portion. This indicated that the actual temperature of the layer was not accurately reflected by the temperature of the sample platform, and that probably only the particles in contact with the sample dish were at 0°C.

### 3.1.2 Experiments at -10°C

Since the parametric study of the effect of reactant spreading area on the purity of $Ca(O_2)_2$ obtained from the subambient disproportionation of $CaO_2 \cdot 2H_2O_2$ indicated that purity was insensitive to reactant layer thickness, a new approach was taken to low temperature scaleup. In this approach, the slurry of $CaO_2 \cdot 2H_2O_2$ and concentrated $H_2O_2$ produced during the normal $CaO_2 \cdot 2H_2O_2$ synthesis process (Sec. 2.2.1.2), was placed in the flask of the freeze-drying apparatus pictured in figure 2-2. After the thick (>5 mm) layer of $CaO_2 \cdot 2H_2O_2$ had been freeze-dried over a temperature range of -20 to -10°C, the material was allowed to disproportionate in the flask at -10°C. It was postulated that better thermal control of the reactant layer could be obtained if it was isolated from the ambient, low-level heat sources of the glass cross reactor walls and was reacted at a lower temperature than in the 0°C reactant spreading area experiments.

After five days of reaction, the pressure in the apparatus had returned to the background value (~0.1 mtorr) and the sample was removed from the flask for analysis. Although the sample was yellow, it contained only 42% $Ca(O_2)_2$. It was postulated that the reactant layer was too densely packed for efficient removal of evolved water vapor. Therefore, a fluffy layer of $CaO_2 \cdot 2H_2O_2$ powder was placed in the flask of the freeze-drying apparatus and was disproportionated at -10°C. However, after 8 h of evacuation, the pressure in the apparatus rose dramatically from chamber background levels. The entire batch of $CaO_2 \cdot 2H_2O_2$ began reacting vigorously, sending most of the powder into the $LN_2$-cooled vapor trap.

These two experiments demonstrated that even at low temperatures, thick layers of $CaO_2 \cdot 2H_2O_2$ could not be successfully converted to $Ca(O_2)_2$ in a static vacuum environment. In the packed reactant layer experiment, there appeared to be effective heat transfer to the cold walls of the flask via interparticular contact, but these packed

layers were unfavorable with regard to water-vapor removal efficiency. When loosely packed layers were reacted, the heat of reaction could be not removed such that the sample remained isothermal and runaway reactions were prevented.

## 3.2 Fluidized Bed Scaleup

An apparent solution to the thermal control problem observed during the subambient scaleup experiments was to remove the heat by flowing an inert gas through the $CaO_2 \cdot 2H_2O_2$ reactant layer. An added advantage of the gas sweep was the efficient removal of evolved water vapor from the reactant layer. Earlier work at the NASA Ames Research Center indicated that a sweep of dry-nitrogen gas was an efficient means of removing evolved water vapor from a thin layer (160 $cm^2/g$ reactant) of disproportionating $CaO_2 \cdot 2H_2O_2$ at 20°C (Sec. 2.2.2). At the higher nitrogen gas velocities tested, the force of the gas molecules was sufficient to partially fluidize the particles of $CaO_2 \cdot 2H_2O_2$. This led to the design of a reactor (fig. 3-1), which could be used to carry out the disproportionation reaction of $CaO_2 \cdot 2H_2O_2$ with the reactant bed fluidized. A detailed description of the disproportionation of $CaO_2 \cdot 2H_2O_2$ in the fluidized bed reactor can be found in references (49), (50) and (6).

In early experiments with the fluidized bed reactor, fluidization of 2 to 5-mm layers of $CaO_2 \cdot 2H_2O_2$ was inhibited by the formation of large agglomerates of statically charged particles. Since the flow of nitrogen gas bypassed the interiors of these agglomerates, they overheated and vigorous disproportionation occurred which resulted in products containing only 37-57% $Ca(O_2)_2$.

To reduce agglomeration, the following approach was taken. A 5 W, 13.56 MHz radiofrequency (RF) glow discharge was used to neutralize the static charge on the $CaO_2 \cdot 2H_2O_2$ particles. The application of the RF field to the sample zone of the reactor was accomplished using external electrodes. The effect of the nitrogen RF glow discharge on the formation of agglomerates was dramatic. After the nitrogen flow was initiated, but before the discharge was turned on, the $CaO_2 \cdot 2H_2O_2$ particles quickly agglomerated. However, the moment that the discharge was turned on, the agglomerates brokeup and the particles fluidized. With an initial reactant loading of 18 $cm^2/g$, 63.5% $Ca(O_2)_2$ was obtained. Increasing the initial reactant layer thickness to a loading of 10 $cm^2/g$ resulted in 59.9% $Ca(O_2)_2$. With the latter reactant loading, the reactor contained 2 g of $CaO_2 \cdot 2H_2O_2$. The apparent trend towards lower purity $Ca(O_2)_2$ with higher loadings suggested that water vapor evolved in one portion of the fluidized bed was reacting with product $Ca(O_2)_2$ before the $H_2O$ had a chance to exit from the top of the bed. Thus, the fluidized bed reactor used here could not be

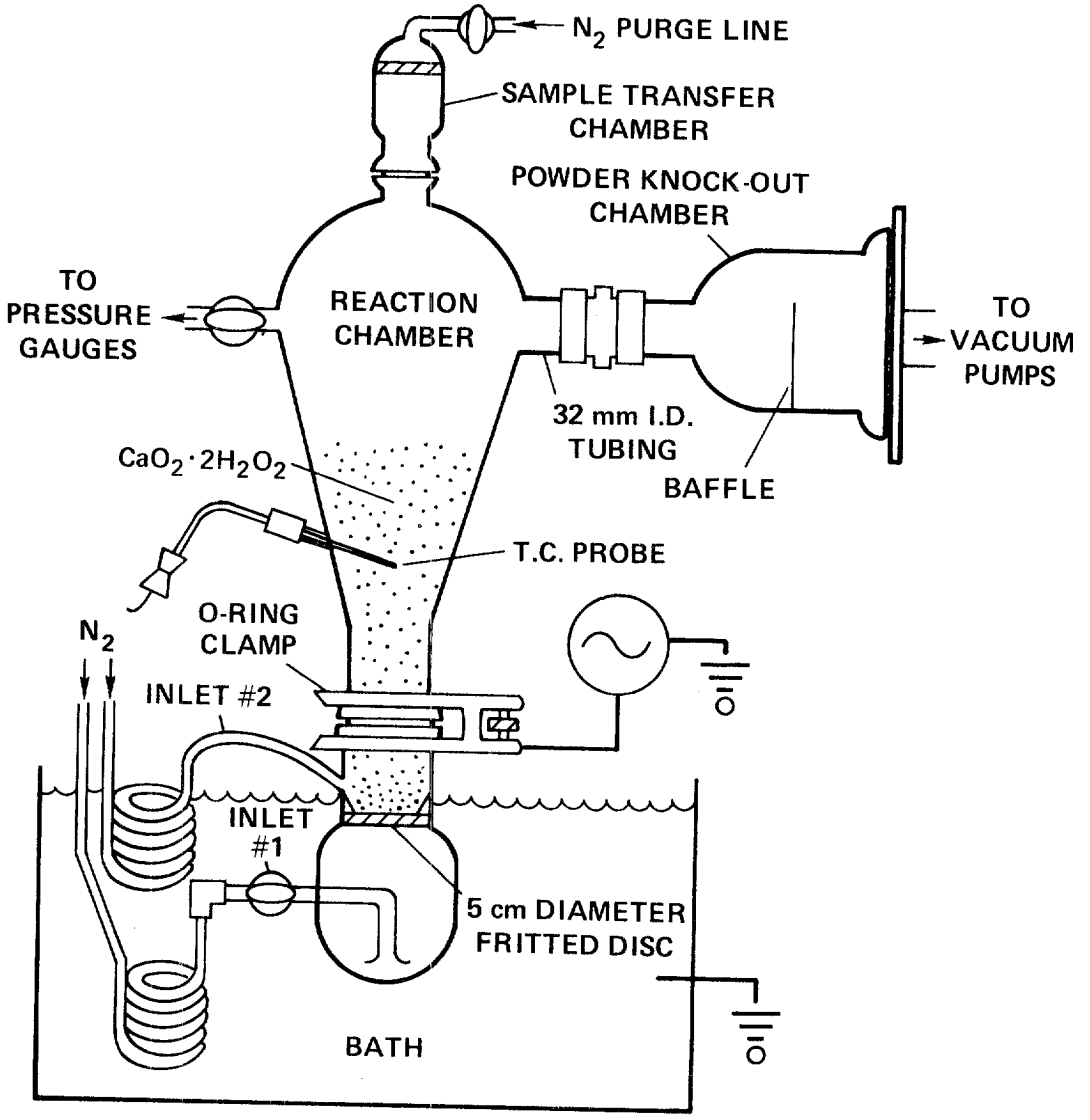


Figure 3-1.- Apparatus for the disproportionation of $CaO_2 \cdot 2H_2O_2$ in a low pressure fluidized bed and radiofrequency glow-discharge. (Copyright 1980 American Society of Mechanical Engineers. NTIS is authorized to reproduce and sell this copyrighted work. Permission for further reproduction must be obtained from the copyright owner.)

employed to process more than about 2 g of $CaO_2 \cdot 2H_2O_2$ at a time and still obtain $Ca(O_2)_2$ at purities greater than 60% when the fluidization process was carried out at 20°C. It is postulated that carrying out the fluidization process at 0°C might decrease the effect of the initial reactant layer thickness on the purity of $Ca(O_2)_2$. However, this postulate has not been tested to date.

### 3.3 Thin Layer, Large Area Scaleup

To obtain larger amounts (>3 g) of 60-67% $Ca(O_2)_2$ it appeared necessary to disproportionate the $CaO_2 \cdot 2H_2O_2$ under conditions similar to those found to be optimum in the initial $Ca(O_2)_2$ synthesis parametric studies, (Sec. 2.2.2.1) but increase the area available for spreading the sample. One way to increase the area available for the reactant layer was to stack trays containing thin layers of $CaO_2 \cdot 2H_2O_2$ in a vacuum chamber. In the earlier parametric study, evolved water vapor had been trapped by a liquid-nitrogen-filled cold finger protruding into the vacuum chamber (fig. 2-3). In the case of stacked reactant layers, each reactant layer was provided with its own water vapor "trap". The water vapor trap used was molecular sieve since it is capable of drying gases to low dew points (down to -100°C), has a moderate capacity for water vapor (4 wt%) and can be regenerated by heating.

In a set of preliminary experiments, the stacking of reactant layers was accomplished by placing the layers of $CaO_2 \cdot 2H_2O_2$ and molecular sieve type 13X pellets (1/16" diam.) on commercially available 20.3-cm-diam., circular sieve trays and then sandwiching each reactant layer between two trays holding the desiccant layers. Two such sandwiched layers were placed into a 38-cm-diam. by 61-cm long cylindrical, stainless-steel vacuum chamber attached to a glove box. The 2.0-g layers of $CaO_2 \cdot 2H_2O_2$ powder were spread over the surface of the stainless-steel metal screen (170-200 mesh) inside a 4°C cold room. Then, the trays were quickly stacked with the metal screen trays (20-42 mesh) containing 150 g of molecular sieve before evacuating the chamber. The molecular sieve had been previously baked at 330°C and cooled under dry nitrogen. A 5.0-cm gap existed between each of the reactant and desiccant layers and the reactant spreading area was 160 $cm^2/g$.

Disproportionation of the $CaO_2 \cdot 2H_2O_2$ was carried out at ambient temperature (20-25°C) for 130 min under static vacuum conditions (i.e., no inert gas flow through chamber). The pressure in the chamber gradually rose from the initial evacuation level of 90 mtorr to a maximum of 120 mtorr and then decreased to below 20 mtorr. No pressure spikes indicative of vigorous reactions were observed on the pressure trace. The disproportionated sample was transferred directly

into the glove box and loaded into glass bottles for storage and analysis. The product contained 67.4% $Ca(O_2)_2$ and 6.4% $CaO_2$. This was the largest quantity of high purity $Ca(O_2)_2$ synthesized in a single batch. In two additional experiments, 4.2 g layers of $CaO_2 \cdot 2H_2O_2$ were processed and yielded 67.1% and 67.2% $Ca(O_2)_2$, respectively.

Once it became apparent that disproportionation of thin-stacked layers of $CaO_2 \cdot 2H_2O_2$ yielded high purity $Ca(O_2)_2$, a new apparatus for holding the sample and desiccant layers was designed and assembled. This new apparatus permited more layers of $CaO_2 \cdot 2H_2O_2$ to be processed simultaneously in the same glove box vacuum chamber that had been used in the preliminary multilayer experiments. The new apparatus consisted of a rack which held two sets of 27.5 X 29 X 1 cm (length x width x depth) stainless steel cloth trays. Each set was made up of six sample-containing metal-cloth trays (200 mesh) and seven molecular-sieve-containing metal-cloth trays (14 mesh). The sets were inserted in the rack such that each sample tray was sandwiched between two molecular sieve trays. The distance between the reactant and desiccant layers was 1 cm. If both sets of trays were loaded with 5.3 g of $CaO_2 \cdot 2H_2O_2$ (spreading area of 150 $cm^2/g$ reactant), 64 g of $CaO_2 \cdot 2H_2O_2$ could be processed at one time.

To test the new apparatus, the number of sample layers processed at one time was increased incrementally during three experiments. In the first experiment, one 5.3-g layer yielded 62.2% $Ca(O_2)_2$, while in the second experiment two 5.5-g layers yielded 63.5% $Ca(O_2)_2$. When three 5.0-g layers of $CaO_2 \cdot 2H_2O_2$ were disproportionated in the third experiment, several pressure spikes were observed during the reaction period and indicated that vigorous reaction were taking place. Analysis of the product indicated that it contained 58.4% $Ca(O_2)_2$, which was 4-5% less than for the one and two layer experiments. The lower purity of $Ca(O_2)_2$ obtained with the greater number of reactant trays may have been due to poor thermal control. Apparently, the temperature rise resulting from the exothermic disproportionation reaction and the heat of absorption of water vapor by the molecular sieve was enough to take the particle layer temperature above 30°C and cause vigorous reactions.

# 4. REACTIVITY OF $Ca(O_2)_2$ WITH $CO_2$ AND WATER VAPOR

## 4.1 Introduction

To date, preparations containing up to 67% $Ca(O_2)_2$ have been synthesized in the work described in this report. Theoretically, the available $O_2$ content and $CO_2$ scrubbing capacity of these preparations, was equivalent to commercially available 90-95% $KO_2$. However, study of the reactivity of $Ca(O_2)_2$ with respiratory gases (i.e., water vapor and $CO_2$) was needed to determine if the potential capacity of $Ca(O_2)_2$ to evolve $O_2$ and absorb $CO_2$ could be realized under conditions simulating those present in the chemical bed of a manned emergency self-rescuer.

Previous research on the reactivity of $Ca(O_2)_2$ with water vapor and $CO_2$ was limited in scope. Vol'nov and Shatunina (44) tested the reactivity of low purity (3-16%) $Ca(O_2)_2$ by exposing it to a gas stream containing 10% $CO_2$ and 90% $N_2$ humidified to a dew point of 23°C. The preparations containing the most $Ca(O_2)_2$ absorbed the most $CO_2$ and evolved the most $O_2$. Materials containing $Ca(O_2)_2$ were found to be more reactive with humidified $CO_2$ than samples that contained only $CaO_2$ and $Ca(OH)_2$. Petrocelli and Capotosto (29) tested the reactivity of $Ca(O_2)_2$ with moist $CO_2$ in a recirculating flow-system loop. They observed that $CO_2$ absorption lagged $O_2$ evolution when $Ca(O_2)_2$ of moderate purity (29-39%) was reacted at 24°C with a gas stream containing 5% $CO_2$ at relative humidities of 48-100%. Prior to the work described here, no research was reported in which the reactivity of $Ca(O_2)_2$ was evaluated in response to the partial pressure of $H_2O$ found in the exhaled human breath (i.e., 47 mm Hg). Furthermore, no data was available in which the rates of reaction of $Ca(O_2)_2$ and $KO_2$ with moist $CO_2$ were compared under similar test conditions.

In the work described in this section, a single-pass flow-system test facility was used to evaluate the reactivity of $Ca(O_2)_2$ with $CO_2$ and water vapor and to compare it with the reactivity of $KO_2$. The reactivity of the superoxides was tested under conditions approximating those which would be present in a manned, self-contained self-rescuer (SCSR) during emergency escape from a coal mine.

## 4.2 Experimental

### 4.2.1 Selection of Flow-System Test Conditions

To completely simulate the reaction conditions existing for a superoxide bed inside a commercially available SCSR during deployment, the following criteria should be met in the laboratory setup:

1. The flow velocity of the test gas entering the face

of the chemical bed should vary in magnitude and frequency in a manner corresponding to the breathing rate of the average person engaged in escape activities while breathing through a unidirectional-flow self-rescuer

2. The composition of the test gas entering the bed should be that of exhaled human breath (i.e. the dew point of the gas should be 37°C and the concentration of $CO_2$ entering the bed should vary between 0 and 5% as the flow velocity goes from 0 to a maximum and back to 0)
3. The sizes of the superoxide granules should be the same as those in the commercial canister
4. The length of the bed should be equivalent to that in the commercial canister.

Two commercial, $KO_2$-based, emergency self-rescuers were used to provide the criteria for the superoxide bed characteristics. These were the MSA 60 Minute, SCSR (Mine Safety Appliance Co., Pittsburgh, PA) and the Drager OXY-SR-60B SCSR (Dragerwerk AG, Lubeck, West Germany)[7]. Table 4-1 shows a summary of superoxide bed characteristics for each device.

The flow-system conditions described below were a compromise between exact simulation of the reaction conditions for a superoxide bed in a self-rescuer during deployment and the practical limits imposed by existing laboratory equipment and the availability of $Ca(O_2)_2$. The latter consideration turned out to be a limiting factor, and a scaled-down [1.06-cm inside diam. (i.d.)] reactor was used in the flow studies. As a result of material limitations, powders and small granules (<2.5 mm) were tested to keep the particle size to reactor diameter ratio in the appropriate range [i.e. 4-10 particles/reactor diam. (9)]. Also, bed heights of only 3.0 to 4.5 cm were used, because of the limited supply of $Ca(O_2)_2$.

A compromise on criteria Nos. 1 and 2 was also made because of the complexity of the equipment needed to generate simultaneous variations in gas velocity and $CO_2$ concentration. Instead of meeting criterion No. 2, 5% $CO_2$ was used so that the bed would be exposed to the maximum $CO_2$ concentration expected during any given exhalation. As will be shown later, this choice resulted in the simulation conditions being more favorable to the reaction of $KO_2$ than would be the case in an actual SCSR. Instead of meeting criterion No. 1, the average linear velocity of the gas to

---

[7] Reference to specific brands, equipment, or trade names in this report is made to facilitate understanding and does not imply endorsement by the Bureau of Mines.

Table 4-1.- $KO_2$ Bed Characteristics of Commercial SCSRs

| Manufacturer | MSA | DRAGER | |
|---|---|---|---|
| Characteristic | | | |
| Bed type | Plug flow, end to end | Semiradial, outside to inside flow | |
| Particle size, mm | (Granules) 5 - 6.5 | (Tablets) 9 x 5 | |
| Bed length, cm | 12 | 9 | |
| Area of bed face, $cm^2$ | 124 | Inside 151 | Outside 270 |
| Bed face velocity, cm/min | | | |
| at 10.5 l/min | 85 | 70 | 39 |
| at 40 l/min | 323 | 265 | 148 |

be used in the laboratory tests was determined based on the average flow velocities existing in the commercial SCSRs. The average velocity of the gas entering the beds of the commercial SCSRs was determined in two steps. First, the geometrical area of the superoxide surface exposed to the entering gas was measured for the MSA and Drager canisters. Then, this bed face area was divided into the average exhalation flow rates given in the Federal Register for sedentary and moderate exercise breathing (11). Since the Drager unit has a semiradial flow design, the velocity of the gas depends on bed depth. A summary of the average face velocities for the two devices at the sedentary breathing rate (10.5 l/min) and the moderate exercise rate (40 l/min) is given in table 4-1 along with the bed face areas. For the reactor (1.06-cm i.d.) used here, flow rates in the range of 34 to 285 $cm^3$/min were necessary to simulate the average flow rate representative of a sedentary to moderate exercise rate. In the tests described below, flow rates of 100 and 300 SCCM (20°C and 760 mm Hg) were used.

### 4.2.2 Flow-System Test Facility

Figure 4-1 is a schematic diagram of the single-pass flow-system test facility (9) which was assembled to test the reactivities of superoxides with $CO_2$ and water vapor. A single-pass flow was used rather than recirculating the gas so that the concentrations of $CO_2$, $O_2$ and $H_2O$ entering the bed were always known and constant. Dry 5% $CO_2$, 95% nitrogen test gas entered the system and was humidified by passage through a gas bubbler before entering the superoxide bed. The chemical composition of the gas leaving the bed was measured before it was vented from the system. Since the composition, pressure, and flow rate of the gas entering and leaving the reaction bed were known, the amounts of $CO_2$ and $H_2O$ absorbed and the amount of $O_2$ evolved by the bed could be determined.

Humidification of the test gas entering the chemical bed was accomplished by flowing the dry test gas through a glass bubbler, which was partially filled with distilled $H_2O$ and immersed in a constant temperature bath. A packing of glass wool above the surface of the distilled $H_2O$ inside the bubbler prevented the entrainment of $H_2O$ droplets or mist in the gas stream. In some of the flow-system experiments the condensation of moisture in the flow system (when the dew point of the test gas was above ambient temperature) was prevented by enclosing all of the parts of the flow system exposed to water vapor in a constant temperature oven set to $40.0 \pm 0.5$°C.

In all the tests described here, the chemical bed was contained in a 1.06-cm-i.d. glass reactor and the bed material was supported on a coarse porosity fritted glass

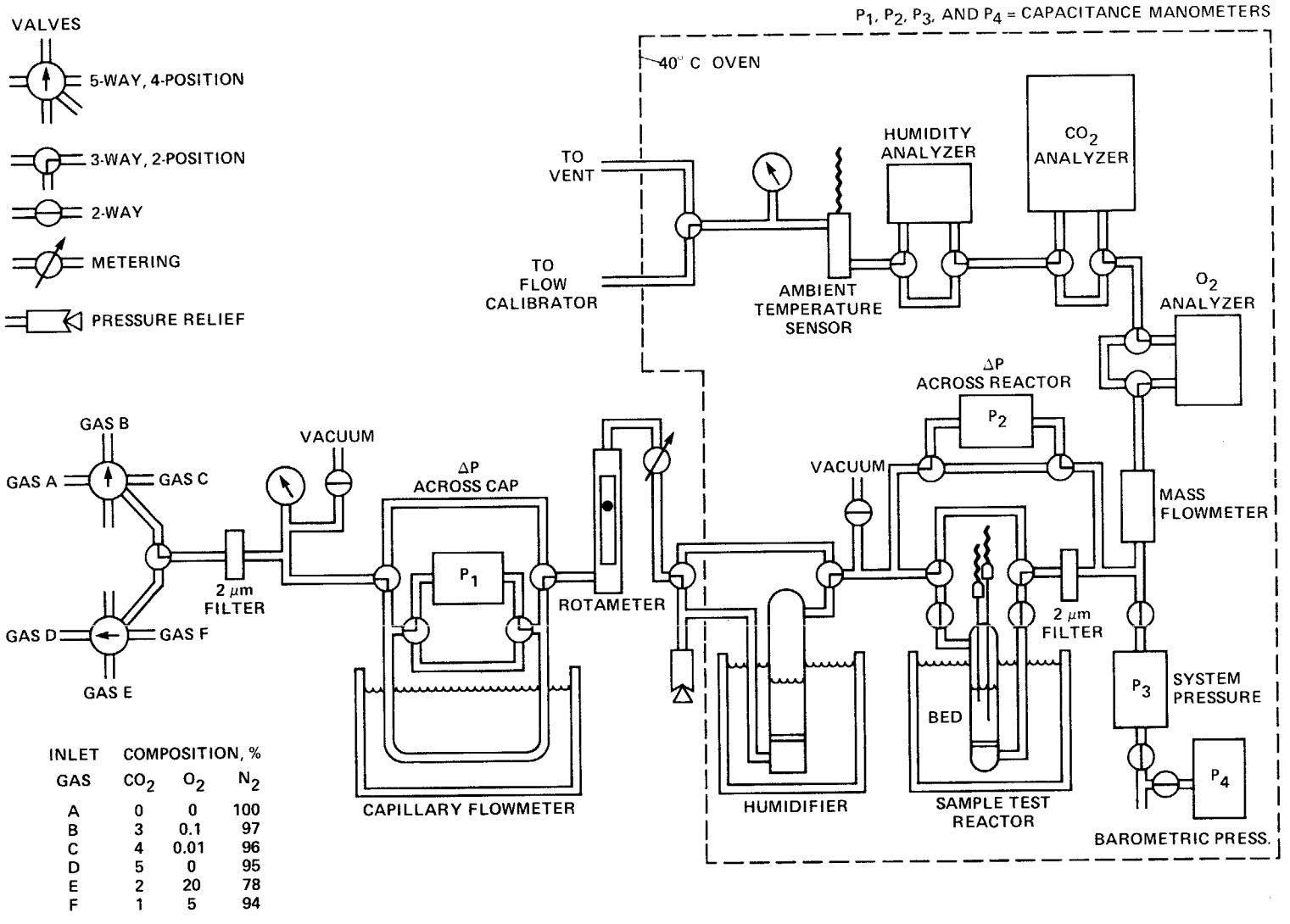


| INLET GAS | COMPOSITION, % $CO_2$ | $O_2$ | $N_2$ |
|---|---|---|---|
| A | 0 | 0 | 100 |
| B | 3 | 0.1 | 97 |
| C | 4 | 0.01 | 96 |
| D | 5 | 0 | 95 |
| E | 2 | 20 | 78 |
| F | 1 | 5 | 94 |

Figure 4-1.- Single-pass flow-system test facility. (Copyright 1983 Society of Automotive Engineers, Inc. NTIS is authorized to reproduce and sell this copyrighted work. Permission for further reproduction must be obtained from the copyright owner.)

disc. Two stainless-steel-sheathed, chromel-constantan thermocouple probes (1.02 mm diam.) were positioned inside the bed so that the probe tips were 1.5 and 3.0 cm, respectively, above the porous support. The thermal environment of the reactor could be varied by suspending it either directly in a constant temperature bath or in an air-well formed by a 5-cm-i.d. plastic tube immersed in the constant temperature bath.

The flow rate of the dry test gas entering the humidifier was determined by measuring the pressure drop across a 60 cm x 1.07 mm i.d. stainless steel capillary also immersed in a constant temperature bath. The pressure drop across the capillary, the pressure drop across the bed, the system pressure and the barometric pressure were measured with capacitance manometers of the appropriate range (models 400-101-SP, 400-100-SP, 220-AH-100 and 310-BAS-1000, respectively, MKS Instruments, Burlington, MA).

The flow rate of the gas leaving the reactor was determined by recording the response of a mass flow meter (model NALL-500, H-100 MS, Teledyne Hastings-Raydist Co.) calibrated for 5% $CO_2$, 95% nitrogen. Since the gas composition leaving the bed deviated considerably at times from that of the dry test gas, the measured flow rate was corrected for the real-time gas composition by the data acquisition program. The correction factor was calculated based on the heat capacities of the gas components.

The composition of the gas downstream from the chemical bed was determined using a model S-3A, N-22n Oxygen Analyzer (Applied Electrochemistry Co., Sunnyvale, CA), a model AR-500R infrared $CO_2$ analyzer (Anarad Inc., Santa Barbara, CA) and a model 911 Dew-All digital humidity analyzer (E.G. and G. Inc., Waltham, MA). The lines connecting the various components of the flow system were made of 1.75 and 4.57-mm i.d. stainless steel tubing.

Data acquisition and reduction were accomplished using an HP 9825B desktop computer interfaced with an HP 3495A 20 channel scanner and an HP 3455A digital voltmeter (Hewlett Packard, Palo Alto, CA). The analog outputs of all of the analyzers, probes, manometers, flowmeters and sensors were connected to the scanner with shielded signal cable. During the flow test, a real-time plot of some of the data was displayed on a CRT monitor driven by an HP 1350A graphics translator.

### 4.2.3 Flow-Test Procedure

The sample to be tested was loaded into the tared reactor under the dry nitrogen atmosphere of a glove box (Vacuum Atmospheres Co., Hawthorne, CA). In four of the

tests described below, laboratory fabricated granules of $Ca(O_2)_2$ or $KO_2$ were reacted with moist $CO_2$. The granules were made by compressing 2.5-$cm^3$ portions of the appropriate superoxide powder (<0.038-mm-diam. particles) in a modified Parr pellet press (Parr Instrument Co., Moline, IL) using a 1.27-cm-diam. punch and die. The pressing operation was carried out inside the dry glove box. Granules were made by breaking up the pellets with a spatula until they were in the desired size range.

Immediately before a flow test, the $O_2$ and $CO_2$ analyzers were calibrated by measuring their response to each of five dry, primary standard gas mixtures (certified to be within 0.02% of the component by Matheson Gas Products, Newark, CA). The calibration procedure was carried out by following the prompts of a custom computer program and the responses of the analyzers were stored by the computer for use during data reduction.

Following the calibration procedure, the flow system (including the lines leading up to the valves on the reactor) was evacuated and filled with dry test gas. In two of the tests, the reactivity of the chemical bed towards dry test gas (5% $CO_2$, 95% nitrogen) was evaluated before reacting the bed with humidified test gas. In these tests, a flow of dry test gas was directed through the reactor until the gas composition and bed temperature had returned to pretest values. Once the dry-mode portion of the reaction was complete, the flow was stopped, the reactor was bypassed and the flow system was equilibrated with moisture by directing the dry-test-gas stream through the humidifier. The humid portion of the test was then initiated by directing the humidified test gas through the reactor. In most of the tests described below, the dry-test-gas purge portion of the test was eliminated and the flow system was equilibrated with moisture before the start of the test.

Table 4-2 summarizes the flow-system test-facility reaction conditions for each of the $Ca(O_2)_2$ samples tested. Table 4-3 summarizes the reaction conditions for each of the $KO_2$ samples. Table 4-4 lists the chemical composition of each of the $Ca(O_2)_2$ samples and table 4-5 gives the composition of the $KO_2$ samples.

## 4.3 Results And Discussion

### 4.3.1 Reactivity of $Ca(O_2)_2$ with $CO_2$ and $H_2O$

Figures 4-2 and 4-3 are plots of the bed temperature and partial pressures of $O_2$, $CO_2$ and $H_2O$ ($pO_2$, $pCO_2$, and $pH_2O$ respectively) downstream from a $Ca(O_2)_2$ bed, as a function of reaction time for test No. CaS-5. The general features of the plot are representative of the data from all

Table 4-2.- Flow System Reaction Conditions for Testing $Ca(O_2)_2$ Samples

| Test No. | Reaction Conditions: Test Gas Parameters: Inlet flow rate, SCCM[3] | Test Gas Parameters: Humidifier temp., °C | Bed Parameters[1,2]: Weight, g | Bed Parameters: Height, cm | Bed Parameters: Particle size, mm | Bed Parameters: Temp. air well, °C | Test duration, ks |
|---|---|---|---|---|---|---|---|
| CaS-1 | 99-101 | 24.8 | 1.034 | 3.0 | <0.98 | 25.0[4] | 16 |
| CaS-2 | 99-101 | 25.0[5] | 1.112 | 3.1 | <0.98 | 25.0 | 18 |
| CaS-3 | 101-103 | 37.0 | 1.138 | 3.3 | <0.98 | 25.0 | 10 |
| CaS-4 | 299-301 | 37.0 | 2.489 | 4.6 | 1.9-2.5 | 37.5[6] | 16 |
| CaS-5 | 98-99 | 37.0 | 0.765 | 3.2 | <0.52 | 37.5 | 15 |
| CaS-6 | 299-301 | 37.0 | 0.835 | 3.2 | <0.52 | 37.5 | 2.6 |

1 See table 4-4 for chemical composition of samples.
2 1.06-cm ID reactor suspended in a 5-cm ID air well.
3 Flow rate for dry test gas (5% $CO_2$, 95% $N_2$); test gas was directed down through chemical bed.
4 Reactor immersed directly in constant temperature bath.
5 Reactor purged with dry test gas prior to humid portion of test.
6 Powder pressed to bulk density of 0.92-1.19 g/cm$^3$, then broken up into granules.

Table 4-3.- Flow System Reaction Conditions for Testing Potassium Superoxide Samples
Reaction Conditions

| Test No. | Test Gas Parameters | | Bed Parameters[1,2] | | | | |
|---|---|---|---|---|---|---|---|
| | Inlet flow rate, SCCM[3] | Humidifier temp., °C | Weight, g | Height, cm | Particle size, mm | Temp. air well, °C | Test duration, ks |
| KS-1 | 296-301 | 24.0 | 2.570 | 4.5 | 1.9-2.5[4] | 25.0 | 10 |
| KS-2 | 299-300 | 37.0 | 2.522 | 4.7 | 1.9-2.5[4] | 37.5 | 10 |
| KS-3 | 299-300 | 37.0[5] | 2.384 | 4.5 | 1.9-2.5[4] | 37.5 | 10 |
| KS-4 | 297-300 | 37.0 | 2.747 | 5.0 | 1.0-1.5[4] | 39.0 | 1.0 |
| KS-5 | 298-300 | 25.0 | 2.723 | 5.0 | 1.0-1.5[4] | 39.0 | 6.5 |
| KS-6 | 299-300 | 25.0[5] | 2.641 | 4.9 | 1.0-1.5[4] | 39.0 | 7.5 |
| KS-7 | 300-301[6] | 25.0 | 2.783 | 5.0 | 1.0-1.5[4] | 39.0 | 2.0 |
| KS-8 | 296-299 | 24.0 | 2.497 | 4.7 | 5 x 9[7] | 25.0 | 3.6 |
| KS-9 | 297-299 | 37.0 | 3.499 | 6.5 | 5 x 9[7] | 25.0[8] | 3.6 |
| KS-10 | 298-300 | 24.0 | 2.145 | 5.2 | 4-13[9] | 25.0 | 3.6 |
| KS-11 | 297-302 | 37.0 | 2.682 | 6.5 | 4-13[9] | 25.0[8] | 3.6 |

1 See table 4-5 for chemical composition of samples.

2 1.06-cm ID reactor suspended in a 5-cm ID air well.

3 Flow rate for dry test gas (5% $CO_2$,95% $N_2$); test gas was directed down through chemical bed.

4 Powder pressed to bulk density of 0.92-1.22 g/cm$^3$, then broken up into granules.

5 Reactor purged with dry test gas prior to humid portion of test.

6 Test gas was 100% $N_2$.

7 Tablets removed from a new, unused Drager SCSR canister.

8 The flow system from the humidifier to the upper portion of reactor was heated to 40-50°C.

9 Granules removed from a new, unused MSA SCSR canister.

Table 4-4.- Composition of the $Ca(O_2)_2$ Samples Used in Flow Studies

| Test No. | Composition of sample,[1] % | | | Theoretical capacities,[2] $cm^3$ STP/g sample | |
|---|---|---|---|---|---|
| | $Ca(O_2)_2$ | $CaO_2$ | $Ca(OH)_2$ | $O_2$ available | $CO_2$ absorption capacity |
| CaS-1 | 59.7 | 11.5 | 28.8 | 210.7 | 251.5 |
| CaS-2 | 55.3 | 14.4 | 30.3 | 201.1 | 255.5 |
| CaS-3 | 55.3 | 14.4 | 30.3 | 201.1 | 255.5 |
| CaS-4 | 57.1 | 12.2 | 30.7 | 203.4 | 253.8 |
| CaS-5 | 56.1 | 13.5 | 30.4 | 202.2 | 254.8 |
| CaS-6 | 55.7 | 14.1 | 30.2 | 201.9 | 255.2 |

1 Samples obtained from the disproportionation of $CaO_2 \cdot 2H_2O_2$.
2 Calculations based on the chemical composition and known reactions of the components.

Table 4-5.- Composition of the $KO_2$ Samples Used in the Flow Studies

| Test No. | Composition of sample, % | | Theoretical capacities[1] $cm^3$ STP/g sample | |
|---|---|---|---|---|
| | $KO_2$ | KOH, $K_2CO_3$, $KHCO_3$ | $O_2$ available | $CO_2$ absorption capacity[2] |
| KS-1 | 85.2 | 14.8 | 201.4 | 163.9-327.7 |
| KS-2 | 87.9 | 12.1 | 207.8 | 162.7-325.4 |
| KS-3 | 87.9 | 12.1 | 207.8 | 162.7-325.4 |
| KS-4 | 87.9 | 12.1 | 207.8 | 162.7-325.4 |
| KS-5 | 87.9 | 12.1 | 207.8 | 162.7-325.4 |
| KS-6 | 87.9 | 12.1 | 207.8 | 162.7-325.4 |
| KS-7 | 87.9 | 12.1 | 207.8 | 162.7-325.4 |
| KS-8 | 76.2 | 23.8 | 180.2 | 167.6-335.3 |
| KS-9 | 76.2 | 23.8 | 180.2 | 167.6-335.3 |
| KS-10 | 91.7 | 8.3 | 217.3 | 161.1-322.2 |
| KS-11 | 91.7 | 8.3 | 217.3 | 161.1-322.2 |

1 Calculations based on the chemical composition and known reactions of the components.

2 Calculations assume negligible quantities of $KHCO_3$ and $K_2CO_3$ in starting material. Lower limit of range is for $K_2CO_3$ as sole product and upper limit of range is for $KHCO_3$ as sole product

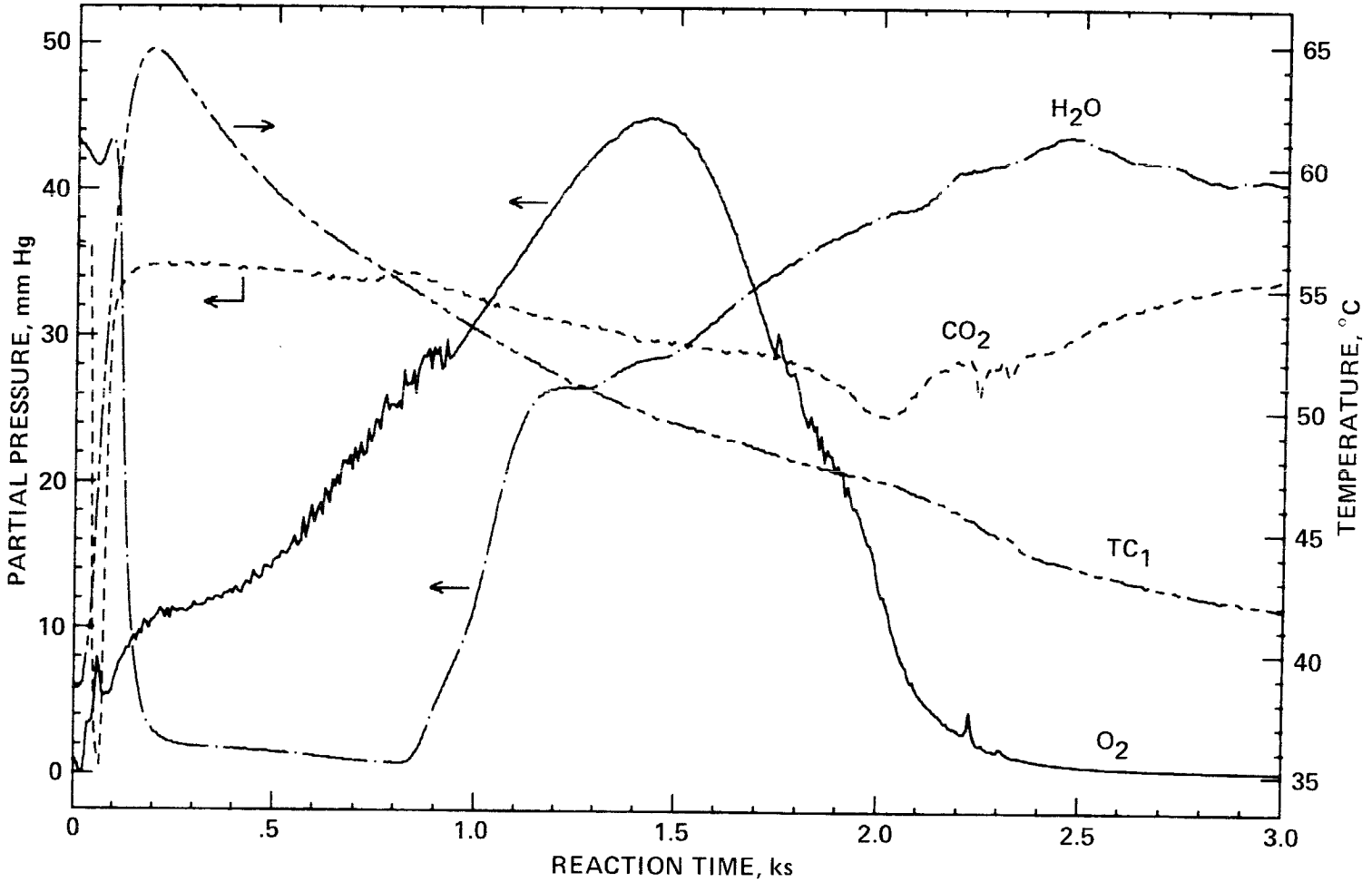


Figure 4-2.- Reaction of $Ca(O_2)_2$ with humidified test gas, phase I (test No. CaS-5). Partial pressures of $O_2$, $CO_2$, and $H_2O$ and bed temperature as a function of reaction time. 

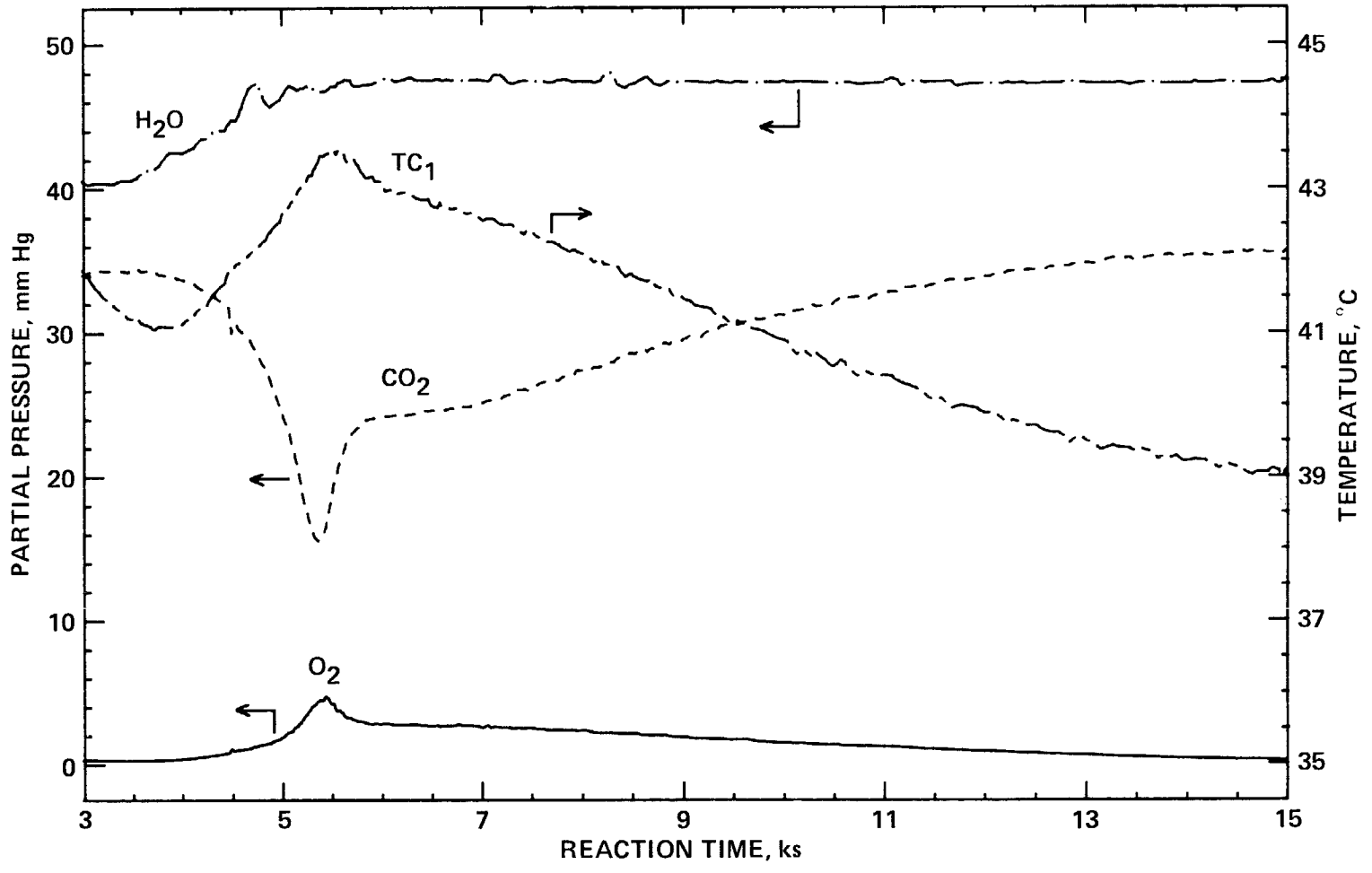


Figure 4-3.- Reaction of $Ca(O_2)_2$ with humidified test gas, phase II (test No. CaS-5). Partial pressures of $O_2$, $CO_2$ and $H_2O$ and bed temperature as a function of reaction time. 

of the tests in which $Ca(O_2)_2$ beds were reacted with a stream of humidified $CO_2$. The reaction of $Ca(O_2)_2$ beds with humidified $CO_2$ can be divided into two time periods or phases. During phase I, the principal reaction that occurred was between the $Ca(O_2)_2$ bed and water vapor. Water vapor was absorbed and $O_2$ was released. Carbon dioxide absorption took place during phase I, but was much less significant than $H_2O$ absorption and $O_2$ evolution. Visual observation of the bed during phase I revealed that the pale yellow color of the $Ca(O_2)_2$ was gradually transformed to white. When the white band reached the glass frit supporting the bed, $pH_2O$, which had been at low levels, increased rapidly. After $H_2O$ breakthrough, $pO_2$ continued to increase to a maximum level and then decreased to almost the background levels. The return of $pO_2$ to low levels marked the end of phase I.

As phase II began, $pO_2$, which had reached a minimum value, began to increase. Concurrent with the increase in $pO_2$ was a drop in $pCO_2$ and an increase in $pH_2O$ and the bed temperature. Before the time that $pO_2$ reached a maximum and $pCO_2$ reached a minimum level, the bed began to evolve water vapor. Visual observation of the reactor at this point revealed condensation in the reactor downstream from the bed. Water vapor evolution continued as long as the bed absorbed $CO_2$. $pO_2$ and the bed temperature reached a maximum during phase II at approximately the same time that $pCO_2$ reached a minimum value.

Table 4-6 lists the maximum rates of $O_2$ evolution and $CO_2$ absorption which were observed during phase I and phase II of the reaction of $Ca(O_2)_2$ beds with humidified $CO_2$. The maximum rates were calculated in terms of μmol/s and then were normalized using the bed weights. Table 4-7 gives the amounts of $O_2$ evolved and $CO_2$ and $H_2O$ absorbed during the two phases of the reaction. When the data given in tables 4-6 and 4-7 for the various $Ca(O_2)_2$ beds are compared and examined in the light of the test conditions for $Ca(O_2)_2$ beds listed in table 4-2, a number of general trends in the reaction behavior becomes apparent. First, during the initial part of Phase I each $Ca(O_2)_2$ bed behaved as a desiccant and all of the incoming $H_2O$ vapor was absorbed by the bed. Therefore, the maximum rate of $H_2O$ absorption by the bed was a function of $pH_2O$ and the flow rate of the test gas entering the bed. When inlet $pH_2O$ was doubled, while keeping the inlet test gas flow rate constant (e.g., tests Nos. CaS-2 and CaS-5), the maximum rate of $H_2O$ absorption doubled. When the inlet $pH_2O$ was held constant and the inlet flow rate was tripled (as in tests Nos. CaS-5 and CaS-6), the maximum rate of $H_2O$ absorption was approximately tripled.

Second, when the rates of $H_2O$ absorption and $O_2$ evolution during phase I are compared for any two $Ca(O_2)_2$

Table 4-6.- Maximum Rates of $O_2$ Evolution and $CO_2$ and $H_2O$ Absorption During Reaction of $Ca(O_2)_2$ Beds with Humidified $CO_2$

| Test No. | Phase of reaction [1] | Time phase begins, ks | $O_2$ evolution | | $CO_2$ absorption | | $H_2O$ absorption | |
|---|---|---|---|---|---|---|---|---|
| | | | Time, ks | Max. rate, μmol/s/g | Time, ks | Max. rate, μmol/s/g | Time, ks | Max. rate, μmol/s/g |
| CaS-1 | I | 0 | 3.48 | 1.74 | 4.72 | 0.55 | 3.30 | 2.07 |
| | II | 6.61 [2] | 11.90 | 0.36 | 11.41 | 1.32 | ND | ND |
| CaS-2 | I | 0 [2] | 3.93 | 1.74 | 5.04 | 0.44 | 2.58 | 1.96 |
| | II | 8.69 | 14.95 | 0.45 | 14.94 | 1.62 | ND | ND |
| CaS-3 | I | 0 | 2.45 | 2.58 | 3.60 | 0.63 | 1.66 | 3.78 |
| | II | 4.68 | 6.38 | 0.90 | 6.40 | 3.15 | ND | ND |
| CaS-4 | I | 0 | 1.11 | 4.64 | 2.13 | 0.60 | 0.30 | 5.29 |
| | II | 3.61 | 7.67 | 0.16 | 7.82 | 0.78 | ND | ND |
| CaS-5 | I | 0 | 1.44 | 5.84 | 2.02 | 1.48 | 0.82 | 5.65 |
| | II | 3.33 | 5.40 | 0.56 | 5.36 | 2.60 | ND | ND |
| CaS-6 | I | 0 [3] | 0.84 | 8.50 | 1.58 | 1.48 | 0.14 | 14.2 |
| | II | 2.67 | NAp | NAp | NAp | NAp | NAp | NAp |

[1] See text for explanation of phase demarcations.
[2] Time corrected for 0.5 ks of dry test gas purge.
[3] Test was terminated following phase I for chemical analysis of sample
NAp = not applicable, ND = not determined.

Table 4-7.- Amounts of $O_2$ Evolved and $CO_2$ and Water Vapor Absorbed During Reaction of $Ca(O_2)_2$ Beds with Humidified $CO_2$

| Test No. | Reaction phase[1] | $O_2$ evolved | | $CO_2$ absorbed | | $H_2O$ absorbed, | $H_2O$ absorbed/ |
|---|---|---|---|---|---|---|---|
| | | $cm^3$ STP/g | $\%O_2$ in bed[2] | $cm^3$ STP/g | % bed capacity[2] | $cm^3$ STP/g | $O_2$ evolved |
| CaS-1 | I | 153.0 | 72.6 | 49.8 | 19.8 | 211.2 | 1.38 |
| | II | 41.2 | 19.6 | 125.1 | 47.8 | 36.1 | 0.88 |
| | I & II | 194.2 | 92.2 | 174.9 | 67.5 | 247.3 | 1.27 |
| CaS-2 | I | 151.6 | 75.4 | 32.0 | 12.5 | 207.3 | 1.37 |
| | II | 23.6 | 11.7 | 71.5 | 28.0 | 19.3 | 0.82 |
| | I & II | 175.2 | 87.1 | 103.4 | 40.5 | 226.6 | 1.29 |
| CaS-3[3] | I | 146.0 | 72.6 | 44.4 | 17.4 | ND | ND |
| | II | 43.0 | 21.4 | 161.9 | 63.3 | ND | ND |
| | I & II | 189.0 | 94.0 | 206.3 | 80.7 | ND | ND |
| CaS-4 | I | 96.1 | 47.2 | 32.2 | 12.7 | 103.2 | 1.07 |
| | II | 24.3 | 12.0 | 106.0 | 41.8 | 7.3 | 0.30 |
| | I & II | 120.4 | 59.2 | 138.2 | 54.4 | 110.4 | 0.92 |
| CaS-5 | I | 150.5 | 74.0 | 50.3 | 19.8 | 178.6 | 1.19 |
| | II | 46.0 | 22.7 | 198.7 | 78.3 | 16.6 | 0.36 |
| | I & II | 196.6 | 96.6 | 249.0 | 98.0 | 195.2 | 0.99 |
| CaS-6[4] | I | 157.8 | 77.6 | 45.1 | 17.8 | 190.6 | 1.21 |

1 See text for explanation of phase demarcations.
2 Calculations based on bed capacities listed in table 4-4.
3 Quantities of $H_2O$ absorbed by bed could not be determined because some $H_2O$ condensed in the reactor. ND = not determined.
4 Test was terminated after phase I for chemical analysis of sample.

beds, the bed exhibiting the higher rate of $H_2O$ absorption also had the higher rate of $O_2$ evolution. For most of the tests, the rate of $O_2$ evolution peaked sooner for the $Ca(O_2)_2$ bed exhibiting the greater rate of absorption. When tests having the same reactor background temperature are compared, the ratio of $H_2O$ absorbed to $O_2$ evolved during phase I is fairly constant. In test, No. CaS-3, the reactor background temperature was lower than the inlet dew point of the test gas and condensation took place in the bed and the reactor during phase I, so no accurate correlation could be made between between the $H_2O$ absorbed and the $O_2$ evolved. In general, the $Ca(O_2)_2$ bed having the highest temperature maximum during phase I had the lowest $H_2O/O_2$ ratio. Apparently the utilization of $H_2O$ for the production of $O_2$ in the $Ca(O_2)_2$ beds is slightly more efficient at higher temperatures.

During phase II of the reaction of $Ca(O_2)_2$ beds with humidified $CO_2$, the overall absorption of $H_2O$ by the bed had a significant effect on the amount of $CO_2$ absorbed by the bed. When tests having the same reactor background temperature (25 or 37.5°C) are compared, the bed which absorbed the most $H_2O$ also absorbed the most $CO_2$ (table 4-7). Also, the bed which absorbed the most $H_2O$ during phase I exhibited the peak rate of $CO_2$ absorption sooner (tables 4-6 and 4-7). In addition, table 4-7 shows that most of the $CO_2$ was absorbed during phase II of each of the tests.

Overall, it is apparent from tables 4-6 and 4-7 that absorption of $H_2O$ by the $Ca(O_2)_2$ bed is the limiting factor in the release of $O_2$ and the absorption of $CO_2$ by the bed. When tests having the same reactor background temperature are compared, the bed which absorbed the most $H_2O$ also absorbed the most $CO_2$ and evolved the most $O_2$.

The bed in test No. CaS-4 had the poorest overall reactivity of all the $Ca(O_2)_2$ beds tested. This was the only bed composed of granules of $Ca(O_2)_2$ made by breaking up pellets of powder pressed to a bulk density of 0.92 $cm^3/g$. Photographs of the $Ca(O_2)_2$ powder using a scanning electron microscope (figure 2-5) had revealed that the powder possessed a very porous structure. It is postulated that pressing the powder may have collapsed some of this porous structure, with the result that less surface was available for reaction with $H_2O$ and $CO_2$.

The reaction behavior exhibited by $Ca(O_2)_2$ beds in contact with humidified $CO_2$ during phase I of the tests is postulated to occur as a result of the following reactions:

$$Ca(O_2)_2 + H_2O = Ca(OH)_2 + 3/2\ O_2 \qquad (4.1)$$

$$Ca(O_2)_2 + xH_2O = CaO_2 \cdot xH_2O + O_2 \qquad (4.2)$$

$$Ca(OH)_2 + yH_2O = Ca(OH)_2 \cdot yH_2O \quad (4.3)$$

$$Ca(OH)_2 \cdot yH_2O + CO_2 = CaCO_3 + (1+y)H_2O \quad (4.4)$$

$$CaO_2 \cdot xH_2O + (z-x)\ H_2O = CaO_2 \cdot zH_2O \quad (4.5)$$

$$CaO_2 + zH_2O = CaO_2 \cdot zH_2O \quad (4.6)$$

$$CaO_2 \cdot zH_2O + CO_2 = CaCO_3 + 1/2\ O_2 + 2H_2O \quad (4.7)$$

These equations were postulated based on two lines of evidence. First of all, it has been shown that anhydrous $CaO_2$ does not react with dry $CO_2$ (27) and tests in our laboratory indicate that $Ca(OH)_2$ also does not react with dry $CO_2$. Therefore, it is necessary for the anhydrous $CaO_2$ and $Ca(OH)_2$ to become hydrated via equations (4.3) and (4.6) before reaction with $CO_2$ occurs via equations (4.4) and (4.7). The extent of hydration necessary for $CO_2$ absorption to take place is not known. However, flow tests carried out on $Ca(OH)_2$ suggest that absorbed $H_2O$ on the $Ca(OH)_2$ powder may be having only a surface catalytic effect, since the amount of $H_2O$ that needs to be absorbed before $CO_2$ absorption occurs is very small. Equation (4.5) is included in the list of reactions because $CaO_2 \cdot xH_2O$ formed as the result of the reaction of $Ca(O_2)_2$ [eq. (4.2) may have to undergo additional hydration before reacting with $CO_2$, via equation (4.7).

The second line of evidence supporting the postulated reaction equations consisted of analytical data obtained on one of the $Ca(O_2)_2$ samples. Flow test No. CaS-6 was terminated at the end of phase I and the bed was analyzed immediately for $Ca(O_2)_2$, $CaO_2$, $Ca(OH)_2$, $CaCO_3$, and $H_2O$, using the pyrolytic analysis method described in Sec. 2.3.1.2. The composition of the sample after phase I is compared with the original sample composition in table 4-8. The increase in the amounts of both $Ca(OH)_2$ and $CaO_2$ at the expense of $Ca(O_2)_2$ upon reaction of the bed with humidified $CO_2$, suggests that water vapor is reacting with $Ca(O_2)_2$ according to equations (4.1) and (4.2). Previous work (3) has established that $Ca(O_2)_2$ reacts with liquid $H_2O$ at $0^oC$ according to equation (4.2) to form hydrated $CaO_2$ and release $O_2$. Since $Ca(OH)_2$ was formed upon exposure of the bed to water vapor, it is apparent that at temperatures greater than $0^oC$ (i.e., $>37.5^oC$ for test No. CaS-6), $Ca(O_2)_2$ reacts (to a significant degree) according to equation (4.1).

Table 4-8 shows that both the amounts of $CaO_2$ and $Ca(OH)_2$ increased by ~10 mole % during phase I. However, the data in table 4-8 also shows that significant $CO_2$ absorption took place during phase I, since there was an increase of ~21 mole % in the amount of $CaCO_3$ in the sample after this

Table 4-8.- A Comparison of the Chemical Compositions of a $Ca(O_2)_2$ [1] Bed Before and After Phase I [2] of the Reaction Period

| Chemical species | Before Phase I [3] | | After Phase I [4] | | |
|---|---|---|---|---|---|
| | Weight % | Mole % | Before heating sample to 110°C, weight % | After heating sample to 110°C, Weight % | Mole % |
| $Ca(O_2)_2$ | 55.65 | 47.03 | 7.01 | 7.31 | 5.69 |
| $CaO_2$ | 14.14 | 17.26 | 21.74 | 24.44 | 27.45 |
| $Ca(OH)_2$ | 29.71 | 35.27 | 37.04 | 41.10 | 44.91 |
| $CaCO_3$ | 0.50 | 0.44 | 24.46 | 27.15 | 21.96 |
| $H_2O$ | 0 | 0 | 9.75 | 0 | 0 |

1 Test No. CaS-6.
2 See text for explanation and demarcation of reaction phases.
3 Composition determined by method described in Sec. 2.3.1.1 of this report, $CaCO_3$ determined by pyrolytic analysis (Sec. 2.3.1.2).
4 Composition determined by pyrolytic analysis (Sec. 2.3.1.2).

period. It was postulated that the $CaCO_3$ was formed via equation (4.4) and/or (4.7) from $Ca(OH)_2$ and $CaO_2$ in the original sample. Since it was of interest to determine whether the reactions in equations (4.1) or (4.2) predominated during phase I, it was necessary to estimate the quantities of $Ca(OH)_2$ and $CaO_2$ that were consumed in producing $CaCO_3$ during this period. It was concluded that most of the $CaCO_3$ produced during phase I resulted from the reaction of $Ca(OH)_2$ with $CO_2$ [eq. (4.1)]; therefore, $Ca(OH)_2$ was the predominate $Ca(O_2)_2$-$H_2O$ reaction product. These conclusions were based on the following reasons:

(a) Recent flow-test data obtained in at the NASA Ames Research Center laboratory showed that $Ca(OH)_2$ exhibited a higher rate of $CO_2$ absorption than $CaO_2$ when each of the anhydrous species was reacted with humidified $CO_2$. Under reaction conditions (table 4-2) identical to that for test No. CaS-5 (except for an inlet test gas-flow rate of 50 SCCM), $Ca(OH)_2$ absorbed $CO_2$ at a maximum rate of 1.22 μmol/s/g. When $CaO_2$ (synthesized by dehydrating $CaO_2 \cdot 8H_2O$ in a dry nitrogen stream) was tested under conditions identical to Test No. CaS-5, the absorption rate of $CO_2$ was less than 0.2 μmol/s/g.

(b) However, $CaO_2 \cdot 8H_2O$ exhibited a $CO_2$ absorption rate of 1.14 μmol/s/g under the same reaction conditions used to test the $CaO_2$. The higher reactivity of $CaO_2 \cdot 8H_2O$ suggested that a higher extent of hydration of $CaO_2$ is necessary for it to be as reactive with $CO_2$ as $Ca(OH)_2$.

(c) During phase I of the tests, $Ca(OH)_2$ and $CaO_2$ originally in the bed before the test had to compete with $Ca(O_2)_2$ for $H_2O$ coming into the bed via the reactions in equations (4.3) and (4.5), to react with $CO_2$. A comparison of the rates of $O_2$ evolution and $CO_2$ absorption during phase I (table 4-6), and the amounts of $O_2$ evolved and $CO_2$ absorbed during phase I (table 4-7), showed that $O_2$ evolution via the reactions in equations (4.1) and (4.2) predominated over $CO_2$ absorption. This suggested that most of the water vapor entering the bed reacts with $Ca(O_2)_2$ (until the superoxide is consumed) and little $H_2O$ is available for hydration reactions. The fact that most of the $CO_2$ absorption took place during phase II, after the $Ca(O_2)_2$ component had reacted, is consistent with postulated competition between the $Ca(O_2)_2$, $CaO_2$ and $Ca(OH)_2$ components for incoming water vapor.

(d) Therefore, since $Ca(OH)_2$ apparently requires only traces of $H_2O$ to react with $CO_2$ while $CaO_2$ probably requires more extensive hydration, it is more likely that $Ca(OH)_2$ would absorb $CO_2$ when most of the $H_2O$ entering the bed is reacting with $Ca(O_2)_2$.

(e) Finally, $CO_2$ absorption continued during the latter part of phase I even after $O_2$ evolution ceased. This would not be the case if $CaO_2$ were reacting with $CO_2$ according to equation (4.7) since 1/2 mole of $O_2$ would be evolved for each mole of $CO_2$ absorbed.

If the above reasons are correct and most of the $CaCO_3$ was produced during phase I by consuming $Ca(OH)_2$, then the mole % composition data in table 4-8 suggests that $Ca(O_2)_2$ reacts predominantly according to equation (4.1). If it is assumed that all of the $CaCO_3$ produced during phase I of test No. CaS-6 came from consumption of $Ca(OH)_2$, then it is apparent from table 4-8 that three times as much $Ca(O_2)_2$ reacted via equation (4.1) than via equation (4.2).

The primary reactions occurring with humidified $CO_2$ during phase II of the tests were postulated to be those given in equations (4.4) and (4.7). Following the reaction of $H_2O$ with $Ca(O_2)_2$ during phase I, the bed continued to absorb $H_2O$ at a slower rate. During this time the $CaO_2$ and $Ca(OH)_2$ originally in the bed, and the amounts produced via the equations (4.1) and (4.2), were being hydrated according to equations (4.3), (4.5) and (4.6). As the hydrated $CaO_2$ and $Ca(OH)_2$ began to react with $CO_2$, water vapor and heat were released. These processes increased the local $pH_2O$ and bed temperature and thereby promoted further $CO_2$ absorption. The maximum bed temperature, $O_2$ evolution, and $CO_2$ absorption occurred simultaneously (e.g., fig. 4-3 and phase II rate data, table 4-7). The simultaneous occurrance of the maximum rates of $O_2$ evolution and $CO_2$ absorption suggested that the reaction in equation (4.7) was occurring. However, the ratio of the maximum rate of $CO_2$ absorption divided by the maximum rate of $O_2$ evolution (table 4-7, last column) ranged from 3.48 to 4.95. The expected $CO_2/O_2$ ratio from equation (4.7) was 2.00; therefore, it was apparent that both $CaO_2$ and $Ca(OH)_2$ were reacting with $CO_2$ [via eq. (4.4) and (4.7), respectively] at this point of phase II.

The minimum extent of hydration of $CaO_2$ necessary for the reactions in equations (4.4) and (4.7) to occur has not been reported in the literature. Therefore, it was important to determine the extent of hydration of $CaO_2$ at the end of phase I since this was just before the time when most of the $CO_2$ absorption took place. This determination of the extent of hydration was made by using the data in table 4-8. It was assumed that all of the water of hydration found in the test No. CaS-6 residue at the end of phase I was combined with the $CaO_2$ in the residue, (i.e., the $H_2O$ bound to $Ca(OH)_2$ is very small and can be neglected). If this assumption is made then the $CaO_2/H_2O$ molar ratio was 1:1.8 (table 4-8). This ratio suggests that the $CaO_2$ must be in the form of the dihydrate ($CaO_2 \cdot 2H_2O$) before absorbing $CO_2$ during phase II.

### 4.3.2 Reactivity of $KO_2$ with $CO_2$ and $H_2O$

#### 4.3.2.1 Tests on Small Laboratory Fabricated $KO_2$ Granules

Figure 4-4 is a plot of the bed temperature and partial pressures of $O_2$, $CO_2$, and water vapor downstream from the $KO_2$ bed, as a function of reaction time, for the first 4 ks of test No. KS-3. The first 1.5 ks of the plotted data was taken when the $KO_2$ bed was exposed to a stream of dry test gas containing 5% $CO_2$ and 95% nitrogen. Visual observations of the bed during this period revealed a white band which moved down through the bed as the test progressed. When the front of the white band reached each of the two thermocouple probe tips a temperature maximum was recorded. By the time the white band approached the bottom of the bed, $pO_2$ downstream had begun to fall and $pCO_2$ had begun to rise. By the end of 1.5 ks of reaction time, $pCO_2$, $pO_2$, and $pH_2O$ levels, as well as the bed temperature, were very close to dry-test-gas background levels. The general features of the first 1.5 ks of plotted data in fig. 4-4 are representative of of the data collected during the dry mode portion of test No. KS-6.

The next 2.5 ks of data shown in figure 4-4 is the response of the $KO_2$ bed to the humidified stream of test gas. The general features of the plotted data after 2.5 ks are representative of the data collected for tests Nos. KS-1, KS-2, and KS-4 - KS-6 which did not include the dry-test-gas purge mode.

DRY-TEST-GAS REACTION WITH $KO_2$ - Since it had been reported that $KO_2$ does not react with dry $CO_2$ (46), at first the reaction behavior of the $KO_2$ bed observed during exposure to dry $CO_2$ was rather surprising. However, the dry-mode reaction phenomena are believed to arise from the reaction of the KOH impurity in the $KO_2$ samples with dry $CO_2$ in the test gas. It was postulated that the following set of reactions occurred during the dry-mode reaction period:

$$2KOH + CO_2 = K_2CO_3 + H_2O \qquad (4.8)$$

$$H_2O + 2KO_2 = 2KOH + 3/2O_2 \qquad (4.9)$$

$$KOH + CO_2 = KHCO_3 \qquad (4.10)$$

$$H_2O + K_2CO_3 = 2(K_2CO_3 \cdot 1/2H_2O) \qquad (4.11)$$

$$3H_2O + 2K_2CO_3 = 2(K_2CO_3 \cdot 3/2H_2O) \qquad (4.12)$$

The reactions given in equations (4.8) and (4.9) were the primary reactions involved in producing the dry-mode reaction behavior of the $KO_2$ bed, and they explain the precipitous drop in $pCO_2$ and the concurrent rise in $pO_2$ seen during the first 1.5 ks of the test. Figure 4-5 illustrates

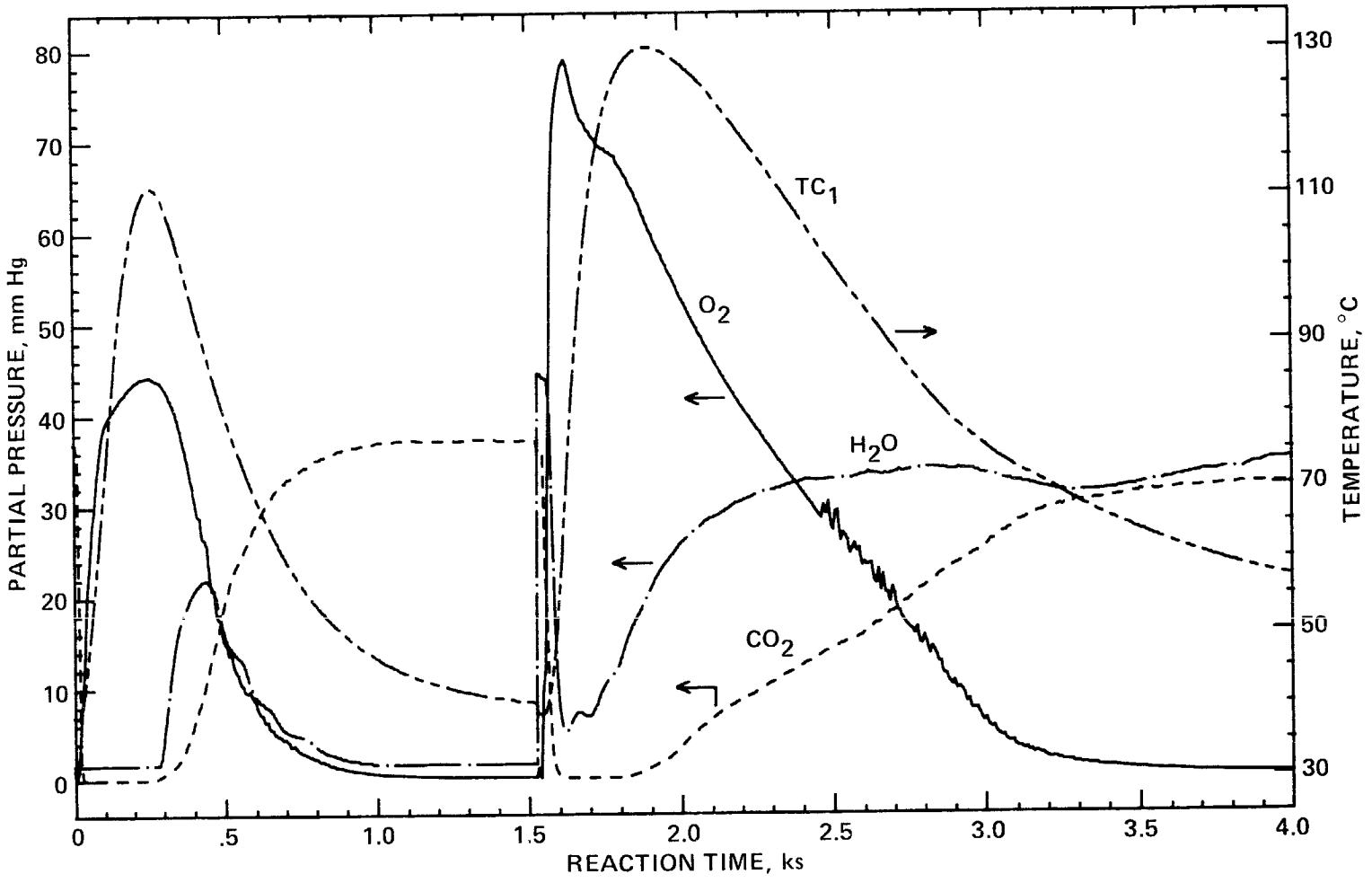


Figure 4-4.- Reaction of $KO_2$ with dry and humidified test gas (test No. KS-3). Partial pressure of $O_2$, $CO_2$ and $H_2O$ and bed temperature as a function of reaction time. 

graphically the postulated dry-mode reactions of $KO_2$. Carbon dioxide in the dry test gas first reacted with KOH impurity at the entrance of the $KO_2$ bed, forming $K_2CO_3$, and releasing $H_2O$. $K_2CO_3$ gave rise to the white coloration of the bed. The $H_2O$ released by the reaction in equation (4.8) could then react with $KO_2$ by equation (4.9). The reaction of equation (4.9) formed additional KOH which could react via equation (4.8), forming additional $K_2CO_3$ and $H_2O$. The reactions of equations (4.8) and (4.9) continued until water vapor generated by reaction of equation (4.8) was removed by either; (a) forming stable hydrates of $K_2CO_3$, as in the reactions of equations (4.11) and (4.12); or (b) being swept out of the bed by the flowing test gas. In addition, KOH originally present in the sample or produced by the reaction of equation (4.9) could react [via eq. (4.10)] forming $KHCO_3$. This reaction did not release $H_2O$ for the continuation of the reaction represented by equation (4.9).

Therefore the explanation of the dry-mode test phenomena described previous is consistent with the earlier published observation that the reaction of $KO_2$ with $CO_2$ does not proceed without the presence of $H_2O$ (46). In the test described here, once the $H_2O$ stored in the bed as KOH had been removed, no further reaction of $KO_2$ with the $CO_2$ occurred.

Table 4-9 lists the amounts of $O_2$ evolved, $CO_2$ absorbed, and $H_2O$ absorbed and evolved by the first three $KO_2$ beds which were tested. It was of interest to determine the relative amounts of $K_2CO_3$ and $KHCO_3$ which were produced during the dry-mode reaction period. Determination of the amount of $KHCO_3$ in a sample containing an equal or greater amount of KOH is not possible by wet chemical methods since the KOH reacts with the $KHCO_3$ to form $K_2CO_3$ when the sample is dissolved. Since the unreacted $KO_2$ in the sample is converted to KOH upon making a solution of the sample in $H_2O$, another method of determining the $KHCO_3$ content was required. Using the data in table 4-9 for the dry-mode portion of test No. KS-3, it was possible to estimate the original amount of KOH in the $KO_2$ sample and the amounts of $K_2CO_3$ and $KHCO_3$ which were produced by the reactions represented by equations (4.8) and (4.10). The calculation was made as follows:

(a) The total amount of KOH available for reaction with $CO_2$ during the 1.5 ks of the dry-test-gas purge [KOH(total)] is equal to the KOH originally present in the bed [KOH(original)] and the KOH produced [KOH(produced)] as a result of the reaction given in equation (4.8);

$$KOH(total) = KOH(original) + KOH(produced) \quad (4.13)$$

(b) From the stoichiometry of equation (4.8),

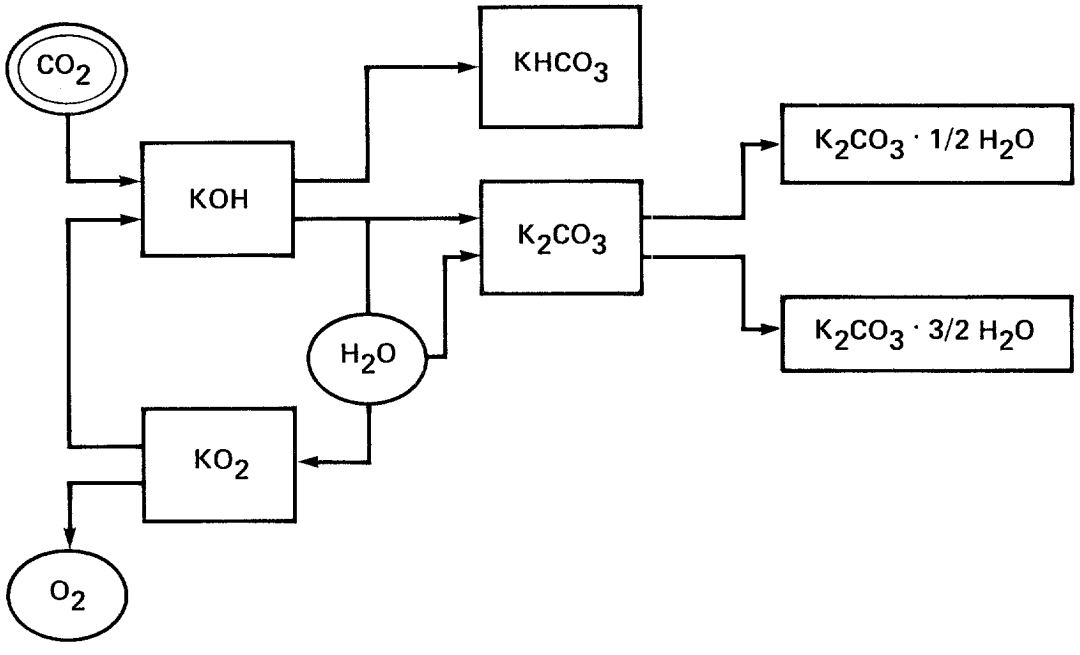


Figure 4-5.- Reaction pathways for the dry-mode reaction of $KO_2$.

Table 4-9.- Amounts of $O_2$ Evolved, $CO_2$ Absorbed, and Water Vapor Absorbed and Evolved During Reaction of $KO_2$ Beds with Dry and Humidified $CO_2$ (Test Nos. KS-1 - KS-3)

| Test No. | Mode of reaction [1] | $O_2$ evolved | | $CO_2$ absorbed | | | $H_2O$ absorbed, $cm^3$ STP/g | $H_2O$ evolved, $cm^3$ STP/g |
|---|---|---|---|---|---|---|---|---|
| | | $cm^3$ STP/g | % $O_2$ available in bed [2] | $cm^3$ STP/g | % bed capacity as $K_2CO_3$ | % bed capacity as $KHCO_3$ | | |
| KS-1 | humid | 203.2 | 100.9 | 175.8 | 107.3 | 53.6 | 117.7 | ND |
| KS-2 | humid | 207.1 | 99.7 | 145.4 | 87.4 | 44.7 | 200.0 | ND |
| KS-3 | dry | 49.0 | 23.6 | 53.9 | 33.1 | 16.6 | 0 | 13.8 |
| | humid | 155.9 | 75.0 | 119.4 | 73.4 | 36.7 | 107.8 | ND |
| KS-3 | total | 204.9 | 98.6 | 173.3 | 106.5 | 53.3 | 107.8 | 13.8 |

[1] See text for explanation of reaction modes.
[2] Calculations based on theoretical capacities given in table 4-5.
ND = not determined.

KOH(produced) is equal to one and one-third times the total amount of $O_2$ evolved during the dry mode;

$$KOH(produced) = 4/3\ O_2(evolved) \qquad (4.14)$$

(c) If it is assumed that all of the KOH present or produced in the bed reacts with $CO_2$, then, according to equations (4.8) and (4.9);

$$KOH(produced) = 2\ K_2CO_3 + KHCO_3 \qquad (4.15)$$

This is a reasonable assumption since the dry mode portion of the test was ended only after the concentrations of $CO_2$ entering and exiting the bed were equal. The total amount of $CO_2$ absorbed during the dry mode is distributed between $K_2CO_3$ and $KHCO_3$;

$$CO_2(absorbed) = KHCO_3 + K_2CO_3 \qquad (4.16)$$

(d) Finally, the total amount of $H_2O$ released via equation (4.8) [$H_2O$(total)] is distributed between $H_2O$ that is evolved from the bed [$H_2O$(evolved)], $H_2O$ tied up in hydrates of $K_2CO_3$ [$H_2O$(hydrates)] and $H_2O$ combined in $KHCO_3$ [$H_2O$(in $KHCO_3$)];

$$H_2O(total) = H_2O(evolved) + H_2O(hydrates) + H_2O(in\ KHCO_3) \qquad (4.17)$$

$H_2O$(in $KHCO_3$) is equal to the amount of $KHCO_3$ produced divided by 2;

$$H_2O(in\ KHCO_3) = KHCO_3/2 \qquad (4.18)$$

To solve equations (4.13-4.18) for $KHCO_3$, $K_2CO_3$ and KOH(original), it was necessary to assume that hydrate formation via equations (4.11) and (4.12) was negligible; therefore, $H_2O$(hydrates) ~0. This assumption was reasonable since the temperature of the reaction front as it moved through the $KO_2$ bed during the dry-test-gas purge was close to the decomposition temperature of the hydrates (100-130°C). When $K_2CO_3$ hydrates were assumed to be absent, it was calculated that the bed originally contained 8.78% KOH and that 6.23 formula weights of $K_2CO_3$ were produced for every formula weight of $KHCO_3$. The ratio of $K_2CO_3/KHCO_3$ in the sample after the dry mode reaction period was not surprising since $KHCO_3$ begins to decompose above ~100 and the reaction front temperature recorded by the thermocouples was as high as 111°C (fig. 4-4).

Once the amount of $KHCO_3$ produced during the dry mode reaction was calculated, it was possible to determine the proportion of water vapor that was evolved by the bed using equation (4.17). It was determined that 79% of the $H_2O$

released via equation (4.8) was evolved from the bed. It was of interest to calculate the maximum number of times the $H_2O$ originally stored in the sample as KOH impurity was "recycled" (absorbed and released) as the reaction front moved through the $KO_2$ bed. The maximum amount of $H_2O$ recycling that took place was calculated by dividing the amount of $O_2$ evolved from the bed by the amount expected if the quantity of $H_2O$ that was evolved by the bed reacted according to equation (4.9). Based on the data in table 4-9 for the dry-mode portion of test No. KS-3, the maximum number of times a molecule of $H_2O$ reacts with the $KO_2$ bed is 2.36.

REACTION OF $KO_2$ WITH HUMIDIFIED TEST GAS - Table 4-10 lists the maximum rates of $O_2$ evolution, $CO_2$ absorption, and $H_2O$ absorption and evolution observed for the first seven $KO_2$ beds which were tested. The rate data were calculated in terms of μmols/s. The rate data for the $KO_2$ beds were not normalized with respect to bed weight as had been done with the $Ca(O_2)_2$ beds (Sec. 4.3.1). Normalization of the rates with respect to bed weights was not done since with $KO_2$ beds it was determined that only a small portion of the beds had reacted by the time the maximum rates were observed. In addition, all the $KO_2$ beds (unlike the $Ca(O_2)_2$ beds) were similar in weight and were reacted at the same test gas-flow rate.

Several general trends become apparent when the rate data in table 4-10 for the humid mode test periods are compared, and the reaction conditions for the tests listed in table 4-3 are consulted:

(a) The differences in the maximum rates of $H_2O$ absorption reflected the differences in $pH_2O$ entering the beds. Three inlet-test-gas dew points were tested; 24°C, 25°C and 37°C ($pH_2O$ = 22.4, 23.8 and 47.0 mm Hg, respectively). In general, the $H_2O$ absorption rate increased with $pH_2O$.

(b) The maximum rate of $CO_2$ absorption was essentially the same for the first six $KO_2$-bed tests (in test No. KS-7, there was no $CO_2$ in the test gas). This was because the maximum rate of $CO_2$ absorption before $CO_2$ breakthrough was a function of the flow rate and $pCO_2$ of the test gas entering the bed and these two parameters were identical for all the tests listed in table 4-10 (except No. KS-7).

(c) The differences in the maximum rates of $O_2$ evolution also reflected the differences in $pH_2O$ entering the beds. In general, the maximum rate of $O_2$ release increased as a function of the inlet $pH_2O$. The major exception to this general trend was test No. KS-7 which had a much lower $O_2$ release rate than the other beds tested at the same inlet $pH_2O$ (e.g., KS-5 and KS-6). The reaction behavior of the bed in test No. KS-7 will be examined later.

The physical properties of the $KO_2$ beds at the end of the flow tests also appeared to be a function of the inlet

Table 4-10.- Maximum Rates of $O_2$ Evolution, $CO_2$ Absorption, and Water Vapor Absorption and Evolution During Reaction of $KO_2$ Beds with Dry and Humdified $CO_2$

| Test No. | Mode of reaction[1] | $O_2$ evolution, μmol/s | $CO_2$ absorption, μmol/s | $H_2O$ absorption, μmol/s | $H_2O$ evolution, μmol/s | Ratio of $CO_2/O_2$ |
|---|---|---|---|---|---|---|
| KS-1 | humid | 15.75 | 10.43 | 4.98 | ND | 0.661 |
| KS-2 | humid | 20.27 | 10.42 | 12.92 | ND | 0.514 |
| KS-3 | dry | 12.19 | 10.48 | 0 | 5.65 | 0.861 |
| | humid | 22.87 | 10.42 | 12.07 | ND | 0.456 |
| KS-4 | humid | 21.65 | 10.41 | 13.26 | ND | 0.481 |
| KS-5 | humid | 17.40 | 10.43 | 6.60 | ND | 0.599 |
| KS-6 | dry | 13.98 | 10.42 | 0 | 8.08 | 0.745 |
| | humid | 14.40 | 10.25 | 5.37 | ND | 0.782 |
| KS-7 | humid | 2.81 | 0 | 6.62 | ND | 0 |

[1] See text for explanation of reaction modes.
ND = not determined.

$pH_2O$. The $KO_2$ granules which had been exposed to test gas with a dew point of 37°C ($pH_2O$ = 47 mm Hg) were soft and mushy at the end of the test. In the case of test No. KS-4, which had the smaller granule size range of the high dew-point tests (table 4-3), the granules had fused and coalesced to the point that the bed became completely plugged after only 1.0 ks of reaction. However, $KO_2$ granules which had been exposed to test gas with dew points of 24 or 25°C ($pH_2O$ = 22.4 or 23.8 mm Hg) were hard and only slightly fused together at the end of the test. It was postulated that the differences in the physical properties of the granules were a result of the ratio of $pH_2O/pCO_2$ in the test gas. This ratio determined whether the rate of KOH production via equation (4.9) exceeded the rate of KOH consumption via reaction with $CO_2$ [eqs. (4.8) and (4.10)]. If KOH production exceeded consumption, then the excess KOH could undergo hydration reactions such as

$$KOH + H_2O = KOH \cdot H_2O \qquad (4.19)$$

$$KOH + 3/4H_2O = KOH \cdot 3/4H_2O \qquad (4.20)$$

$$KOH + 2H_2O = KOH \cdot 2H_2O \qquad (4.21)$$

These hydrated KOH products were postulated to be the cause of the intergranule fusion and the soft, mushy consistency of the granules exposed to the highest $pH_2O/pCO_2$ ratio. When the rates of KOH production and consumption were similar in magnitude, then the amount of excess KOH would be small and the principal hydrate species formed on the granule surfaces would be those produced via equations (4.11) and (4.12). Unlike hydrated KOH, hydrated $K_2CO_3$ does not fuse or melt even upon prolonged exposure to water vapor.

The $O_2$ and $CO_2$ rate data in table 4-10 were used to calculate the maximum rates of KOH production and consumption for each of the $KO_2$ beds. These calculated rates are given in table 4-11. The values in table 4-11 were calculated based on the following reasoning.

(a) The rate of KOH production was assumed to be directly proportional to the rate of $O_2$ release. The stoichiometry of equation (4.9) gave the following relationship between the rates of $O_2$ and KOH production:

$$d(KOH)/dt = 4/3 \times d(O_2)/dt \qquad (4.22)$$

where $d(KOH)/dt$ and $d(O_2)/dt$ are the rates expressed in terms of umol/s.

(b) Potassium hydroxide can be consumed by reaction with $CO_2$ via either equation (4.8) or (4.10). For the comparison of the rates of KOH production and consumption given in table 4-11, the KOH was assumed to be consumed

Table 4-11.- Maximum Rates of KOH Production and Consumption During Reaction of $KO_2$ Beds with Dry and Humidified $CO_2$

| Test No. | Mode of reaction [1] | Mole ratio of $H_2O/CO_2$ in inlet test gas | KOH production, d(KOH)/dt, μmol/s | KOH consumption, -d(KOH)/dt, umol/s | |
|---|---|---|---|---|---|
| | | | | $K_2CO_3$ as product | $KHCO_3$ as product |
| KS-1 | humid | 0.589 | 21.00 | 20.86 | 10.43 |
| KS-2 | humid | 1.24 | 27.03 | 20.84 | 10.42 |
| KS-3 | dry | 0 | 16.25 | 20.96 | 10.48 |
| | humid | 1.24 | 30.49 | 20.84 | 10.42 |
| KS-4 | humid | 1.24 | 28.87 | 20.82 | 10.41 |
| KS-5 | humid | 0.625 | 23.20 | 20.86 | 10.43 |
| KS-6 | dry | 0 | 18.64 | 20.84 | 10.42 |
| | humid | 0.625 | 19.20 | 20.50 | 10.25 |
| KS-7 | humid | NAp [2] | 3.75 | 0 | 0 |

[1] See text for explanation of reaction modes.
[2] No $CO_2$ in test gas, NAp = not applicable.

exclusively either by equation (4.8) producing $K_2CO_3$ or by equation (4.10) producing $KHCO_3$. The stoichiometry of equations (4.8) and (4.9) gave the following relationships between the rates of $CO_2$ absorption, $K_2CO_3$ or $KHCO_3$ production and KOH consumption:

$$-d(KOH)/dt = 2 \times d(K_2CO_3)/dt = 2 \times d(CO_2)/dt \quad (4.23)$$

or

$$-d(KOH)/dt = d(KHCO_3)/dt = d(CO_2)/dt \quad (4.24)$$

It was shown previously that ~6 times as much $K_2CO_3$ was formed than $KHCO_3$ during the dry mode reaction of $KO_2$. The predominance of the $K_2CO_3$-forming, KOH-$CO_2$ reaction pathway was also expected during the period when the maximum humid-mode reaction rates were observed since the high temperature of the bed (>100°C) was unfavorable towards the formation of $KHCO_3$.

The data compiled in table 4-11 supports the postulate that the formation of excess KOH (and subsequently, hydrated KOH) was the cause of the differences in physical properties between the various reacted $KO_2$ samples. For the tests in which the ratio of $H_2O/CO_2$ in the test gas was high (i.e., test Nos. KS-2, KS-3 and KS-4), the rate of KOH production was much larger than the rate of consumption via the formation of $K_2CO_3$. As was mentioned previously, the $KO_2$ granules from these tests were highly fused and very soft. For the other humid mode tests (except KS-6), the rates of KOH production were only slightly higher than the rates of KOH consumption. The beds in these tests were moderately fused and but the reacted granules were hard. For the dry mode portion of test No. KS-3 and for both the dry and humid modes of KS-6 the rates of KOH production were slightly lower than KOH consumption via the formation of $K_2CO_3$. In these tests some KOH was being consumed by the formation of $KHCO_3$.

The $KO_2$ test results described here give insight into how to minimize two fundamental problems which occur when $KO_2$ is used as the air revitalization chemical in portable life support systems such as SCSRs. These problems have been discussed previously in Sec. 1.2. The first problem with $KO_2$ is that it overproduces $O_2$ relative to the amount of $CO_2$ it absorbs. This overproduction of $O_2$ is theoretically expected if $K_2CO_3$ is the principal $CO_2$ reaction product. In actual use, the overproduction of $O_2$ is greater than is theoretically predicted. By comparing the last column in table 4-10 and the third column of table 4-11 it can be seen that the ratio of the maximum rates of $CO_2$ absorption to $O_2$ evolution increased as the mole ratio of $H_2O/CO_2$ in the test gas decreased. The highest $CO_2/O_2$ rate ratios were observed

during the dry mode portions of test Nos. KS-3 and KS-6. The only source of water vapor to drive the reaction in equation (4.9) during the dry mode came from the reaction of KOH with $CO_2$ to produce $K_2CO_3$ [eq. (4.8)]. Once this $H_2O$ was evolved from the bed, $O_2$ evolution and $CO_2$ absorption ceased. The lowest ratio of $CO_2/O_2$ was seen for the tests having $H_2O/CO_2$ ratios of 1.24. These results suggest that inlet $H_2O/CO_2$ ratios lower than ~0.6 would probably decrease the overproduction of $O_2$ without affecting the rate of $CO_2$ absorption.

The data in table 4-12 also show that a decrease in the inlet $H_2O/CO_2$ ratio increased the ratio of the volumes of $CO_2$ absorbed/$O_2$ evolved. Table 4-12 lists the volumes of $O_2$ evolved, $CO_2$ and $H_2O$ absorbed and $H_2O$ evolved for test Nos. KS-4 - KS-7. These tests were conducted using identical reaction conditions except for inlet test-gas dew point, and, in the case of test No. KS-7, the absence of $CO_2$ in the test gas (table 4-3). The data are listed for two time ranges during the tests; 0.00-0.72 ks and 0.0-2.0 ks. The first time range was selected because it was the range over which useful data was obtained for test No. KS-4 before the $KO_2$ bed became plugged. The second time range encompassed the duration of the dry mode reactions of test No. KS-6 and the entire reaction period of test No. KS-7. Using data from these two time ranges allowed for the maximum comparison of the four tests.

When the 0.72 ks columns of table 4-12 are examined, it is apparent that the $KO_2$ beds in test Nos. KS-4 - KS-6 absorbed nearly identical amounts of $CO_2$ but differed significantly in the amount of $O_2$ they released. The amounts of $O_2$ evolved decreased and the $CO_2/O_2$ ratio increased as the inlet $H_2O/CO_2$ ratio was decreased (consult column 3, table 4-11 for the $H_2O/CO_2$ ratios). This relationship between the inlet $H_2O/CO_2$ ratio and the $CO_2/O_2$ ratio again suggests that $H_2O/CO_2$ ratios lower than ~0.6 would decrease the amount of excess $O_2$ produced without decreasing the $CO_2$ scrubbing efficiency of the $KO_2$ bed.

Test No. KS-7 examined the effect of "very large" $H_2O/CO_2$ ratios, since there was no $CO_2$ present in the test gas. In this limiting case, there was a dramatic difference in the reaction behavior exhibited by the $KO_2$ bed. The differences between the bed in test No. KS-7 and the beds in test Nos. KS-4 - KS-6 are as follows.

(a) The rate of $O_2$ evolution was 1/6 that for test No. KS-5 which was tested with the same inlet test-gas dew point (table 4-10).

(b) The $KO_2$ granules gradually turned white and melted together as $H_2O$ was absorbed from the bed. The reacted portion of the bed shrunk into a single plug of hydrated KOH.

(c) Water vapor had not broken through the bed when the

Table 4-12.- Volumes of $O_2$ Evolved, $CO_2$ Absorbed, and Water Vapor Absorbed and Evolution During Reaction of $KO_2$ Beds with Dry and Humidified $CO_2$ (Test Nos. KS-4 - KS-7)

| Test No. | Mode of reaction[1] | Gas evolved or absorbed (after elapsed reaction time), $cm^3$ STP/g bed | | | | | | | | | |
|---|---|---|---|---|---|---|---|---|---|---|---|
| | | $O_2$ evolved | | $CO_2$ absorbed | | $H_2O$ absorbed | | $H_2O$ evolved | | ratio of $CO_2/O_2$ | |
| | | 0.72 ks | 2.0 ks | 0.72 ks | 2.0 ks | 0.72 ks | 2.0 ks | 0.72 ks | 2.0 ks | 0.72 ks | 2.0 ks |
| KS-4[2] | humid | 109.2 | NAp | 60.1 | NAp | 72.6 | NAp | ND | NAp | 0.550 | NAp |
| KS-5 | humid | 93.4 | 184.8 | 60.3 | 139.6 | 34.5 | 43.2 | ND | ND | 0.645 | 0.755 |
| KS-6 | dry | 69.4 | 79.9 | 59.8 | 75.8 | 0 | 0 | 6.2 | 19.4 | 0.862 | 0.949 |
| KS-7 | humid | 11.7 | 38.8 | 0 | 0 | 35.5 | 103.9 | ND | ND | 0 | 0 |

[1] See text for explanation of reaction modes.
[2] Test was terminated after 1 ks.
NAp = not applicable, ND = not determined.

test was terminated at 2.0 ks. After 2.0 ks of reaction, the bed had absorbed 2.4 times the amount of $H_2O$ as the bed in test No. KS-5 (table 4-12). Both beds were exposed to the same test gas-dew point (table 4-3).

(d) The temperature of the bed reached a maximum of only 64°C. In the other tests, maximum temperatures of 135-173°C were attained (table 4-13).

The reaction behavior of the bed in test No. KS-7 led to an important conclusion. It seemed apparent that $KO_2$ cannot be used efficiently as an $O_2$ source apart from also being used as a $CO_2$ scrubber. It was postulated that the KOH-$CO_2$ reaction is necessary both to supply heat to drive the $KO_2$-$H_2O$ reaction and to maintain the structure and reactive surface area of the $KO_2$ granules. The primary reactions of $KO_2$ with water vapor and $CO_2$ [eqs. (4.8) and (4.9)] are exothermic. However, the KOH-$CO_2$ reaction releases 33.7 kcal/gm mole while the $KO_2$-$H_2O$ reaction releases 1/3 that amount (9.7 kcal/gm mole). The KOH hydration reactions also release heat. The reactions given in equations (4.19), (4.20) and (4.21) release 16.6, 20, and 33.8 kcal/gm mole, respectively. However, in the absence of $CO_2$ the $KO_2$ granules fuse into a mass of hydrated KOH. The decrease in active surface of $KO_2$ available for reaction and the diffusion barrier presented to the $H_2O$ reactant by the hydrated KOH layer on the granules both contribute to a decrease in the rate of $O_2$ evolution.

The second problem which occurs when $KO_2$ is used as the air revitalization chemical in portable life support systems is that the utilization efficiency of the available $O_2$ and $CO_2$ scrubbing capacity is as low as 50%. In the tests described here it appeared that low utilization efficiency was a result of the formation of a fused hydroxide coating on the granules. For example, in test No. KS-4, the extent of utilization of the $O_2$ capacity was only ~52% since the bed became completely plugged shortly after 0.72 ks of reaction (tables 4-12 and 4-5). In contrast to this low-utilization efficiency, the bed in test No. KS-5 did not plug and continued to evolve $O_2$ after 0.72 ks. It had an $O_2$ utilization efficiency of 89% by 2.0 ks. The only difference between the reaction conditions of these two tests was that the inlet $H_2O/CO_2$ ratio in test No. KS-5 was 1/2 that in test No. KS-4 (table 4-11). The higher $H_2O/CO_2$ ratio for test No. KS-4 resulted in the formation of a significant excess of KOH which became hydrated and fused.

#### 4.3.2.2 Tests on Breathing-Canister-Size $KO_2$ Tablets and Granules

It has been reported that the $O_2$ utilization efficiency of the $KO_2$ in SCSRs ranges from 50-85% (18,8). However, no information concerning utilization efficiency of state-of-

Table 4-13.- Maximum Temperatures Recorded by Thermocouples in $KO_2$ Beds During Reaction with Dry and Humidified $CO_2$

| Test No. | Thermocouple No. 1[1] | | Thermocouple No. 2[2] | |
|---|---|---|---|---|
| | Time, ks | Temperature, °C | Time, ks | Temperature, °C |
| KS-1 | 0.18 | 100 | 0.30 | 117 |
| KS-2 | 0.32 | 136 | 0.52 | 124 |
| KS-3 | 0.14 | 95 | 0.26 | 111 |
| KS-4 | 0.46 | 173 | 0.83 | 170 |
| KS-5 | 0.29 | 149 | 0.66 | 155 |
| KS-6 | 0.16 | 135[3] | 0.41 | 160[3] |
| KS-7 | 2.00[4] | 64 | 2.00[4] | 58 |

1 Thermocouple tip was 3.0 cm from bottom face of bed.
2 Thermocouple tip was 1.5 cm from bottom face of bed.
3 Temperature is for dry mode reaction only.
4 Temperature of thermocouple was still rising slowly when test was terminated.

the-art $KO_2$-based SCSRs was found in the literature. An analysis of two commercially available $KO_2$-based SCSRs indicated that the canisters contain about twice as much $KO_2$ than is necessary to meet the $O_2$ requirement of the 95% percentile coal miner engaged in 60 min of escape activity (Sec. 6.2). A recent paper in which these devices were tested using human subjects and a breathing machine simulator indicated that the devices generally met or exceeded the 60 min. of required operation while performing test No. 4 of CFR Title 30 (11).

For these manned SCSR tests, the utilization efficiency of the bed would theoretically be determined by analyzing the $KO_2$ in the bed after one of the following criteria had been met:

1. The inhaled $CO_2$ concentration was >1.5%.
2. The $O_2$ concentration fell below 19%.
3. The breathing bag collapsed due to a lack of $O_2$ generation.
4. The device had exceeded the target use period of 60 min operation.

Criteria Nos. 1-3 could occur before reaching the 60 min of required operation. No work has been reported in which this evaluation of $KO_2$ utilization efficiency has been done.

Therefore, it was important to estimate experimentally the extent of utilization of the $O_2$ evolution and $CO_2$ absorption capacities of the $KO_2$ in these SCSRs when the tablets or granules of $KO_2$ were tested for 60 min under flow conditions which approximated those existing in a SCSR during escape activities. The flow system used in these experiments limited the size of the $KO_2$ bed that could be tested. Beds with cross sections approaching those in the SCSRs would require flow rates of up to 100 l/min to simulate the flow conditions existing during manned tests. The equipment required to match the variations in exhalation gas velocity and $CO_2$ concentration which would be seen by a $KO_2$ bed (on a breath-by-breath time scale) in a manned SCSR was also not available. Because of the limitations of the laboratory flow system, small beds were tested for 60 min under conditions giving the average bed-face velocity which would be seen by $KO_2$ in an SCSR.

The flow-system tests conducted during this preliminary study were carried out on $KO_2$ material taken from new Drager and MSA 60 min SCSRs. All the tests were carried out using a flow rate giving a bed face velocity approximating the average value expected for the SCSR beds tested under the conditions listed in Title 30 of the CFR (11) [table 4-3, test Nos. KS-8 - KS-11]. Potassium superoxide from each of the two SCSRs was tested at dew point levels of 24o and 37°C. The tablets or granules of $KO_2$ were loaded into the same 1.06-cm-i.d. reactor that was used for the tests on

$Ca(O_2)_2$ and smaller granules of $KO_2$ (Sec. 4.2.1). When the large granules or tablets of $KO_2$ were tested in this small diameter reactor, breakthrough of $CO_2$ from the bed occurred almost immediately after the test was begun. However, since the goal of the test was to estimate the extent of utilization of the $KO_2$ after 60 min of reaction, the test was continued until 60 min had elapsed. After breakthough of $CO_2$, $pO_2$ steadily decreased and $pCO_2$ steadily increased.

During the flow tests, the $KO_2$ tablets taken from the Drager SCSR gradually turned from an initial greenish yellow to a brownish gray color with black blotches. $KO_2$ granules from the MSA SCSR turned from bright yellow to white. Immediately following each of the tests, the $KO_2$ granules or tablets were removed from the reactor and cut in half with a spatula. The tablets from the Drager device had a hard gray shell covering a softer yellow-green center, while the MSA granules had a white coating which covered a canary-yellow center. The product coating on both the granules and tablets could be easily broken away from the unreacted centers.

Table 4-14 gives the amounts of $O_2$ evolved and $CO_2$ absorbed by the $KO_2$ beds during the flow tests. Table 4-3 lists the inlet dew points used during the tests.It is apparent that the utilization efficiency of both types of $KO_2$ decreased upon exposure to an inlet water vapor dew point of 37°C, although the effect was greater in the case of the tablets taken from the Drager SCSR. Under the conditions most closely simulating those seen by $KO_2$ in manned SCSRs, (i.e., inlet water-vapor dew point of 37°C), the $O_2$ utilization efficiency for both types of $KO_2$ was below 70%.

As mentioned previously, the reaction conditions used here were different than those which would be seen by $KO_2$ in the bed of a SCSR during man testing. However, it was postulated that the differences in reaction conditions (i.e., size of the $KO_2$ bed, peak flow velocities, breath-by-breath flow velocity and gas composition variations) would only result in a further decrease in the utilization efficiency of the $KO_2$. This postulate is based on several factors.

First, it was shown previously (Sec. 4.3.2.1) that the formation of KOH hydrates on the $KO_2$ granules affects the utilization efficiency of the $KO_2$. The extent that hydration reactions of KOH can occur in a $KO_2$ bed was found to be dependent on the ratio of the partial pressures of $H_2O$ and $CO_2$ entering the bed. In the case of a SCSR, $pH_2O$ is constant at 47 mm Hg. This value for $pH_2O$ corresponds to the dew point of the lungs; i.e., 37°C. However, the $pCO_2$ varies from $pCO_2$ in the dead-space volume of the lungs to ~40 mm Hg ($pCO_2$ of the lung alveolar volume) depending on the extent of the exhalation. The partial pressure of $CO_2$ in the lung

Table 4-14.- Amounts of $O_2$ Evolved and $CO_2$ Absorbed During Reaction of $KO_2$ Beds with Humidified $CO_2$ (Test Nos. KS-8 - KS-11)

| Test No. | $O_2$ evolved[1] | | $CO_2$ absorbed[1] | |
|---|---|---|---|---|
| | $cm^3$ STP/g | % bed capacity[2] | $cm^3$ STP/g | % bed capacity[3] |
| KS-8 | 137.6 | 76.3 | 102.2 | 61.0 |
| KS-9 | 123.8 | 68.7 | 71.9 | 42.9 |
| KS-10 | 136.0 | 62.6 | 118.2 | 73.4 |
| KS-11 | 132.8 | 61.1 | 95.1 | 59.0 |

1 After 3.6 ks of reaction time.
2 Calculations based on the theoretical capacities given in table 4-5.
3 Calculations based on the theoretical capacities given in table 4-5 and $K_2CO_3$ being the sole $CO_2$ reaction product.

dead space volume is dependent on the concentration of $CO_2$ in the breathing bag of the SCSR (e.g., 0-3.8 mm Hg). Therefore, during each exhalation, the ratio of $pH_2O/pCO_2$ entering the $KO_2$ bed would go from a very large value (at least 10) down to about 1.2. The initially high $H_2O/CO_2$ ratio would result in the extensive formation of fused hydroxide coatings. In the tests described here, the inlet $H_2O/CO_2$ ratio was constant at either 0.589 or 1.24. Therefore, it seemed reasonable that excess hydroxide formation would be more extensive in the case of an SCSR than in the laboratory tests and would result in even lower utilization efficiency of the $KO_2$ tablets or granules in the SCSRs.

Second, the temperature in the $KO_2$ bed of an SCSR would be significantly higher than that observed here for a small reactor (~100°C). The primary reason for the higher temperature is that there would be a lower percentage of the granules undergoing thermal exchange with the outside air (via the canister wall). In the case of the reactor used in the laboratory tests, nearly all of the granules could undergo thermal exchange through the reactor walls and this tended to moderate the temperature of the bed. In addition, the maximum bed face velocity of the exhaled gas mixture would be higher in the real case than the averaged value which was tested here because there is a variation in metabolic load and ventilation rate occurring during the use of an SCSR in performing Test No. 4 of the CFR Title 30 (11). This higher velocity would also contribute to higher bed temperatures since the rates of the $H_2O$ and $CO_2$ reactions with $KO_2$ are mass transfer limited except at high space velocities. Therefore, the higher gas velocities increase the rates of reaction and heat generation. The increase in bed temperature would probably result in increased fusion of reaction products (i.e., KOH and its hydrates), and thereby decrease the diffusion of gaseous reactants (i.e., $CO_2$ and $H_2O$) into the $KO_2$.

Finally, since the useful lifetime of the SCSR in the real case would be determined by one of three failure modes listed previously (in criteria Nos. 1-3) it is likely that the downstream portion of the bed remains essentially unreacted. In the tests employed here, the granules were exposed to humidified $CO_2$ during the entire 60 min-reaction period. Therefore, the tests carried out here simulated the conditions that granules or tablets at the entrance to the $KO_2$ bed in an SCSR would be exposed to. Therefore, it was postulated, that the utilization efficiencies determined here for the granules and tablets would be the upper bound of what would be expected in the real case for the utilization efficiency of the entire bed.

### 4.3.3 Comparison of the Reactivities of $Ca(O_2)_2$ and $KO_2$ with $H_2O$ and $CO_2$

To compare the reactivities of $Ca(O_2)_2$ and $KO_2$, granules of the two superoxides having a similar bulk density (0.92-1.2 $g/cm^3$), were flow tested under identical reaction conditions (e.g., tests Nos. CaS-4 and KS-2). To compare the maximum rates of $O_2$ evolution, and $CO_2$ and $H_2O$ absorption exhibited by the $Ca(O_2)_2$ and $KO_2$ beds (tables 4-6 and 4-10), it is necessary to multiply the rates of the $Ca(O_2)_2$ sample by the bed weight since the rates of the $KO_2$ were not normalized to the bed weight. When this is done, the maximum rates of $O_2$ release and $CO_2$ and $H_2O$ absorption for the $Ca(O_2)_2$ bed during phases I and II are 11.55, 1.94 and 13.16 $\mu mol/s$, respectively.

A comparison of the maximum rates of $O_2$ evolution, and $CO_2$ and $H_2O$ absorption exhibited by the $Ca(O_2)_2$ and $KO_2$ beds (tables 4-6 and 4-10), along with a comparison of the extent of utilization of the available $O_2$ and $CO_2$ scrubbing capacities of the two beds (tables 4-7 and 4-9), indicated that the $Ca(O_2)_2$ bed was much less reactive with $H_2O$ and $CO_2$ than the $KO_2$ bed. Although the $Ca(O_2)_2$ bed absorbed $H_2O$ at a slightly higher rate than the $KO_2$ bed, the maximum rate of $O_2$ evolution was only 57% of the rate for the $KO_2$ bed. Whereas $CO_2$ absorption was simultaneous with $O_2$ evolution for the $KO_2$ bed, in the case of $Ca(O_2)_2$ most of the $CO_2$ scrubbed by the bed was absorbed <u>after</u> the bulk of the $O_2$ evolution had taken place.

The differences in the reactivity of $Ca(O_2)_2$ and $KO_2$ can be explained, on the basis of the differences in reactivity of the products of the superoxide-$H_2O$ reactions. Both $KO_2$ and $Ca(O_2)_2$ react first with $H_2O$ to form the respective hydroxides, KOH and $Ca(OH)_2$. In the case of $Ca(O_2)_2$, $CaO_2$ is also formed, but to a lesser extent than $Ca(OH)_2$. Potassium hydroxide reacts directly with dry $CO_2$ to form $KHCO_3$ or $K_2CO_3$, while $Ca(OH)_2$ and $CaO_2$ must first be hydrated to absorb $CO_2$. Because it does not require $H_2O$ for reaction with $CO_2$, KOH produced by the $KO_2$-$H_2O$ reaction does not have to compete with the remaining $KO_2$ for $H_2O$. Therefore, $CO_2$ absorption by KOH can take place simultaneously with $O_2$ evolution. Since $Ca(OH)_2$ and $CaO_2$ must compete with $Ca(O_2)_2$ for $H_2O$, complete hydration of $Ca(OH)_2$ and $CaO_2$ cannot take place until after most of the $O_2$ has been released from $Ca(O_2)_2$. Table 4-15 summarizes the comparison of the reactivities of $KO_2$ and $Ca(O_2)_2$.

The extent of utilization of the available $O_2$ in the $Ca(O_2)_2$ bed in test No. CaS-4 could probably be improved by increasing the porosity of the granules through different granule fabrication techniques. Superior utilization of the $Ca(O_2)_2$ beds was seen when powdered $Ca(O_2)_2$ was tested. The

Table 4-15.- Comparsion of the Reactivities of $KO_2$ and $Ca(O_2)_2$ with $CO_2$ and $H_2O$

| | $KO_2$ | $Ca(O_2)_2$ |
|---|---|---|
| I. Reactivity of superoxide with $H_2O$. | high | moderate |
| II. Product(s) of $H_2O$/superoxide reaction. | KOH | $Ca(OH)_2$, $CaO_2$ |
| A. Product(s) react with dry $CO_2$? | yes | no |
| B. Reactivity of Products with humidified $CO_2$. | high | low to moderate |
| C. $CO_2$ absorption simultaneous with $O_2$ evolution? | yes | no |
| III. Product(s) of $CO_2$ reaction. | $K_2CO_3$, $KHCO_3$ | $CaCO_3$ |
| IV. Formation of a fused, hydrous product coating? | yes | no |

higher utilization was apparently due to the increased surface area exposed to $H_2O$ and $CO_2$.

## 4.4 Summary and Conclusions

The reactivity of beds of $Ca(O_2)_2$ and $KO_2$ with water vapor and carbon dioxide was evaluated under reaction conditions which approximated those existing in manned SCSRs. Calcium superoxide preparations containing $Ca(O_2)_2$, $CaO_2$, and $Ca(OH)_2$ reacted with $H_2O$ and $CO_2$; evolving $O_2$ and absorbing $H_2O$ and $CO_2$. Most of the $O_2$ which was available for release from the $Ca(O_2)_2$ beds was evolved when the $Ca(O_2)_2$ component of the bed reacted with water vapor and produced $Ca(OH)_2$ and $CaO_2$. Calcium hydroxide and $CaO_2$ originally in the bed and that which was produced during the reaction of $Ca(O_2)_2$ with $H_2O$ had to become hydrated before absorption of $CO_2$ took place. Furthermore, since both $Ca(OH)_2$ and $CaO_2$ compete poorly with $Ca(O_2)_2$ for $H_2O$ entering the bed, most of the $CO_2$ absorption took place following the $Ca(O_2)_2$-$H_2O$ reaction. Release of the $O_2$ present in $CaO_2$ occurred as $CO_2$ was being absorbed by the hydrated $CaO_2$. The results of the $Ca(O_2)_2$ flow tests described here indicated that the most important factor in releasing the available $O_2$ and absorbing $CO_2$ was supplying an abundant amount of $H_2O$ to the bed.

Potassium superoxide beds containing significant quantities of KOH impurity reacted with dry $CO_2$ and released $O_2$ and water vapor. This dry-mode reaction of the $KO_2$ bed proceeded until the $H_2O$ released by the reaction of KOH and $CO_2$ was combined in stable hydrates of $K_2CO_3$, or in $KHCO_3$, or was swept out of the bed by the stream of test gas. Potassium superoxide without KOH impurity did not react with dry $CO_2$. During the dry-test-gas purge, KOH reacted with $CO_2$ producing six times as much $K_2CO_3$ as $KHCO_3$. This suggested that at bed temperatures above at least ~100°C, the formation of $KHCO_3$ is not favored, and that $K_2CO_3$ was the predominate $KO_2$-$CO_2$ reaction product.

When $KO_2$ beds were reacted with humidified test gas it was found that the ratio of $pH_2O/pCO_2$ in the inlet was determinative with respect to the ratio of $CO_2$ absorbed to $O_2$ evolved, the utilization efficiency and physical properties of the bed. A ratio of $pH_2O/pCO_2$ in the inlet gas of 1.24 resulted in an overall $CO_2/O_2$ ratio of 0.55, 52% $O_2$ utilization efficiency, and extensive fusion and plugging of the $KO_2$ bed. The cause of the fusion and plugging of the bed was that the rate of KOH production greatly exceeded the rate of KOH consumption via reaction with $CO_2$. With a ratio of $pH_2O/pCO_2$ in the inlet gas of 0.625 the fusion of the granules was greatly reduced and the plugging of the bed was eliminated. The lower $H_2O/CO_2$ ratio resulted in an overall $CO_2/O_2$ ratio of 0.75 and 89% $O_2$ utilization efficiency.

When a $KO_2$ bed was reacted with water vapor in the absence of $CO_2$, the $O_2$ generation rate was 1/6 of that for an identical bed reacted with 5.0% $CO_2$ and the sample inlet $pH_2O$. The granules of $KO_2$ bed were gradually converted to a single plug of hydrated KOH. This test indicated that $KO_2$ cannot be used to efficiently generate $O_2$ via reaction with water vapor unless it is also used to concurrently scrub $CO_2$.

Granules and tablets of $KO_2$ which were removed from commercial SCSRs and tested for 60 min (the rated life of the devices) under conditions approximating those seen during escape activity, exhibited chemical utilization efficiencies of 60-70%. It was postulated that this utilization efficiency represents the upper bound of what would be expected for the entire bed of current SCSRs.

Flow tests in which beds of $Ca(O_2)_2$ and $KO_2$ were reacted with humidified $CO_2$ under identical conditions indicated that $Ca(O_2)_2$ was much less reactive toward $H_2O$ and $CO_2$ than is $KO_2$. Both the rates of $O_2$ evolution and $CO_2$ absorption were significantly lower for $Ca(O_2)_2$ that those obtained for $KO_2$. Carbon dioxide absorption was simultaneous with $O_2$ evolution during the reaction of $KO_2$, whereas $CO_2$ absorption lagged $O_2$ release in the case of $Ca(O_2)_2$. Although preparations containing 55-67% $Ca(O_2)_2$ have equivalent $O_2$ evolution and superior $CO_2$ absorption capacities compared to commercially available $KO_2$, these test results suggest that $Ca(O_2)_2$ would not be a suitable replacement for $KO_2$ in SCSRs at the present time.

Some preliminary work has been done in which the effect of a catalyst on the reactivity of $Ca(O_2)_2$ with $H_2O$ and $CO_2$ was studied (Sec. 5.1). However, more work needs to be done before it can be determined whether catalysts will be effective in significantly enhancing the reactivity of $Ca(O_2)_2$ towards humidified $CO_2$. Since $KO_2$ tends to overproduce $O_2$ (relative to the amount of $CO_2$ absorbed) under conditions simulating those existing in manned SCSRs, and this overproduction of $O_2$ is the result of an oversupply of $H_2O$ relative to $CO_2$ to the bed, improved balance in the reactivity of $KO_2$ may be obtained by mixing $Ca(O_2)_2$ with $KO_2$. $Ca(O_2)_2$ would then act as an $O_2$-producing, $CO_2$-absorbing desiccant in the $KO_2$. This possibility is explored in the next section of this report.

## 5. PREPARATION AND TESTING OF SUPEROXIDE MIXTURES

A preliminary study of the preparation and reaction characteristics of mixtures of $Ca(O_2)_2$ and $KO_2$ was begun with two primary objectives:

(a) To determine if the addition of $KO_2$ to $Ca(O_2)_2$ could be used to catalytically enhance the rates of $O_2$ evolution and $CO_2$ absorption by $Ca(O_2)_2$ (with $Ca(O_2)_2$ as the major component);

(b) To determine if pelletized mixtures of powdered $KO_2$ and $Ca(O_2)_2$ (with $KO_2$ as the major component) possessed superior reaction characteristics and chemical utilization efficiencies when compared to $KO_2$ alone.

### 5.1 $Ca(O_2)_2/KO_2$ Mixtures with $Ca(O_2)_2$ as the Major Component.

#### 5.1.1 Introduction

An evaluation of the reactivity of $Ca(O_2)_2$ with humidified $CO_2$ (Sec. 4.) demonstrated that the reactivity of $Ca(O_2)_2$ with simulated respiratory gases was inferior to that of $KO_2$. This evaluation also suggested that if $Ca(O_2)_2$ was to be used as a replacement for $KO_2$ in a SCSR, the reactivity of $Ca(O_2)_2$ with humidified $CO_2$ would have be enhanced.

Since $Ca(O_2)_2$ obtained from the disproportionation of $CaO_2 \cdot 2H_2O_2$ also contains significant quantities of $CaO_2$ and $Ca(OH)_2$, and since the latter two compounds are also produced upon reaction of $Ca(O_2)_2$ with water vapor, it seemed reasonable that the reactivity of the $CaO_2$ and $Ca(OH)_2$ components with $CO_2$ [and, therefore, the overall reactivity of the $Ca(O_2)_2$)] might be enhanced by adding a suitable catalyst.

Pavlyuchenko and Rubinchik (27) demonstrated that the addition of sodium hydroxide (NaOH) and manganese dioxide ($MnO_2$) to $CaO_2$, resulted in increased reactivity of the peroxide with humidified $CO_2$. They postulated that NaOH and $MnO_2$ were involved in the decomposition of the $H_2O_2$ formed from the reaction of $H_2O$ with $CaO_2$.

Industrially, NaOH and KOH are added to $Ca(OH)_2$ to increase its reactivity with $CO_2$. The resulting mixture, called soda lime or sodasorb (78% $Ca(OH)_2$, 2.5% NaOH, 2% KOH, and 17.5% $H_2O$), is used extensively as a $CO_2$ absorption agent (7,12,48). Another commercial $CO_2$ absorbent containing $Ca(OH)_2$ as the major component is Baralyme (78% $Ca(OH)_2$, 18% $Ba(OH)_2 \cdot 8H_2O$, and 4% KOH) (20). It has been postulated that the minor components of these mixtures act as $CO_2$ transfer agents for $Ca(OH)_2$; therefore, the agents function as

catalysts (20). For example, in the case of soda lime the following reactions could occur when the surface of the material reacts with humidified $CO_2$:

$$CO_2 + H_2O = H_2CO_3 \quad (5.1)$$

$$H_2CO_3 + 2Na^+ + 2OH^- = 2Na^+ + CO_3^{2-} + 2H_2O \quad (5.2)$$

$$Ca(OH)_2 = Ca^{2+} + 2OH^- \quad (5.3)$$

$$Ca^{2+} + 2OH^- + 2Na^+ + CO_3^{2-} = CaCO_3 + 2Na^+ + 2OH^- \quad (5.4)$$

The net reactions are

$$2NaOH + CO_2 = Na_2CO_3 + H_2O \quad (5.5)$$

$$Ca(OH)_2 + Na_2CO_3 = CaCO_3 + 2NaOH \quad (5.6)$$

Similar reactions could be written for the KOH component of soda lime.

In the case of $Ca(O_2)_2$, it was desirable to either add a catalyst that was effective in very small proportions (such that the $O_2$ capacity/unit weight of the mixture would not be significantly decreased) or add one that also evolved $O_2$ so that the $O_2$ capacity of the resulting mixture would be comparable to that for moderate purity (55-67%) $Ca(O_2)_2$. Since the product of the $KO_2/H_2O$ reaction is KOH, it appeared reasonable that the admixture of $KO_2$ to $Ca(O_2)_2$ might improve the reactivity of the latter compound without decreasing its $O_2$ capacity.

### 5.1.2 Flow Tests of Mixtures of Powdered $Ca(O_2)_2$ and $KO_2$

Initially, it was postulated that mixing and grinding powdered $KO_2$ and $Ca(O_2)_2$ together would provide intimate enough contact for the proposed catalytic effect of KOH reaction products to be exhibited. Therefore, a mixture was made by blending the two superoxide powders and then grinding the mixture with a mortar and pestle. The $Ca(O_2)_2$ material was obtained from the disproportionation of $CaO_2 \cdot 2H_2O_2$ and had the composition 58.3% $Ca(O_2)_2$, 14.5% $CaO_2$, and 27.2% $Ca(OH)_2$). The $KO_2$ material consisted of 86.9% $KO_2$ and 13.1% KOH, $K_2CO_3$ and $KHCO_3$. Samples of the mixture were reacted with humidified 5% $CO_2$, 95% $N_2$ using the flow system described previously in Sec. 4.2.2. Table 5-1 summarizes the flow-test reaction conditions for the two $Ca(O_2)_2/KO_2$ mixture samples.

Although both samples contained $KO_2$, no dry-mode-reaction behavior characteristic of $KO_2$ samples containing KOH contamination was exhibited (Sec. 4.3.2.1). This observation is believed to be the result of the absorption

Table 5-1.- Flow-System Reaction Conditions for Testing $Ca(O_2)_2/KO_2$ Mixture Samples

| Test No. | Material | Reaction Conditions | | | |
|---|---|---|---|---|---|
| | | | Bed Parameters[1] | | |
| | | Inlet flow rate, SCCM[2] | Weight, g | Height, cm | Particle size, mm |
| CaS/KS-1 | $Ca(O_2)_2/KO_2$[3] | 95-101 | 1.126 | 3.0 | <0.038 |
| CaS/KS-2 | $Ca(O_2)_2/KO_2$[3,4] | 97-100 | 1.075 | 3.0 | <0.038 |

1 1.06-cm ID reactor suspended in a 5-cm ID, 25°C air well.
2 Flow rate for dry test gas (5% $CO_2$, 95% $N_2$). After 0.5 ks of dry-test-gas purge, the test gas was humidified to a dew point of 25°C and directed down through chemical bed for 9.5 ks.
3 Mixture consisted of 66.3% $CaO_2 \cdot 2H_2O_2$ disproportionation product (58% $Ca(O_2)_2$, 14.5% $CaO_2$, 27.2% $Ca(OH)_2$) and 33.7% $KO_2$ (86.9% $KO_2$, 13.1% KOH, $K_2CO_3$, and $KHCO_3$).
4 Mixture pressed to a bulk densisty of 0.825 g/cm$^3$, then reground to powder with mortar and pestle.

of the evolved $H_2O$ from the $KOH/CO_2$ reaction [forming $K_2CO_3$, eq. (4.8)] by the $Ca(O_2)_2$ which prevents recycling of water vapor in the bed.

Table 5-2 lists the maximum rates of $O_2$ evolution and $CO_2$ and $H_2O$ absorption which were observed during the flow tests of the superoxide mixture samples and compares them with the rates obtained with a $Ca(O_2)_2$ sample under similar test conditions. Despite the fact that the sample in test No. CaS/KS-1 exhibited maximum $O_2$ evolution and $CO_2$ absorption rates sooner than the $Ca(O_2)_2$ sample tested under similar conditions (test No. CaS-2), the magnitude of the rates for the mixture were not significantly different than for the $Ca(O_2)_2$ material. However, unlike the $Ca(O_2)_2$ sample, the maximum rates of $O_2$ evolution and $CO_2$ absorption for the mixture occurred simultaneously. The juxposition of the $O_2$ evolution and $CO_2$ absorption for the mixture may be due solely to the reaction of the $KO_2$ component and not to any enhancement of the reactivity of the $Ca(O_2)_2$.

It was postulated that more intimate contact of the two powdered materials might be achieved by pressing the mixture into a pellet and than regrinding the pelletized mixture. In test No. CaS/KS-2 this postulate was evaluated and although slightly higher maximum reaction rates were observed, the differences between the two samples did not appear significant.

Table 5-3 compares the chemical utilization efficiencies of the $Ca(O_2)_2/KO_2$ mixtures with that for $Ca(O_2)_2$. The major difference between the two materials is seen in the absorption of $CO_2$. The mixture appears to be superior to $Ca(O_2)_2$ as a $CO_2$ absorbent. However, the low percentage utilization of the $CO_2$ capacity for the mixture indicates that absorption of $CO_2$ by $Ca(OH)_2$ via equations (5.1)-(5.6) above was not proceeding to a significant extent.

### 5.1.3 Cosynthesized Mixture of $Ca(O_2)_2$ and $KO_2$

It seemed apparent that using the proportions of $Ca(O_2)_2$ and $KO_2$ described above, a simple mechanical mixing of superoxide powders was not effective in significantly enhancing the reactivity of $Ca(O_2)_2$. Since materials such as soda lime are made by drying a slurry of $Ca(OH)_2$ in a NaOH solution, it seemed that a better approach would be to synthesize both superoxides simultaneously in such a way that there would be either a mixed crystal structure formed or at least some more intimate contact of potassium and calcium ions in the final product. Since both superoxides could be synthesized by disproportionation of their respective peroxide diperoxyhydrates, a study was undertaken to determine the feasiblity of synthesizing a mixture of $Ca(O_2)_2$ and $KO_2$ from an intimate mixture of $CaO_2 \cdot 2H_2O_2$ and

Table 5-2.- Maximum Rates of $O_2$ Evolution and $CO_2$ and Water Vapor Absorption During Reaction of $Ca(O_2)_2/KO_2$ and $Ca(O_2)_2$ Beds with Humidified $CO_2$

| Test No. | $O_2$ evolution | | $CO_2$ absorption | | $H_2O$ absorption | |
|---|---|---|---|---|---|---|
| | Time,[1] ks | Max. rate, μmol/s/g | Time,[1] ks | Max. rate, μmol/s/g | Time,[1] ks | Max. rate, μmol/s/g |
| CaS/KS-1 | 1.49 | 1.57 | 1.48 | 1.79 | 1.48 | 1.70 |
| CaS/KS-2 | 1.58 | 1.77 | 1.53 | 1.97 | 1.71 | 1.85 |
| CaS-2[2] | 3.93 | 1.74 | 14.94 | 1.62 | 2.58 | 1.96 |

[1] Reaction time corrected for 0.5 ks of dry-test-gas purge.
[2] Values taken from table 4-6.

Table 5-3.- Amounts of $O_2$ Evolved and $CO_2$ Absorbed During Reaction of $Ca(O_2)_2/KO_2$ and $Ca(O_2)_2$ Beds with Humidified $CO_2$

| Test No. | $O_2$ evolved[1] | | $CO_2$ absorbed[1] | |
|---|---|---|---|---|
| | $cm^3$ STP/g | % bed capacity | $cm^3$ STP/g | % bed capacity |
| CaS/KS-1 | 161.7 | 77.4[2] | 131.8 | 59.2[3] |
| CaS/KS-2 | 159.7 | 76.4[2] | 125.1 | 56.2[3] |
| CaS-2[4] | 154.4 | 76.8[5] | 36.9[6] | 14.4[5] |

1 After 13.0 ks of reaction time.
2 Calculations based on the chemical composition given in table 5-1.
3 Calculations based on the chemical composition given in table 5-1 with $CaCO_3$ and $K_2CO_3$ being the only $CO_2$ reaction products
4 Same test as in table 4-2, but the first 13 ks of reaction time were selected.
5 Calculations based on the theoretical capacities given in table 4-4.
6 Maximum $CO_2$ absorption occurred after 13.0 ks (i.e., at 14.9 ks). The $CO_2$ absorbed by 18 ks was 103.4 $cm^3$ STP/g or 40.5% of bed capacity.

$K_2O_2 \cdot nH_2O_2$ (where n = 2-4.5).

The mixture of $CaO_2 \cdot 2H_2O_2$ and $K_2O_2 \cdot nH_2O_2$ was made by reacting $CaO_2 \cdot 8H_2O$ and KOH with 89% $H_2O_2$ at -15.5°C. The resulting slurry was then freeze-dried at -65°C to -15°C (see fig. 2-2 in Sec. 2.2.1.2, for a sketch of the apparatus). Since the KOH completely dissolved in the concentrated $H_2O_2$, the peroxyhydrates of the calcium and potassium were in intimate contact. A dry white product was scraped from the freeze-drying flask. It was analyzed for peroxide content by titration with $KMnO_4$, base content by back-titrating a sample dissolved in standard $HNO_3$ with NaOH, and calcium content by EDTA titration. The solid contained 67.5% $CaO_2 \cdot 2H_2O_2$ and 32.5% $K_2O_2 \cdot 4.5H_2O_2$. Peroxyhydrates of $K_2O_2$ with 2-4.6 associated molecules of $H_2O_2$ were also reported by Kazarnovskii and Neiding (16) in their work on the synthesis of $KO_2$. Examination of the sample synthesized in this work under a light microscope revealed that the individual particles had a tree-like structure, with agglomerates of particles forming branches.

Samples of the peroxide peroxyhydrate mixture were disproportionated in the apparatus described in Sec. 3.3. They were disproportionated under the same conditions which had been used to produce 67% $Ca(O_2)_2$, except that the samples were reacted for longer than the usual 1.75-2.25-h reaction period. The longer reaction period was necessary to allow the residual pressure in the reaction chamber to fall below 20-25 mtorr. This pressure range had indicated complete reaction in the case of the disproportionation of $CaO_2 \cdot 2H_2O_2$. Three samples of the mixed peroxide peroxyhydrate were disproportionated.

The first sample was reacted for 3 h, and exhibited a light yellow color similar to that of $CaO_2 \cdot 2H_2O_2$ disproportionation products containing 67% $Ca(O_2)_2$. However, analysis of the sample indicated that it contained only 1/3 the superoxide anion ($O_2^-$) content of 67% $Ca(O_2)_2$ (i.e., 13.7% $O_2^-$ vs 41.4% $O_2^-$). The yellow color gradually faded over a period of several days. It was concluded that the disproportionation reaction had not gone to completion in 3 h, and so a second sample was reacted for 4.5 h. The product from the second sample contained a slightly higher $O_2^-$ content (15.0%), and a more intense yellow color which also faded over a period of several days.

A third sample was reacted for 24 h and contained a $O_2^-$ content of only 14.8%. Table 5-4 summarizes the analysis results from the three samples and also gives the later analyses of each of the samples after storage from 3-28 days. Upon storage, the $O_2^-$ content of the last two samples increased slightly, while the peroxide anion content decreased, suggesting that disproportionation was still

Table 5-4.- Superoxide and Peroxide Content of $CaO_2 \cdot 2H_2O_2/K_2O_2 \cdot 4.5H_2O_2$ Disproportionation Products

| Sample No. | Storage time, days | $\%O_2^-$ (superoxide anion) | $\%O_2^{2-}$ (peroxide anion) | Disproportionation reaction time, h |
|---|---|---|---|---|
| 1 | 0 | 13.7 | 24.2 | 3 |
| | 3 | 10.3 | 17.6 | |
| | 28 | 11.0 | 13.2 | |
| 2 | 0 | 15.0 | 23.3 | 4.5 |
| | 23 | 16.1 | 12.3 | |
| 3 | 0 | 14.8 | 20.8 | 24 |
| | 26 | 18.1 | 13.8 | |

continuing even after 24 h of reaction in the vacuum chamber.

To better understand the results obtained from the cosynthesized mixture disproportionation experiments it was decided to perform a similar test on a sample consisting of only $K_2O_2 \cdot 4.5H_2O_2$. This material was obtained by reacting KOH with concentrated $H_2O_2$ and freeze-drying the solution to precipitate the sample. After removing most of the sample from the flask, the residue was evacuated in the flask at room temperature, to note the time of appearance of the yellow superoxide. It took 3 days for a pale yellow color to appear. The flask was then heated to 55-60°C and the residue in the flask became bright canary yellow in color after only 3 h.

Analysis of the residue showed 69% $KO_2$. The conclusion drawn from these experiments was that the $K_2O_2 \cdot 4.5H_2O_2$ (or at least the $K_2O_2 \cdot 2H_2O_2$ formed by loss of $H_2O_2$ during evacuation) had a significantly greater thermal stability than did $CaO_2 \cdot 2H_2O_2$.

### 5.1.4 Conclusions

The difference in the thermal stability and, therefore, the disproportionation rates of the $K_2O_2 \cdot nH_2O_2$ and $CaO_2 \cdot 2H_2O_2$ materials suggests that further long term (>24 h) disproportionation experiments should be attempted or the mixture should be disproportionated at a higher temperature to increase the rate. Further work may produce a $Ca(O_2)_2/KO_2$ mixture which will have improved $CO_2$ absorption properties when compared with $Ca(O_2)_2$.

Although mixtures of powdered $KO_2$ and $Ca(O_2)_2$ which had been blended by grinding and pressing did not produce a material which had significantly superior reactivity with $CO_2$, it may be possible to further increase the intimacy of the superoxide mixture by sintering the powder under pressure below the Tamman temperature. The Tamman temperature is equal to 2/3 of the melting point of one of the components in degrees Kelvin (33). Sintering the superoxide mixture near the Tamman temperature might promote significant ion migration in the lattices and facilitate catalytic activity on the part of the KOH product species.

## 5.2 $KO_2/Ca(O_2)_2$ Mixtures with $KO_2$ as the Major Component

### 5.2.1 Introduction

In the past, there have been two main approaches to solving the problems associated with the use of $KO_2$ as a life support chemical. In the first approach, engineering solutions to the fusing of the chemical have been sought

through changing the $KO_2$ bed configuration. This was done by either by changing the bed dimensions, or by breaking up the bed into multiple thin layers (18,19,32).

The second approach has been to dilute the $KO_2$ bed with granules of other materials such as molecular sieve desiccants or $CO_2$ absorbents (8,25). These mixed granule beds were not significantly different in reaction properties from pure $KO_2$ beds and in many cases exhibited poorer performance.

Neither of these approaches has been completely successful and so current portable breathing devices employing $KO_2$ carry up to twice as much $KO_2$ than is theoretically required to meet the metabolic requirements of the user (consult Sec. 6.2, for an an analysis of commercially available SCSRs). Since the size of the $KO_2$ bed has a direct impact on the overall weight and bulkiness of the portable breathing device, it is desirable to eliminate, if possible, this extra $KO_2$.

Little work has been reported on a third approach to improving the reaction characteristics of $KO_2$. In this approach, improvement in the reactivity of $KO_2$ was sought by mixing it with other chemicals prior to the fabrication of granules. Some research has been focused on adding transition metal catalysts (such as CuOCl and $KMnO_4$) to $KO_2$ to improve the rate of the $O_2$ release reaction (24). Some work has also been done on adding alkali metal hydroxide and peroxides to $KO_2$ before the chemical was fabricated into rippled plates for use in a large-chamber life-support system (24). The addition of lithium hydroxid (LiOH) to $KO_2$ improved the $O_2$ utilization efficiency, but the $O_2$ capacity of the mixture (l/kg bed) was lower than $KO_2$. Also, there was no improvement in $CO_2$ absorption capacity when the mixture was compared to pure $KO_2$. It was not clear from the work described in (24) how well the $KO_2$-additive mixtures were blended prior to fabrication into the rippled plates.

It was postulated mixing $Ca(O_2)_2$ powder as a minor component with $KO_2$ powder prior to the formation of granules or tablets might improve the utilization efficiency of $KO_2$ by preventing the formation of fused hydroxide coatings. Calcium superoxide would act as an $O_2$-yielding desiccant inside the granule and tie up excess water vapor. Excess water vapor would be derived from the exhalation gas or from the formation of $K_2CO_3$ from KOH [eq. (4.8)]. Also, because the reaction products of $Ca(O_2)_2$ with $H_2O$ (i.e., $CaO_2$, and $Ca(OH)_2$) do not melt below their decomposition temperatures, $Ca(O_2)_2$ might help to maintain an open structure in the granule for further penetration by reactant gases.

Conversely, the reactivity of $Ca(O_2)_2$ could potentially

be helped by: (a) the higher temperatures created from the reaction of the $KO_2$ in the granules, (b) the $H_2O$ released by the $K_2CO_3$ forming reaction, and (c) carbonate group transfer reactions between $K_2CO_3$ and $Ca(OH)_2$. Although significant improvement in the reactivity of $Ca(O_2)_2$ was not seen upon admixture of $KO_2$ as a minor component, it was postulated that the close proximity of the superoxide powders brought about by pelletization at high pressure and the potential potassium ion migration in the high temperature reaction zone environment would permit catalytic activity on the part of $KO_2$ and thereby increase the reactivity of the $Ca(O_2)_2$ component with humidified $CO_2$.

### 5.2.2 Flow Tests with $KO_2/Ca(O_2)_2$ Mixtures

To determine the effectiveness of $Ca(O_2)_2$ in improving the utilization efficiency of $KO_2$ granules, a series of flow tests were carried out on the system described in Sec. 4.2.2. Three pairs of samples were tested. Each sample pair consisted of granules of a $KO_2/Ca(O_2)_2$ mixture and granules of $KO_2$ fabricated under identical pelletizing conditions from $KO_2$ powder having the same grain size. The members of each sample pair were tested under identical conditions. A summary of the flow system conditions is given in table 5-5.

Since $Li_2O_2$ has an equivalent $O_2$ capacity to $KO_2$ but a superior $CO_2$-scrubbing capacity, and since $Li_2O_2$ should not form fused hydrous coatings (melting point of LiOH = 450°C) during reaction with humidified $CO_2$, it seemed reasonable that an admixture of $Li_2O_2$ with $KO_2$ might also improve the utilization efficiency of $KO_2$ granules. Therefore, a $KO_2/Li_2O_2$ mixture was tested and the conditions are given in table 5-5. The $KO_2/Li_2O_2$ mixture is compared with the $KO_2$ granules of test No. KS-10.

Figures 5-1, 5-2, 5-3 and 5-4 are plots of the $O_2$ utilization efficiency and $CO_2$-scrubbing capacity as a function of the concentration of $CO_2$ downstream from the bed for each pair of samples tested. For the sake of comparison, data was plotted for $CO_2$ breakthrough concentrations up to 3.5% even though in real use the maximum allowable $CO_2$ concentration downstream from the bed would be 0.5% (11). It is apparent that for each pair tested, the superoxide-mixture granules exhibited superior performance to the $KO_2$ granules. For test Nos. KS/CaS-1 and KS-8 the utilization efficiency at low $CO_2$ breakthrough levels (i.e., 0.5-1.0%) was less than for the other sample pairs. This lower utilization efficiency was postulated to be a result of the shorter (~3 cm), bed lengths which allowed breakthrough to occur sooner. Therefore, the granules at the entrance to the bed were not exposed to the reactant gases for as long a period as the granules in the ~4.5 cm beds.

Table 5-5.- Flow-System Reaction Conditions for Testing Various Superoxide Mixture Samples

| Test No. | Material [4] | Reaction Conditions: Inlet flow rate, SCCM [2] | Bed Parameters [1]: Weight, g | Height, cm | Particle size, mm [3] |
|---|---|---|---|---|---|
| KS/CaS-1 | $KO_2/Ca(O_2)_2$ [5] | 299-305 | 1.569 | 3.2 | 1.3-2.5 |
| KS-8 | $KO_2$ | 298-299 | 1.615 | 2.9 | 1.3-2.5 |
| KS/CaS-2 | $KO_2/Ca(O_2)_2$ [5] | 299-304 | 2.187 | 4.7 | 1.3-2.5 |
| KS-9 | $KO_2$ | 301-303 | 2.517 | 4.7 | 1.3-2.5 |
| KS/CaS-3 | $KO_2/Ca(O_2)_2$ [6] | 298-300 | 2.228 | 4.5 | 1.9-2.5 |
| KS-10 | $KO_2$ | 296-301 | 2.570 | 4.5 | 1.9-2.5 |
| KS/LiP-1 | $KO_2/Li_2O_2$ [7] | 300-303 | 2.557 | 4.6 | 1.9-2.5 |

1 1.06-cm ID reactor was suspended in a 5-cm ID, 25°C air well.
2 Flow rate for dry test gas (5% $CO_2$, 95% $N_2$). Test gas was humidified to a dew point of 24°C and directed down through the chemical bed for 10.0 ks.
3 Material pressed to a bulk density of 0.99-1.19 g/cm$^3$, then broken up into granules.
4 Origin and composition of $O_2$ sources:
A - $KO_2$, MSA, granules, ground to a grain size of <0.38 mm., 85.2% $KO_2$, 14.8% KOH, $K_2CO_3$, $KHCO_3$,
B - $Ca(O_2)_2$, from disproportionation of $CaO_2 \cdot 2H_2O_2$, powder, 55.3% $Ca(O_2)_2$, 14.4% $CaO_2$, 30.3% $Ca(OH)_2$,
C - $Li_2O_2$, Alpha Inorganics, powder, 95.3% $Li_2O_2$.
5 Mixture consisted of 75.7% of A and 24.3% of B (see 4 above).
6 Mixture consisted of 74.1% of A and 25.9% of B (see 4 above).
7 Mixture consisted of 79.0% of A and 21.0% of C (see 4 above).

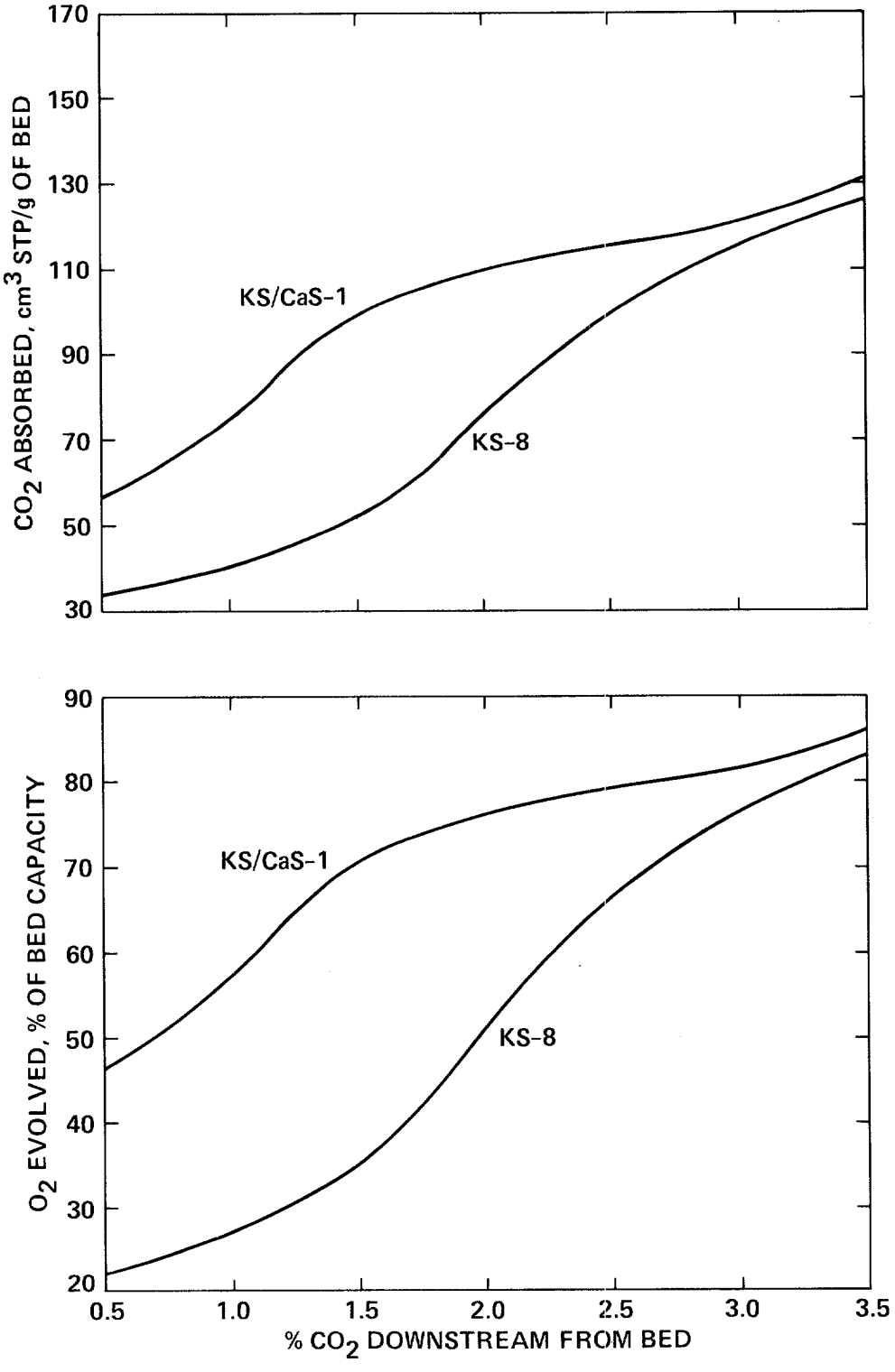


Figure 5-1.- Comparison of the chemical utilization efficiencies for granules of $KO_2/Ca(O_2)_2$ mixture and $KO_2$. Oxygen evolved and $CO_2$ absorbed as a function of the $CO_2$ concentration downstream from the superoxide bed. (Test Nos. KS/CaS-1 and KS-8.)

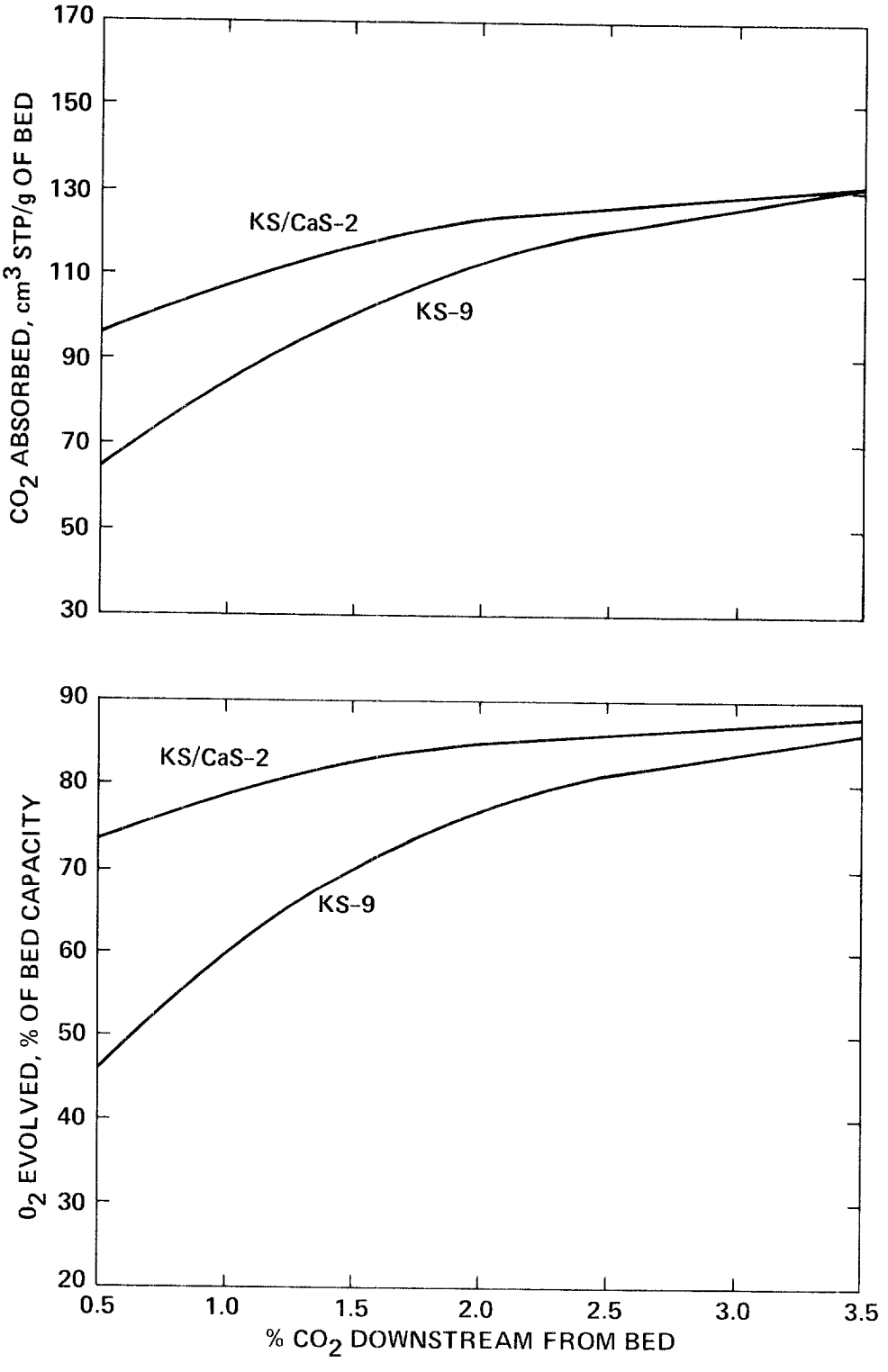


Figure 5-2.- Comparison of the chemical utilization efficiencies for granules of $KO_2/Ca(O_2)_2$ mixture and $KO_2$. Oxygen evolved and $CO_2$ absorbed as a function of the $CO_2$ concentration downstream from the superoxide bed. (Test Nos. KS/CaS-2 and KS-9.)

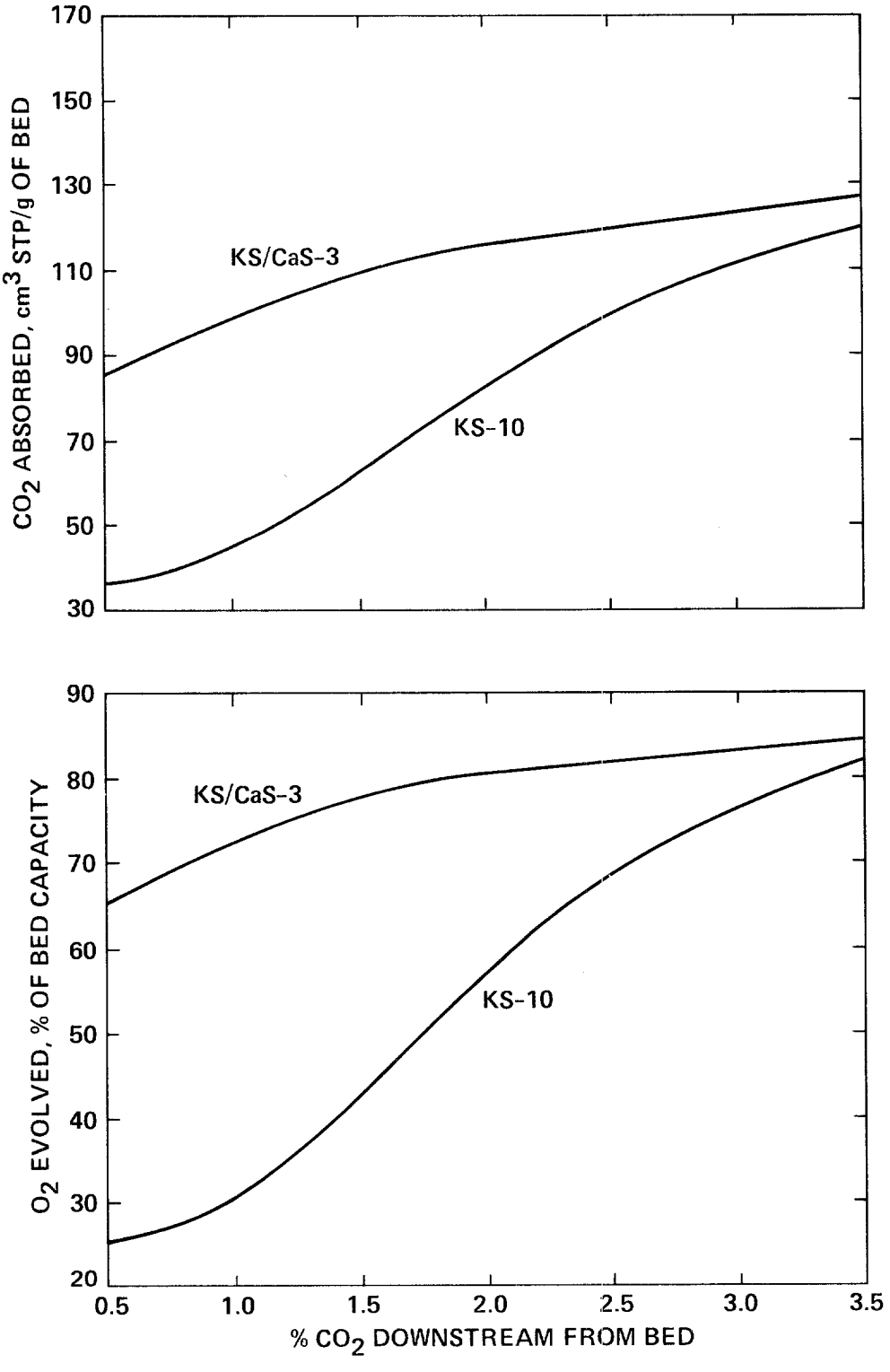


Figure 5-3.- Comparison of the chemical utilization efficiencies for granules of a $KO_2/Ca(O_2)_2$ mixture and $KO_2$. Oxygen evolved and $CO_2$ absorbed as a function of the $CO_2$ concentration downstream from the superoxide bed. (Test Nos. KS/CaS-3 and KS-10.)

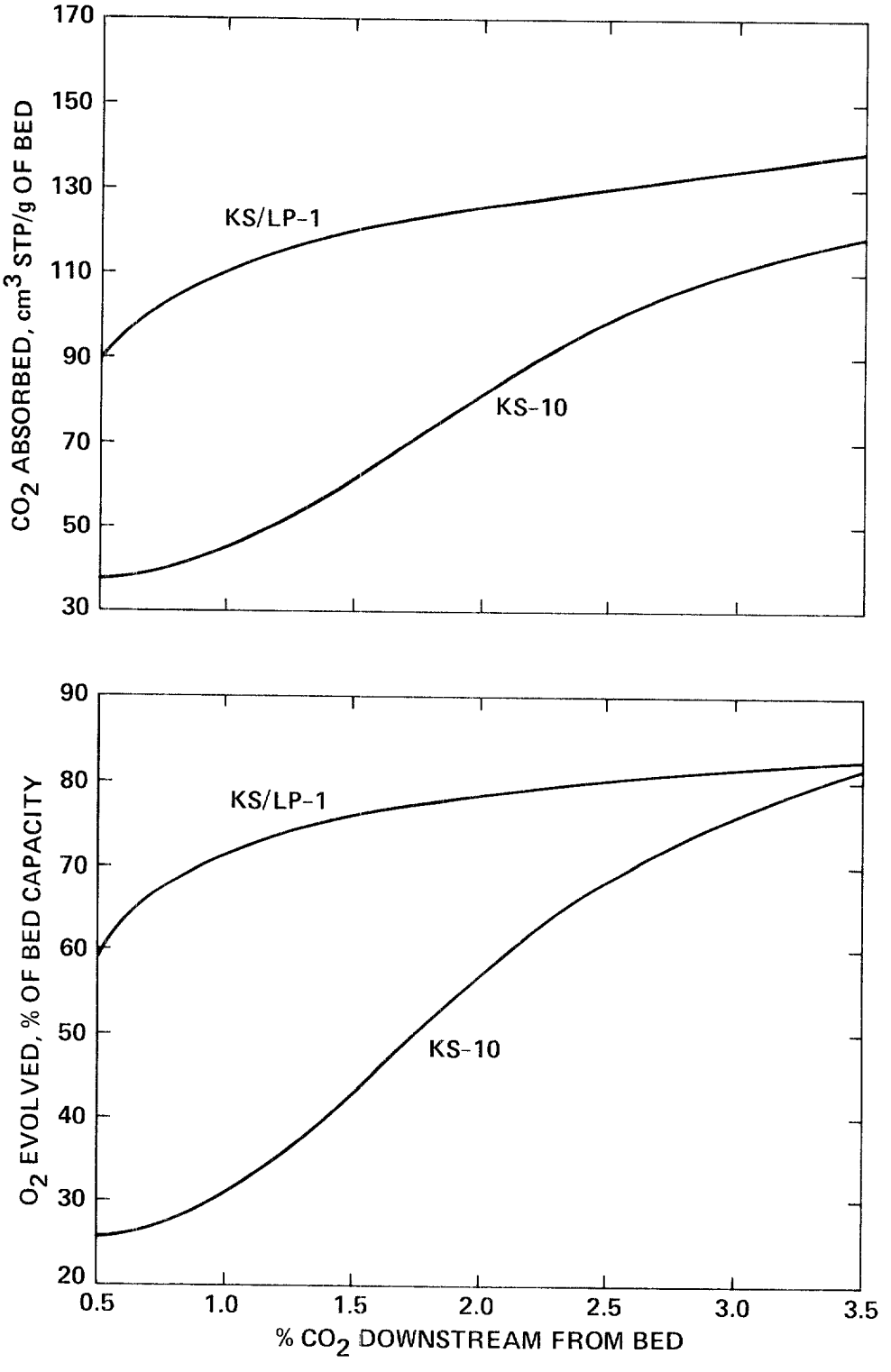


Figure 5-4.- Comparison of the chemical utilization efficiencies for granules of a $KO_2/Li_2O_2$ mixture and $KO_2$. Oxygen evolved and $CO_2$ absorbed as a function of the $CO_2$ concentration downstream from the superoxide bed. (Test Nos. KS/LP-1 and KS-10.)

For test Nos. KS/CaS-3, KS-10, and KS/LP-1, a narrower granule-size distribution was used than with the other two sample pairs. With the elimination of the smallest size granules (1.3-1.9-mm diam.), the difference in $O_2$ utilization efficiency was the most dramatic between the superoxide-mixture granules and the $KO_2$ granules. The decrease in the performance of the $KO_2$ bed upon elimination of the smallest sized granules is postulated to result from the lowering of the surface area to volume ratio of the granules and the formation of a fused, hydrous coating. Since the addition of $Ca(O_2)_2$ or $Li_2O_2$ to $KO_2$ is postulated to prevent the formation of fused coatings on the granules, only a slight decrease in utilization efficiency was observed for the superoxide-mixture beds. For the $KO_2/Ca(O_2)_2$ mixture-$KO_2$ sample pair, the $O_2$ utilization efficiency at or below a $CO_2$ breakthrough level of 2.0% was doubled upon addition of $Ca(O_2)_2$ to the granules. Of all the samples tested, the $KO_2/Li_2O_2$ mixture had the highest $CO_2$-scrubbing capacity.

For each sample pair there was also dramatic differences between the physical properties of the mixture granules when compared to the $KO_2$ granules. Whereas the spent mixture granules could be poured out of the reactor at the end of the flow test and were still intact, the spent $KO_2$ granules at the exit to the bed were fused together and those at the entrance were soft and mushy. The spent $KO_2$ granules were removed from the reactor with great difficulty using a spatula.

It should be noted that no attempts were made in this preliminary study to optimize the granule fabrication technique so that the porosity and mechanical properties of the granules were equivalent to commercial $KO_2$ granules. It is postulated that improved utilization efficiency of the $KO_2/Ca(O_2)_2$ mixtures could be achieved if the porosity of the granules was increased.

### 5.2.3 Summary and Conclusions

Preliminary work on the reactivity of granules fabricated from an intimate mixture of 75% $KO_2$ and 25% $Ca(O_2)_2$ showed no evidence of fused hydrous coatings. The utilization efficiency of the mixture with respect to both $O_2$ release and $CO_2$ absorption was up to 100% greater than $KO_2$ granules prepared and reacted under identical conditions. It is postulated that the $Ca(O_2)_2$ aids the $KO_2$ by reacting with excess moisture, and thereby preventing the formation of fused hydroxide-hydrate coatings. The $KO_2$ can aid the reactivity of $Ca(O_2)_2$ by acting as a catalyst for the reaction of $CO_2$ with $Ca(OH)_2$ and $CaO_2$. Since $Ca(O_2)_2$ also releases $O_2$ and scrubs $CO_2$, the overall $O_2$ capacity of the $KO_2/Ca(O_2)_2$ mixture is nearly identical to commercial $KO_2$. By adding $Ca(O_2)_2$ to $KO_2$ in the proper proportions it

should be possible to increase the ratio of $CO_2$ absorbed to $O_2$ released such that this ratio more closely matches the RQ of man engaged in moderate activity. Significant improvement in the reaction behavior of $KO_2$ was also induced by fabricating granules from a mixture of 25% $Li_2O_2$ and 75% $KO_2$. Further research on these mixed superoxide granules may provide a new generation of air revitalization chemicals which could reduce the size of current portable life support systems.

## 6. SELF-CONTAINED SELF-RESCUER WEIGHT/VOLUME REDUCTION CALCULATIONS

### 6.1 Introduction

Currently there are two commercially available, $KO_2$-based, 60 min SCSRs which have approval from the National Institute of Occupational Safety and Health (NIOSH) for use by miners during an emergency escape from a coal mine; the Drager model "Oyy SR 60B" and the MSA model No. 464213. Tables 6-1 and 6-2 give a weight breakdown of the major components for each device. The values in the two tables were obtained by dismantling device in a glove box, removing the $KO_2$, and weighing the components. The study described next was undertaken based on the postulate that improving the utilization efficiency of the $KO_2$ or replacing it with a chemical that had superior $O_2$-releasing and $CO_2$-scrubbing capacities would result in substantial savings in weight and volume in the Drager and MSA SCSRs.

The overall method used in estimating the weight and volume savings that could result from improving the utilization of $KO_2$ or replacing it with a superior chemical involved the following steps:

(a) The weight of chemical required to meet the metabolic requirement of the most demanding user for 1 h was calculated

(b) The reductions in the chemical bed weight and volume which would be realized for each of the two commercial SCSRs was determined

(c) The reductions in weight and volume which would be realized in the canister and case of each SCSR as a result of the reduction in bed volume was estimated.

### 6.2 Oxygen Requirement

To calculate the amount of superoxide to use in a 60 min SCSR, it was first necessary to know the amount of $O_2$ required by the most demanding user and his average respiratory quotient (RQ). Kamon, Bernard and Stein (15) determined that a 95th percentile miner requires 105 l of $O_2$ and eliminates 105 l of $CO_2$ during the course of performing the tasks listed for Test 4 in Title 30, Part II of the Code of Federal Regulations (11). The average RQ for the 95th percentile miner during the 60 min test was 1.0.

### 6.3 Determination of Superoxide Bed Size

Knowing the $O_2$ requirement and RQ of the most demanding SCSR user, it was possible to estimate the amount of chemical necessary to sustain his metabolic requirements for 60 min Buban and Gray (8) give the following formula for determining the weight of chemical required to meet a given

Table 6-1.- Component Weights of the Drager "Oxy SR 60B" Self-Contained, Self-Rescuer (No. 880 A06913)[1]

| Item | Weight, g | % of total weight |
|---|---|---|
| POTASSIUM SUPEROXIDE (tablets, volume of bed = 1462 $cm^3$, $O_2$ content = 180 $cm^3$ STP/g or 207.5 std. l/canister) | 1153 | 30.7 |
| OUTER PLASTIC CASE (includes seals, clamps, desiccant, nylon straps, volume = 6754 $cm^3$) | 1263 | 33.7 |
| STAINLESS STEEL CANISTER (includes perchlorate candle [fired], screens, baffles) | 881 | 23.5 |
| BREATHING BAG (includes nose plug, valves, breathing hose) | 381 | 10.1 |
| GOGGLES | 74 | 2.0 |
| TOTAL | 3752 (= 8.27 lbs) | 100.0 |

[1] Reference to specific brands, equipment, or trade names in this section is made to facilitate understanding and does not imply indorsement by the Bureau of Mines.

Table 6-2.- Component Weights of the MSA 464213 Self-Contained, Self-Rescuer

| Item | Weight, g | % of total weight |
|---|---|---|
| POTASSIUM SUPEROXIDE (granules, volume of bed = 1552 $cm^3$, $O_2$ content = 217 $cm^3$ STP/g or 211.1 std. l/canister) | 973 | 24.3 |
| OUTER METAL CASE (includes seals, clamps, clips, nylon straps, volume = 5700 $cm^3$) | 1654 | 41.3 |
| STAINLESS STEEL CANISTER (includes perchlorate candle, screens, felt insulation, baffles) | 1095 | 27.4 |
| BREATHING BAG (includes nose plug, valves, breathing hose) | 254 | 6.4 |
| GOGGLES | 26 | 0.6 |
| TOTAL | 4002 (= 8.82 lbs) | 100.0 |

set of metabolic requirements:

$$W = (V \times RQ\text{-man})/(C \times E \times RQ\text{-chem}) \qquad (6.1)$$

where W is the calculated weight of the chemical required in grams, V is the liters of $O_2$ required for 60 min of activity, RQ-man is the average RQ of the miner during the activity period, C is the $O_2$ capacity of the chemical in l/g, E is the utilization efficiency in decimal percent, and RQ-chem is the molar ratio of $CO_2$ absorbed to $O_2$ evolved for the chemical. The factor RQ-chem was introduced into the equation to take into account the fact that superoxides generally tend to overproduce $O_2$ relative to the amount of $CO_2$ they absorb. For $KO_2$, Buban and Gray used 0.68 for RQ-chem, based on their analysis of spent, 10 min SCSR canisters. Use of the RQ-chem factor was based on the assumption that the chemical must absorb the $CO_2$ eliminated by the user or else the $CO_2$ levels in the SCSR will exceed the specifications listed in the CFR Title 30 (11). However, if the $CO_2/O_2$ molar ratio of the chemical was greater than 1.0, 1.0 was used since otherwise the $O_2$ capacity of the chemical would be erroneously increased.

Based on the total available $O_2$ values given in tables 6-1 and 6-2 (listed under the $KO_2$ heading) it is apparent that both the Drager and MSA SCSRs contain twice as much $O_2$ than is needed by the 95th percentile miner during simulated escape activities for 60 min. Using equation (6.1) it was possible to estimate the design utilization efficiency used by the two manufacturers of 60 min SCSRs. For example, in the case of the MSA SCSR, the superoxide bed contained 92.0% $KO_2$. If the remainder is assumed to be KOH, the RQ-chem is theoretically 0.741 and the projected utilization efficiency E is 67.0%. If 0.68 is used for RQ-chem (as in the work of Buban and Gray), then E is 73.1%. At 67% utilization efficiency, 35 l of $O_2$ is vented, and at 73% utilization efficiency, 48 l of $O_2$ is vented. On the basis of these calculations it is apparent that the SCSRs carry a large excess of $KO_2$ because RQ-chem < RQ-man (and the SCSRs overproduce $O_2$ which is vented) and/or the utilization efficiency is low. It is interesting to note that in a 1973 paper (31), Perry and Wagner of Lockheed described a NIOSH approved prototype SCSR which used 681 g (1.5 lbs) of $KO_2$ yet weighed only 2061 g (4.54 lbs) and occupied a volume of 2912 $cm^3$ (177.7 $in^3$). Although this Lockheed unit later had some problems with overheating (137, it should be noted that current SCSRs have evolved into devices with nearly twice the weight and volume.

It is apparent from equation (6.1) that there are three ways to decrease the weight of chemical required to meet a given metabolic load; increase the utilization efficiency of the existing chemical, use a chemical with a similar utili-

zation efficiency but a a higher $O_2$ capacity, and/or use a chemical which has a similar $O_2$ capacity and utilization efficiency but a higher RQ-chem.

## 6.4 Potential Replacement Chemicals For $KO_2$

Table 6-3 contains a listing of the theoretical $O_2$-evolution and $CO_2$-scrubbing capacities of commercial purity $KO_2$, of $Ca(O_2)_2$ at various purity levels and of two $Ca(O_2)_2/KO_2$ mixtures. These capacities were calculated based on the known reactions of each of the components present in the superoxide materials. Also included in the table are the theoretical RQ-chem factors for each superoxide material. It should be noted that the rates at which each superoxide material reacts with H2O and $CO_2$ were not taken into account in making these calculations. Material "A" is $KO_2$ at the purity level found in the MSA SCSR. The $Ca(O_2)_2$ materials are chemicals which have theoretically superior $O_2$ capacities and/or higher RQ-chem factors. 100% $Ca(O_2)_2$ has not yet been synthesized; 67.4% $Ca(O_2)_2$ is the highest purity of $Ca(O_2)_2$ which has been synthesized, and 55.4% $Ca(O_2)_2$ is easily synthesized and is indefinitely stable (Sec. 2). Materials "E" and "F" are mixtures of $KO_2$ and $Ca(O_2)_2$ which have comparable $O_2$ capacities to MSA $KO_2$ but which have higher theoretical RQ-chem values. Material "E" has been evaluated in the flow system and preliminary results indicated that when this superoxide mixture was compared with MSA $KO_2$ tested under identical conditions, superior chemical utilization efficiencies were obtained (Sec. 5.2).

## 6.5 Determination of SCSR Weight And Volume Reductions

Tables 6-4 and 6-5 list the calculated bed weights for each superoxide material at various utilization efficiencies and the resulting reductions in the bed weight and volume, canister weight and case weight and volume which would be realized for the Drager and MSA SCSRs. The values given in tables 6-4 and 6-5 were calculated based on the following assumptions:

(a) The superoxide material in question could be fabricated into granules or tablets of similar bulk density as the $KO_2$ in the commercial SCSRs and so the reduction in the volume of the bed would be directly proportional to the reduction in weight of the bed.

(b) The minimum reduction of weight to the canister and case could be estimated by determining the reduction in bed length which would occur for a given reduction in bed volume. The shape of the bed was assumed to change in only one dimension. Any optimization of the design of the canister and case permitted by the reduction of bed volume would only result in additional reductions in canister and case

Table 6-3.- Theoretical $O_2$ Evolution and $CO_2$ Absorption Capacities of Various Superoxide Materials

| Material | Chemical composition | $O_2$ evolution capacity, $cm^3$ STP/g | $CO_2$ absorption capacity, $cm^3$ STP/g | RQ-chem [1] |
|---|---|---|---|---|
| A | 91.0% $KO_2$, 9.0% KOH | 215.2 | 161.4 [2] | 0.750 |
| B | 100% $Ca(O_2)_2$ | 323.0 | 215.4 | 0.667 |
| C | 67.4% $Ca(O_2)_2$, 6.4% $CaO_2$, 26.2% $Ca(OH)_2$ | 227.7 | 244.3 | 1.07 |
| D | 55.4% $Ca(O_2)_2$, 14.4% $CaO_2$, 30.2% $Ca(OH)_2$ | 201.4 | 255.4 | 1.27 |
| E | 75% A, 25% D | 211.7 | 184.9 [2] | 0.874 |
| F | 50% A, 50% D | 208.3 | 208.4 [2] | 1.01 |

[1] RQ-chem = vol. $CO_2$ absorbed/vol. $O_2$ evolved.
[2] Carbon dioxide absorption capacity calculations based on $K_2CO_3$ being the sole $CO_2/KO_2$ reaction product.

Table 6-4.- Weight and Volume Reductions in Drager Self-Contained, Self-Rescuer as a Function of Decreased Superoxide Bed Size

| Material[3] | Utilization efficiency, % $O_2$ available | Required[2] bed weight, g | Reductions in Drager SCSR[1]: Superoxide bed Weight g | Weight % | Height cm | Volume $cm^3$ | Metal canister Weight g | Weight % | Outer case Weight g | Weight % | Volume % | Total Weight g | Weight % |
|---|---|---|---|---|---|---|---|---|---|---|---|---|---|
| A | 90 | 723 | 430 | 37.3 | 5.6 | 546 | 240 | 27.2 | 117 | 9.3 | 18.7 | 787 | 21.0 |
| | 80 | 813 | 340 | 29.5 | 4.4 | 431 | 189 | 21.5 | 93 | 7.3 | 14.7 | 622 | 16.6 |
| | 70 | 929 | 224 | 19.4 | 2.9 | 284 | 125 | 14.1 | 61 | 4.8 | 9.7 | 410 | 10.9 |
| | 60 | 1084 | 69 | 6.0 | 0.9 | 88 | 38 | 4.4 | 19 | 1.5 | 3.0 | 126 | 3.4 |
| B | 90 | 542 | 611 | 53.0 | 8.0 | 775 | 340 | 38.6 | 167 | 13.2 | 26.5 | 1118 | 29.8 |
| | 80 | 609 | 544 | 47.1 | 7.1 | 689 | 303 | 34.4 | 148 | 11.7 | 23.6 | 994 | 26.5 |
| | 70 | 697 | 456 | 39.6 | 5.9 | 579 | 254 | 28.8 | 124 | 9.9 | 19.8 | 835 | 22.3 |
| | 60 | 813 | 340 | 29.5 | 4.4 | 431 | 190 | 21.5 | 93 | 7.4 | 14.8 | 623 | 16.6 |
| C | 90 | 512 | 641 | 55.6 | 8.3 | 812 | 357 | 40.5 | 175 | 13.8 | 27.8 | 1172 | 31.2 |
| | 80 | 576 | 577 | 50.0 | 7.5 | 731 | 321 | 36.4 | 157 | 12.5 | 25.0 | 1055 | 28.1 |
| | 70 | 659 | 494 | 42.9 | 6.4 | 627 | 275 | 31.2 | 135 | 10.7 | 21.4 | 904 | 24.1 |
| | 60 | 769 | 384 | 33.3 | 5.0 | 487 | 214 | 24.3 | 105 | 8.3 | 16.7 | 703 | 18.7 |
| D | 90 | 579 | 574 | 49.8 | 7.5 | 727 | 320 | 36.3 | 156 | 12.4 | 24.9 | 1050 | 28.0 |
| | 80 | 652 | 501 | 43.5 | 6.5 | 636 | 279 | 31.7 | 137 | 10.8 | 21.7 | 917 | 24.4 |
| | 70 | 745 | 408 | 35.4 | 5.3 | 518 | 227 | 25.8 | 111 | 8.8 | 17.7 | 747 | 19.9 |
| | 60 | 869 | 284 | 24.6 | 3.7 | 360 | 158 | 18.0 | 78 | 6.1 | 12.3 | 520 | 13.9 |
| E | 90 | 631 | 522 | 45.3 | 6.8 | 662 | 291 | 33.0 | 142 | 11.3 | 22.6 | 955 | 25.5 |
| | 80 | 710 | 443 | 38.4 | 5.8 | 562 | 247 | 28.0 | 121 | 9.6 | 19.2 | 811 | 21.6 |
| | 70 | 811 | 342 | 29.6 | 4.4 | 433 | 190 | 21.6 | 93 | 7.4 | 14.8 | 625 | 16.7 |
| | 60 | 946 | 207 | 17.9 | 2.7 | 262 | 115 | 13.1 | 56 | 4.5 | 9.0 | 378 | 10.1 |
| F | 90 | 560 | 593 | 51.4 | 7.7 | 752 | 330 | 37.5 | 162 | 12.8 | 25.7 | 1085 | 28.9 |
| | 80 | 630 | 523 | 45.4 | 6.8 | 663 | 291 | 33.0 | 143 | 11.3 | 22.7 | 957 | 25.5 |
| | 70 | 720 | 433 | 37.5 | 5.6 | 549 | 241 | 27.4 | 118 | 9.3 | 18.8 | 792 | 21.1 |
| | 60 | 840 | 313 | 27.1 | 4.1 | 572 | 174 | 19.8 | 85 | 6.8 | 13.6 | 572 | 15.3 |

1 Percentage value calculations based on the original weights and volumes of the components listed in table 6-1.
2 Calculated using equation (6.1) in text and RQ-chem values listed in table 6-3 (for RQ-chem values >1, 1.0 was used, see text).
3 See table 6-3 for identity and composition of superoxide materials.

Table 6-5.- Weight and Volume Reductions in MSA Self-Contained, Self-Rescuer as a Function of Decreased Superoxide Bed Size

| Material[3] | Utilization efficiency, % $O_2$ available | Required[2] bed weight, g | Reductions in MSA SCSR[1]: Superoxide bed Weight g | Superoxide bed Weight % | Superoxide bed Height cm | Superoxide bed Volume $cm^3$ | Metal canister Weight g | Metal canister Weight % | Outer case Weight g | Outer case Weight % | Outer case Volume % | Total Weight g | Total Weight % |
|---|---|---|---|---|---|---|---|---|---|---|---|---|---|
| A | 90 | 723 | 250 | 25.7 | 3.1 | 399 | 163 | 14.9 | 156 | 9.5 | 12.3 | 597 | 14.2 |
| | 80 | 813 | 160 | 16.4 | 2.0 | 255 | 104 | 9.5 | 100 | 6.0 | 7.9 | 364 | 9.1 |
| | 70 | 929 | 44 | 4.5 | 0.5 | 70 | 28 | 2.6 | 27 | 1.7 | 2.2 | 100 | 2.5 |
| | 60 | 1084 | NR | NR | NR | NR | NR | NR | NR | NR | NR | NR | NR |
| B | 90 | 542 | 431 | 44.3 | 5.3 | 688 | 280 | 25.6 | 270 | 16.3 | 21.3 | 981 | 24.5 |
| | 80 | 609 | 364 | 37.4 | 4.5 | 580 | 236 | 21.6 | 227 | 13.7 | 17.9 | 827 | 20.7 |
| | 70 | 679 | 276 | 28.4 | 3.4 | 441 | 180 | 16.4 | 173 | 10.4 | 13.6 | 629 | 15.7 |
| | 60 | 813 | 160 | 16.5 | 2.0 | 256 | 104 | 9.5 | 100 | 6.1 | 7.9 | 365 | 9.1 |
| C | 90 | 512 | 461 | 47.3 | 5.7 | 735 | 300 | 27.4 | 289 | 17.4 | 22.7 | 1048 | 26.2 |
| | 80 | 576 | 397 | 40.8 | 4.9 | 632 | 258 | 23.6 | 248 | 15.0 | 19.6 | 902 | 22.5 |
| | 70 | 659 | 314 | 32.3 | 3.9 | 501 | 204 | 18.7 | 196 | 11.9 | 15.5 | 715 | 17.9 |
| | 60 | 769 | 204 | 21.0 | 2.5 | 326 | 133 | 12.1 | 128 | 7.7 | 10.1 | 465 | 11.6 |
| D | 90 | 579 | 394 | 40.5 | 4.9 | 628 | 256 | 23.4 | 246 | 14.9 | 19.4 | 896 | 22.4 |
| | 80 | 652 | 321 | 33.0 | 4.0 | 512 | 209 | 19.1 | 201 | 12.1 | 15.9 | 731 | 18.3 |
| | 70 | 745 | 228 | 23.5 | 2.8 | 364 | 148 | 13.6 | 143 | 8.6 | 11.3 | 519 | 13.0 |
| | 60 | 869 | 104 | 10.7 | 1.3 | 166 | 68 | 6.2 | 65 | 3.9 | 5.1 | 237 | 5.9 |
| E | 90 | 631 | 342 | 35.2 | 4.2 | 546 | 222 | 20.3 | 214 | 12.9 | 16.9 | 778 | 19.4 |
| | 80 | 710 | 263 | 27.1 | 3.2 | 420 | 171 | 15.6 | 164 | 9.9 | 13.0 | 599 | 15.0 |
| | 70 | 811 | 162 | 16.6 | 2.0 | 368 | 105 | 9.6 | 101 | 6.1 | 8.0 | 368 | 9.2 |
| | 60 | 946 | 27 | 2.7 | 0.3 | 43 | 17 | 1.6 | 17 | 1.0 | 1.3 | 61 | 1.5 |
| F | 90 | 560 | 413 | 42.4 | 5.1 | 659 | 268 | 24.5 | 258 | 15.6 | 20.4 | 939 | 23.5 |
| | 80 | 630 | 343 | 35.2 | 4.2 | 547 | 223 | 20.4 | 214 | 13.0 | 16.9 | 780 | 19.5 |
| | 70 | 720 | 253 | 26.0 | 2.1 | 403 | 164 | 15.0 | 158 | 9.6 | 12.5 | 575 | 14.4 |
| | 60 | 840 | 133 | 13.7 | 1.6 | 302 | 86 | 7.9 | 83 | 5.0 | 6.6 | 302 | 7.6 |

1 Percentage value calculations based on the original weights and volumes of the components listed in table 6-2, NR = no reduction.
2 Calculated using equation (6.1) in text and RQ-chem values listed in table 6-3 (for RQ-chem values >1, 1.0 was used, see text).
3 See table 6-3 for identity and composition of superoxide materials.

weights.

The estimation of the reductions of weight and volume for each SCSR was made as follows:

1. Once the reductions in bed weight were determined by subtracting the theoretical bed weights [calculated using equation (6.1)] from the bed weight listed in tables 6-1 and 6-2 for the two SCSRs, the reductions in bed volume were calculated.

2. Next, the reductions in bed height were calculated by dividing the cross-sectional area of the bed into the reductions in volume. The cross-sectional area of the MSA SCSR bed (129.3 $cm^2$) was taken as the section normal to the direction of gas flow, whereas the cross-sectional area of the radial Drager bed (97.4 $cm^2$) was taken as the section normal to the axis of the central gas-exit tube (parallel to gas flow).

3. The reductions in canister weight were estimated by multiplying the reductions in bed height by the circumference of the canister, and then multiplying the resulting reductions in surface area of the canister by the surface density. Since reductions in bed height would affect the number of baffles and screens in the interior of the canister, the surface density of each SCSR canister type was estimated by dividing the total weight of the canister shell (tables 6-1 and 6-2) by the total outside surface area. The surface densities of the Drager and MSA canisters are 0.951 and 1.127 $g/cm^3$, respectively and the circumferences of the two canisters are 45 and 47 cm respectively.

4. The reductions in the case weight for each SCSR were estimated in the same way as for the canister weight. The case circumference of the Drager and MSA SCSRs were 51 and 67 cm, respectively, whereas the corresponding surface densities were 0.466 and 0.756 $g/cm^3$, respectively.

5. The reductions in case volume for each SCSR were estimated by multiplying the reductions in bed height by the cross-sectional area of the case. The cross-sectional areas of the SCSR cases were determined normal to the same axis that had been used in determining the bed cross sectional areas (see step 2). The cross-sectional areas of the Drager and MSA cases are 224 and 228 $cm^2$, respectively.

6. Finally, the total reductions in the weight which would be realized for each SCSR were calculated by adding up the reductions in weight of the chemical bed, the canister and the case. With the overall design optimization which could be possible based on a smaller chemical bed size, the reductions in overall weight and volume would probably be

even greater than those estimated here.

## 6.6 Results and Conclusions

It is apparent from the data tabulated in tables 6-4 and 6-5 that substantial weight and volume savings could be realized by utilizing $Ca(O_2)_2$ or a mixture of $KO_2$ and $Ca(O_2)_2$ in place of $KO_2$ in the Drager or MSA SCSR. The weight and volume savings are slightly higher for the Drager SCSR because it contained $KO_2$ of a lower $O_2$ capacity than the MSA SCSR. Even at a modest 80% utilization of the 55% $Ca(O_2)_2$, over 900 g (~2 lb) could be eliminated from the weight of the Drager SCSR and over 700 g (1.5 lb) from the MSA SCSR. However, in Sec. 4.3.1, an evaluation of the reactivity of $Ca(O_2)_2$ towards humidified $CO_2$ indicated that the rates of reaction of water vapor and $CO_2$ with the superoxide were too low to allow $Ca(O_2)_2$ to be currently used to replace $KO_2$ in SCSRs. The study described in this section indicated that <u>if</u> the rates of $CO_2$ absorption and $O_2$ evolution could be enhanced by means of a catalyst, then $Ca(O_2)_2$ <u>could</u> be considered as a $KO_2$-replacement in SCSRs.

Weight and volume reductions of similar magnitude to those calculated for 55% $Ca(O_2)_2$ could be obtained if the 50% $KO_2$-50% $Ca(O_2)_2$ or 75% $KO_2$-25% $Ca(O_2)_2$ mixtures listed in table 6-3 were substituted for $KO_2$. In the case of the 75% $KO_2$-25% $Ca(O_2)_2$ mixture, results from flow tests have demonstrated that it exhibited superior chemical utilization efficiency compared to $KO_2$ tested under identical conditions while the rates of $CO_2$ absorption and $O_2$ evolution were equal to $KO_2$. Therefore, these superoxide mixtures are chemicals which could be used in the future as replacements for $KO_2$ in SCSRs.

# 7. RECOMMENDATIONS FOR FUTURE WORK

## 7.1 Catalysts for $Ca(O_2)_2$/Humidified $CO_2$ Reaction

For $Ca(O_2)_2$ to be used as an air revitalization chemical in portable a breathing apparatus the problem of its low reactivity with humidified $CO_2$ must be overcome. This problem was discussed in detail in Sec. 4.3. Some work has already been done on testing $KO_2$ as a catalyst in $Ca(O_2)_2$ (Sec. 5.1). Further work should be done in which other materials such as transition metal oxides and/or NaOH are added to $Ca(O_2)_2$ and the resulting mixtures flow-tested to compare their reactivity with untreated $Ca(O_2)_2$.

## 7.2 Superoxide Mixtures

In Sec. 5., preliminary research was described in which mixtures of $KO_2$ and $Ca(O_2)_2$ or $Li_2O_2$ were fabricated into granules and their reactivity was compared to $KO_2$. These mixtures exhibited significantly superior utilization efficiency and improved post reaction physical properties compared to $KO_2$ when tested under the same conditions. Additional work on these mixtures should be done to further characterize the properties and reactivity of the materials over a wider range of reaction conditions.

## 8. REFERENCES


1. Adriani, J., and E. A Rovenstein. Experimental Studies on Carbon Dioxide Absorbers for Anesthesia. Anesthesiology, v. 2, 1941, pp. 1-19.

2. Bakulina, V. M., A. N. Zimina, and A. B. Tsentsiper. X-ray Phase Study of the Product of the Decomposition of Calcium Peroxide Diperhydrate. Acad. of Sci. of the USSR, Gen. and Inorg. Chem., v. 3, 1968, pp. 646-647, (Eng. Trans. of Izvest. Akad. Nauk SSSR, Ser. Khim., v. 3, 1968, pp. 666-667).

3. Ballou, E. V., P. C. Wood, L. A. Spitze, and T. Wydeven. The Preparation of Calcium Superoxide from Calcium Peroxide Diperoxyhydrate. Ind. Eng. Chem., Prod. Res. Dev., v. 16, 1977, pp. 180-186.

4. Ballou, E. V., P. C. Wood, L. A. Spitze, and T. Wydeven. The Preparation of Calcium Superoxide at Subambient Temperatures and Pressures. J. Eng. Ind., v. 100, 1978, pp. 26-30.

5. Ballou, E. V., P. C. Wood, L. A. Spitze, and T. Wydeven. Process for the Preparation of Calcium Superoxide," U. S. Patent 4,101,644, July 1978a.

6. Ballou, E. V., P. C. Wood, L. A. Spitze, T. Wydeven, and R. L. Stein. The Reduction of Particle Agglomeration in a Fluidizing Gas Stream in the Presence of a Radiofrequency Glow Discharge. Ind. Eng. Chem. Fundam., v. 19, 1980, pp. 315-316.

7. Brosset, C., and N. G. Vannerberg. Formation of Calcium Superoxide. Nature, v. 177, 1956, p. 238.

8. Buban, E. E., and R. E. Gray. Short Duration Self-rescue Breathing Apparatus. BuMines CR HO220071, 1974.

9. Difford, A. M. R., and H. S. Spencer. Catalyst Test Reactor Types and Examples of Their Applications. A. I. Ch. E. Symp. Series, v. 70, n. 143, 1974, pp. 42-48.

10. Dresser, K. J. Lithium Peroxide for Portable Life Support System Atmospheric Regeneration. NASA SP-234, April 1964, pp. 343-371.

11. Federal Register, Title 30, Ch. 1, sec. 11.85.3 and 11.85.12, v. 37, n. 59, March 25, 1972, U. S. Govt. Printing Office, Washington D. C.

12. Grace, W. R., and Co., Dewy and Almy Chemical Division. The Sodasorb Manual of Carbon Dioxide Absorption. 1962, pp. 1-57.

13. Handbook of Chemistry and Physics, 52nd ed., R. C. Weast, Ed., Chemical Rubber Co., Cleveland, Ohio, 1972, p. B-230

14. Johnston, R. S., E. D. Osgood, and R. R. Miller. Analysis of Mixed Oxides of Calcium. Anal. Chem., v. 30, 1958, pp. 511-513.

15. Kamon, E., T. Bernard, and R. Stein. Steady State Respiratory Responses to Tasks Used in Federal Testing of Self-Contained Breathing Apparatus. Amer. Ind. Hyg. Assoc. J., v. 36, 1975, pp. 886-896.

16. Kazarnovskii, I. A., and A. B. Neiding. Research on the Mechanism of Decomposition of Hydrogen Peroxide in Some Diperoxyhydrates. Eng. Trans. of Dokl. Akad. Nauk, SSSR, v. 86, n. 4, 1952, pp. 717-720.

17. Kubaschewski, O., and I. LL. Evans. Metallurgical Thermochemistry. Pergamon Press Ltd., 3rd ed., London, 1958, pp. 5-18, 225-283, 310-325.

18. Li, Y. S. One-Hour Self-Rescue Breathing Apparatus. BuMines CR H0220040, Oct. 1974.

19. Li, Y. S. A Potassium Superoxide ($KO_2$) Life Support System for Deep Quest. Proceedings of Ocean '79, The Technical Change of Inner Space, IEEE and Ocean Eng. Council, Marine Tech. Soc., 1979, pp. 752-757.

20. Lower, B. R. Removal of $CO_2$ from Closed Circuit Breathing Apparatus. Equipment for the Working Diver. Symposium Proceedings, D. Landreman, Ed., Marine Technology Society, 1970, pp. 261-282.

21. Makarov, S. Z., and N. K. Grigoreva. Systems Containing Concentrated Hydrogen Peroxide V. Thermal Characteristics of the Solid Phases of the System $Ca(OH)_2$-$H_2O_2$-$H_2O$. Bull. Acad. Sci. U.S.S.R., Div. Chem. Sci., v. 1954, pp. 511-514 (Eng. Trans. of Izvest. Akad. Nauk, S.S.S.R., Otdel. Khim. Nauk, v. 1954, pp. 598-603).

22. Makarov, S. Z., and N. K. Grigoreva. Systems Containing Hydrogen Peroxide at High Concentration, Communication 15. The 10° Solubility Isotherm of the Ternary System $Ca(OH)_2$-$H_2O_2$-$H_2O$ and Further Characterization of the Solid Phases. Bull. Acad. Sci., USSR, Div. Chem. Sci., (Eng. Trans. of Izv. Akad. Nauk, SSSR, Otd. Khim. Nauk), v. 11, 1958, pp. 1245-1250.

23. Marriott, J. A., A. Capotosto, Jr., and A. W. Petrocelli. The Effect of Catalysts on the Thermal Decomposition of Sodium Superoxide. Anal. Chim. Acta, v. 41, 1968, pp. 121-128.

24. McGoff, M. J., and J. C. King. Superoxide Configurations for Atmosphere Control Systems. Aerospace Medical Research Laboratories, Aerospace Medical Division, Air Force Systems Command, Wright Patterson AFB, Ohio, Report No. AMRL-TR-66-167, Nov. 1966.

25. Optican, A. W. Potassium Superoxide Canister Evaluation for Manned Space Vehicles. Aeronautical Systems Division, Dir/Aero Mechanics, Flight Accessories Laboratory, Wright Patterson AFB, Ohio, Report No. ASD-TDR-62-583, Sept. 1962.

26. Patel, P. S., and B. S. Baker. Development of a Prototype Regeration Carbon Dioxide Absorber. Final Report, on Contract No. NAS2-9265, Oct. 1977.

27. Pavlyvchenko, M. M., and Ya. S. Rubinchik. The Decomposition of Calcium Peroxide in Gaseous Carbon Dioxide. Zh. Neorg. Khim., v. 4, 1959, pp. 19-21, (Eng. translation).

28. Petrocelli A. W., and A. Capotosto, Jr. Some Notes on the Use of Superoxides in Non Regenerative Air Revitalization Systems. Aerospace Med., v. 35, 1964, pp. 440-443.

29. Petrocelli, A. W., and A. Capotosto, Jr. The Synthesis of Low Molecular Weight Ozonides for Air Revitalization Purposes, Interim Report. NASA Contract No. NASw-559, 1965.

30. Petrocelli, A. W. The Role of Active Chemicals for Air Revitalization. NASA SP-234, April 1969, pp. 331-337.

31. Perry, E. N., and P. A. Wagner. One-hour Self-Rescue Breathing Apparatus. AIAA Paper 73-1358, Nov. 1973.

32. Presti, J., H. Wallman, and A. Petrocelli. Superoxide Life Support System for Submersibles. UnderSea Technology, June 1967, pp. 20-21.

33. Schenk, P. W., and G. Brauer. Preparative Methods - Powder Reactions. Handbook of Preparative Inorganic Chemistry, G. Brauer, Ed., Academic Press, New York, v. 1, 2nd ed., 1963, pp. 103-104.

34. Schumb, W. C., C. N. Satterfield, and R. L. Wentworth. Hydrogen Peroxide. Reinhold Publishing Corp., New York, 1955, p. 533.

35. Seyb, E., Jr., and J. Kleinberg. Determination of Superoxide Oxygen. Anal. Chem., v. 23, 1951, pp. 115-117.

36. Skoog D. A., and D. M. West. Fundamentals of Analytical Chemistry. Holt, Rinehart and Winston, Inc., 2nd ed., New York, 1969, pp. 355-357.

37. Stein, R. L. Development of Two New Oxygen Self-Rescuers. BuMines, RI 8102, 1976.

38. Tokareva, S. A., G. P. Pilipenko, V. L. Khimanov, and I. I. Vol'nov. Synthesis of New Alkaline and Alkaline Earth Metal Superoxides and Ozonides. Tezisy Dokl. Vses. Soueshch. Khim. Neorg. Perekisnykh Soedin., 1973, 14 (Russ), Chem. Abstracts 83:21009p, 1975.

39. Vannerberg, N. G. On the System $SrO_2$-$H_2O$-$H_2O_2$ 1. The Crystal Structure of Alpha- and Beta-$SrO_2 \cdot 2H_2O_2$. Arkiv. Kemi., v. 13, 1958, pp. 29-41.

40. Vannerberg, N. G. The Formation and Structure of Peroxy Compounds of Group IIa and IIb Elements. Thesis, Doktorsarhandlingar Chalmers Tekn. Hogskola, v. 21, 1959, pp. 1-22.

41. Vannerberg, N. G. On the System $BaO_2$-$H_2O$-$H_2O_2$ 1. Investigation of the Existing Phases and Their Preparation 2. The Structure of $BaO_2 \cdot H_2O_2$. Arkiv. Kemi., v. 14, 1959, pp. 147-159.

42. Vannerberg, N. G. On the System $BaO_2$-$H_2O$-$H_2O_2$ 3. The Crystal Structure of Alpha-, Beta-, and Gamma-$BaO_2 \cdot H_2O_2$ and $BaO_2 \cdot H_2O_2 \cdot 2H_2O$. Arkiv. Kemi., v. 14, 1959, pp. 125-145.

43. Vol'nov, I. I., V. N. Chamova, and E. I. Latysheva. Studies in Synthesis of Alkaline Earth Superoxides," Russ. J. Inorg. Chem. (Eng. Trans. of Zh. Neorg. Khim.), v. 2, n. 2, 1957a, pp. 263-267.

44. Vol'nov, I. I., and A. N. Shatunina. Reactivity of Alkali Earth Metal Superoxides in Relation to $H_2O$ and $CO_2$. Russ. J. Inorg. Chem., v.2. n. 7, 1957, pp. 1474-1478, (Eng. Trans. of Zh. Neorg. Khim., v. 2, n. 7, 1957, pp. 1474-1478).

45. Vol'nov, I. I., and V. N. Chamova. The Mechanism of Conversion of $CaO_2 \cdot 2H_2O_2$ Into $Ca(O_2)_2$. Russ. J. Inorg. Chem., v. 5, n. 3, 1960, pp. 249-250, (Eng. Trans. of Zh. Neorg. Khim., v. 5, n. 3, 1960, pp. 522-523).

46. Vol'nov, I. I. Peroxides, Superoxides, and Ozonides of Alkali and Alkaline Earth Metals. A. W. Petrocelli, Translation editor., Plenum Press, New York, 1966a, pp. 95-140.

47. Vol'nov, I. I., and A. N. Shatunina. New Data on the Formation of $Ca(O_2)_2$ by Means of $CaO_2 \cdot 2H_2O_2$. Eng. Trans. of Izv. Akad. Nauk, SSSR, Ser. Khim., no. 11, 1966b, pp. 2032-2033.

48. Wilson, R. E. Soda Lime a an Absorbent for Industrial Purposes. J. of Ind. and Eng. Chem., v. 12, 1920, pp. 1000-1007.

49. Wood, P. C., E. V. Ballou, L. A. Spitze, and T. Wydeven. The Preparation of Calcium Superoxide in A Flowing Gas Stream and Fluidized Bed. ASME Paper 80-ENAs-18, Tenth Intersociety Conference on Environmental Systems, San Diego, Calif., July 14-17, 1980.

50. Wood, P. C., E. V. Ballou, L. A. Spitze, and T. Wydeven. Use of Glow Discharge in Fluidized Beds. U. S. Patent 4,303,961, Dec. 1981.

| 1. Report No. | 2. Government Accession No. | 3. Recipient's Catalog No. |
|---|---|---|
| | | |

| 4. Title and Subtitle | 5. Report Date |
|---|---|
| IMPROVED OXYGEN SOURCES FOR BREATHING APPARATUS - FINAL REPORT | August 1983 |
| | 6. Performing Organization Code |

| 7. Author(s) | 8. Performing Organization Report No. |
|---|---|
| Peter C. Wood (San Jose State University, San Jose, CA 95192) and Theodore Wydeven | |
| | 10. Work Unit No. |
| 9. Performing Organization Name and Address<br>Ames Research Center<br>National Aeronautics and Space Administration<br>Moffett Field, California 94035 | 11. Contract or Grant No.<br>HO242047 |
| | 13. Type of Report and Period Covered<br>Final 4/74-9/82 |
| 12. Sponsoring Agency Name and Address<br>United States Bureau of Mines<br>Cochrans Mill Road, P. O. Box 18070<br>Pittsburgh, Pennsylvania 15236 | 14. Sponsoring Agency Code |

15. Supplementary Notes

Point of Contact: John Kovak, United States Bureau of Mines, Cochrans Mill Road, P. O. Box 18070, Pittsburgh, Pennsylvania 15236
FTS 8-723-6471, 412-675-6971

16. Abstract

This report describes research directed toward the preparation of chemical oxygen ($O_2$) sources which exhibited improved $O_2$ storage and reaction characteristics when compared to potassium superoxide ($KO_2$). The initial focus of the research was the preparation of calcium superoxide ($Ca(O_2)_2$) by the disproportionation of calcium peroxide diperoxyhydrate. The $Ca(O_2)_2$ was characterized by chemical, thermal, and x-ray analyses. Several methods for scaling up the $Ca(O_2)_2$ synthesis process were studied. Next, the reactivity of $Ca(O_2)_2$ toward humidified carbon dioxide ($CO_2$) was evaluated and was compared to that of $KO_2$ under flow-test conditions approximating those existing in portable breathing apparatus. The reactivities of mixtures of $KO_2$ and $Ca(O_2)_2$ or lithium peroxide towards humidified $CO_2$ were also studied. Finally, an analysis of two commercial, $KO_2$-based, self-contained self-rescuers was conducted to determine the potential weight and volume savings which would be possible if $Ca(O_2)_2$ or a mixture of $KO_2$ and $Ca(O_2)_2$ were used as a replacement for $KO_2$.

| 17. Key Words (Suggested by Author(s)) | 18. Distribution Statement |
|---|---|
| Calcium superoxide, Peroxides<br>Potassium superoxide<br>Superoxide mixtures<br>Self-contained self-rescuers<br>Chemical oxygen storage | Unclassified - Unlimited |

| 19. Security Classif. (of this report) | 20. Security Classif. (of this page) | 21. No. of Pages | 22. Price* |
|---|---|---|---|
| Unclassified | Unclassified | 160 | |

*For sale by the National Technical Information Service, Springfield, Virginia 22161